

South Dakota State University
**Open PRAIRIE: Open Public Research Access Institutional
Repository and Information Exchange**


Theses and Dissertations

2017

UAV-Based Bridge Inspection and Computational Simulations

Luis Duque
South Dakota State University

Follow this and additional works at: <https://openprairie.sdstate.edu/etd>

 Part of the [Civil Engineering Commons](#), [Structural Engineering Commons](#), and the [Transportation Engineering Commons](#)

Recommended Citation

Duque, Luis, "UAV-Based Bridge Inspection and Computational Simulations" (2017). *Theses and Dissertations*. 2159.
<https://openprairie.sdstate.edu/etd/2159>

This Thesis - Open Access is brought to you for free and open access by Open PRAIRIE: Open Public Research Access Institutional Repository and Information Exchange. It has been accepted for inclusion in Theses and Dissertations by an authorized administrator of Open PRAIRIE: Open Public Research Access Institutional Repository and Information Exchange. For more information, please contact michael.biondo@sdstate.edu.

UAV– BASED BRIDGE INSPECTION AND COMPUTATIONAL SIMULATIONS

BY

LUIS DUQUE

A thesis submitted in partial fulfillment of the requirements for

Master of Science

Major in Civil Engineering

South Dakota State University

2017

El fruto de mis esfuerzos es dedicado a Dios que me dio fortaleza en los momentos difíciles que afronte durante mis estudios en la universidad. Gracias a Dios por permitirme completar este logro tan grande en mi carrera y por permitirme continuar aprendiendo y luchando por mis sueños.

Quiero también dedicar este logro a personas especiales que por motivos del destino no pueden celebrar conmigo este gran logro. Mis abuelitos Hernando Duque y Fabio Aristizabal que siempre me enseñaron a ser bondadoso y agradecido por lo que la vida me ofrece. A ellos, les debo muchos de mis logros y hacen gran parte de este logro en mi vida.

A toda mi familia, que a pesar de la distancia siempre sentí el amor y apoyo conmigo a lo largo de este camino. Su constante apoyo me ayudo a seguir adelante y sentirlos a todos cerca de mí.

Por último, este logro es dedicado a mi esposa Callie Duque, mis padres Roberto Duque y Gloria Aristizabal y hermano Juan Duque por su constante apoyo y motivación. Sin ellos, este logro no hubiese sido posible.

“Confía en el Señor con todo tu corazón, y no te apoyes en tu propio entendimiento. En todas sus maneras lo reconocen y él enderezara tus veredas.” – Proverbios 3:5,6

ACKNOWLEDGMENTS

I would like to thank Dr. Junwon Seo for his encouragement and assistance during every stage of the research process. He constantly pushed me to give more than what I thought possible of myself and allowed me to surpass my own expectations. The guidance provided by Dr. Seo for the completion of all the written work pertaining to the research project was much appreciated, and it allowed me to greatly improve my writing skills.

I want to extend my gratefulness to Dr. Wehbe, Dr. Tazarv, and Dr. Burckhard for their assistance in my learning process while completing my Master's program.

I would like to also thank the United States Department of Agriculture – Forest Service (USDA-FS) for sponsoring the project. The assistance and cooperation of the South Dakota Department of Transportation (SDDOT) was greatly appreciated.

Finally, I would like to thank my wife Callie Duque, my parents Roberto Duque and Gloria Aristizabal, my brother Juan Duque, and my parents-in-law Matthew and Dee Sleep for their constant support and encouragement to overcome the adversities I faced during my research project. Their words of inspiration allowed me to achieve all my goals and successfully complete my studies.

TABLE OF CONTENTS

ABSTRACT.....	x
INTRODUCTION	1
RESEARCH OBJECTIVES	2
SCOPE OF RESEARCH.....	2
OUTLINE OF THESIS.....	3
CHAPTER 1: SYNTHESIS OF UNMANNED AERIAL VEHICLE APPLICATIONS FOR INFRASTRUCTURES	4
1.1 ABSTRACT.....	5
1.2 INTRODUCTION.....	6
1.3 FAA REGULATIONS FOR UAVs.....	8
1.4 VISUAL INSPECTION OF INFRASTRUCTURES	9
1.4.1 BRIDGES	9
1.4.2 BUILDINGS.....	11
1.4.3 OTHER STRUCTURES.....	12
1.5 VISUAL INSPECTION-BASED ANALYTICAL METHODS	14
1.5.1 BRIDGES	14
1.5.2 BUILDINGS.....	17
1.5.3 OTHER STRUCTURES.....	18
1.6 INFRASTRUCTURE INSPECTION WITH INTEGRATED SENSORS	20

1.7	UAV SELECTION	22
1.8	SURVEY	28
1.9	SUMMARY AND CONCLUSION.....	33
1.10	REFERENCES.....	36
CHAPTER 2: BRIDGE INSPECTION PROTOCOL USING DRONE TECHNOLOGY		47
2.1	ABSTRACT.....	48
2.2	INTRODUCTION.....	49
2.3	DRONE AND BRIDGE SELECTION.....	51
2.3.1	SELECTED DRONE.....	51
2.3.2	SELECTED BRIDGE.....	53
2.4	BRIDGE INSPECTION PROTOCOL	54
2.5	APPLICATION OF INSPECTION PROTOCOL TO TIMBER GIRDER BRIDGE.....	57
2.5.1	STAGE 1.....	57
2.5.2	STAGE 2.....	58
2.5.3	STAGE 3.....	60
2.5.4	STAGE 4.....	61
2.5.5	STAGE 5.....	63
2.5.5.1	Underside of Deck.....	63

2.5.5.2	Abutment	65
2.5.5.3	Girders	66
2.6	COMPARISON TO CONVENTIONAL INSPECTION METHODS	68
2.6.1	UNDERSIDE OF DECK.....	70
2.6.2	ABUTMENTS	71
2.6.3	GIRDERS	72
2.7	CONCLUSIONS AND CHALLENGES	74
2.8	ACKNOWLEDGMENTS.....	76
2.9	REFERENCES.....	77
CHAPTER 3: BRIDGE DAMAGE QUANTIFICATION PROTOCOL USING UAV ..		80
3.1	ABSTRACT.....	81
3.2	INTRODUCTION.....	82
3.3	UAV AND BRIDGE SELECTION.....	84
3.3.1	UAV SELECTION	84
3.3.2	BRIDGE SELECTION.....	86
3.4	UAV-IMAGE-BASED BRIDGE DAMAGE QUANTIFICATION PROTOCOL.....	87
3.5	APPLICATION OF PROTOCOL TO KEYSTONE WYE BRIDGE DAMAGE	91
3.5.1	STAGE ONE	92

3.5.2	STAGE TWO.....	95
3.5.2.1	Image Quality Assessment Method.....	95
3.5.2.1.1	Entropy Definition.....	96
3.5.2.1.2	Sharpness Definition.....	97
3.5.2.1.3	Entropy-Sharpness Relationship.....	98
3.5.2.2	High Quality Image Determination.....	98
3.5.3	STAGE THREE.....	102
3.5.3.1	Pixel-Based Measurements Results.....	102
3.5.3.2	Photogrammetry-Based Measurements Results.....	107
3.5.4	STAGE FOUR.....	109
3.6	CONCLUSIONS.....	111
3.7	ACKNOWLEDGEMENTS.....	113
3.8	REFERENCES.....	114
CHAPTER 4: UAV DATA-DRIVEN FINITE ELEMENT ANALYSIS FOR BRIDGE PERFORMANCE EVALUATION.....		116
4.1	ABSTRACT.....	117
4.2	INTRODUCTION.....	118
4.3	BACKGROUND AND LITERATURE REVIEW.....	119
4.3.1	UAV-ENABLED BRIDGE INSPECTION.....	119
4.3.2	FE MODELING AND SIMULATION.....	121

4.3.3	SUMMARY	122
4.4	STUDIED BRIDGE DESCRIPTION AND MODELING	123
4.4.1	BRIDGE DESCRIPTION.....	123
4.4.2	FE MODELING.....	124
4.5	UAV SELECTION AND DAMAGE IDENTIFICATION	126
4.5.1	UAV SELECTION	126
4.5.2	DAMAGE IDENTIFICATION	128
4.5.2.1	Underside of Deck.....	128
4.5.2.2	Stringers.....	129
4.5.2.3	Abutments.....	130
4.6	FE ANALYSIS	131
4.6.1	DAMAGE APPLICATION.....	131
4.6.2	LIVE-LOAD DFs	134
4.6.3	STRUCTURAL CAPACITY ESTIMATE.....	141
4.6.4	LOAD RATING FACTORS	142
4.7	CONCLUSIONS	147
4.8	REFERENCES.....	150

ABSTRACT

UAV– BASED BRIDGE INSPECTION AND COMPUTATIONAL SIMULATIONS

LUIS DUQUE

2017

The use of Unmanned Aerial Vehicles (UAV), commonly known as drones, has significantly increased in the field of civil engineering due to the poor condition of the United States' infrastructure. The American Society of Civil Engineers (ASCE) recently reported that more than 9.1% of the United States' bridges were structurally deficient and required attention and maintenance to ensure appropriate structural performance. Meanwhile, current practices are expensive and unsafe for bridge inspectors, requiring innovative and safer methods for the study of bridges. The goal of this paper was to identify better techniques to not only inspect, quantify, and determine the effect of damage on bridges to minimize the risk for inspectors, but also to determine their live-load performance using UAV-based computational simulation updating techniques. To accomplish the objective, an extensive literature review and survey to state departments of transportation (DOTs) was conducted to gain technical knowledge on current UAV-based inspection practices. To evaluate the efficiency of the UAV, the Keystone Interchange Bridges (i.e., Keystone Wye timber arch bridge and timber girder bridge) in the Black Hills National Forest near the city of Keystone, South Dakota (SD), were studied. To provide a more systematic and efficient UAV-enabled bridge inspection method, a five-stage recommended bridge inspection protocol was developed. A UAV-image-based bridge damage quantification protocol involving image quality assessment and image-based damage measurement was recommended. Finally, using the damage information from the

inspection and quantification of the bridges, a Finite Element (FE) model to determine the live-load performance of the Keystone Wye timber arch bridge in terms of Distribution Factors (DF) and Load Rating Factors (RF) was developed. It was concluded that the UAV served as an effective tool to supplement current inspection practices and provide damage information that can be used to update FE models to rationally estimate bridge performance.

INTRODUCTION

An Unmanned Aerial Vehicle (UAV), referred to as a drone, is an aircraft without an aviator aboard. UAVs are equipped with high resolution cameras capable of capturing images, recording videos, and having infrared vision to examine bridges, among other uses. They are capable of carrying additional attachments, such as flashlights or thermal cameras, to perform a wider variety of damage identification. This emerging technology presents great potential for the inspection of bridges, as these structures often present inaccessible areas for inspectors. To date, limited research for UAV-enabled bridge inspection in junction to computational simulations have been made.

The American Society of Civil Engineers (ASCE) has provided a structural integrity assessment of the United States' infrastructure. Recently, the ASCE released the 2017 Infrastructure Report Card indicating that approximately 9.1% of the 614,387 bridges currently in-service are considered structurally deficient. Additionally, over 41% of the bridges are over 40 years old and approaching the end of their service life. Although the percentage of the structurally deficient bridges has slightly declined in past years, a visual inspection of such bridges should be conducted to better identify damage and determine appropriate retrofit methods. Due to increasing costs and limited accessibility of bridge inspection with current inspection technology, the use of remote-controlled UAVs equipped with high-resolution cameras may shed light on efficient and effective bridge inspection techniques. UAV technology provides a more efficient tool for enhancing current bridge inspection practices to identify visible damage and decay in inaccessible areas that could cause structural degradation.

RESEARCH OBJECTIVES

The main objective of this study was to identify better techniques to not only inspect, quantify, and determine the effect of damage on bridges to minimize the risk for inspectors, but also to determine their live-load performance using UAV-based computational simulation updating techniques

SCOPE OF RESEARCH

The scope of work is detailed as follows:

- Conduct a literature review on the state-of-the-art on UAV-enabled bridge inspection techniques along with a technical survey to gather relevant UAV-enabled inspection techniques.
- Provide a recommended UAV-enabled bridge inspection protocol for future generation bridge inspections.
- Complete a comparison of results for the UAV-enabled and conventional bridge inspection techniques.
- Provide a recommended UAV-image-based bridge damage quantification protocol to minimize risk for inspectors.
- Provide a damage state classification following the American Association of State Highway and Transportation Officials (AASHTO) Bridge Element Inspection Manual standards.
- Determine the effect of damage on the bridge load-carrying capacity using an integrated UAV and finite element analysis.

- Establish a finite element model updating technique to account for damage on the bridge
- Evaluate the variation of DFs and RFs due to the identified damage on the bridge.

OUTLINE OF THESIS

This thesis contains four research papers, detailed in four different chapters, investigating the use of UAVs to inspect, quantify, and conduct computational simulations to determine the live-load performance of bridges. Chapter One summarizes current research efforts from different investigators and includes the summary of a technical survey to all 50 state DOTs to identify inspection practices for different types of infrastructure. Additionally, an UAV selection based on the knowledge from the literature review to recommend a suitable UAV for bridge inspection was conducted. Chapter Two entails a recommended UAV-enabled bridge inspection protocol to efficiently and effectively identify damage on the structure. A field investigation of the timber girder bridge was conducted following the recommended protocol, and the corresponding results were compared to historical inspection reports provided by the SDDOT. Chapter Three presents a UAV-image-based bridge damage quantification protocol to provide more systematical and straightforward damage classification method. In detail, the use of image quality parameters such as entropy and sharpness and damage quantification techniques including pixel- and photogrammetry-based measurements provided an efficient method to quantify damage on the Keystone Wye timber arch bridge. Finally, Chapter Four presents a computational simulation to determine the bridge load-carrying capacity using an integrated UAV and FE analysis, following the AASHTO Manual for Bridge Evaluation.

CHAPTER 1: SYNTHESIS OF UNMANNED AERIAL VEHICLE APPLICATIONS FOR INFRASTRUCTURES

Luis Duque, S.M. ASCE, EIT

Graduate Research Assistant

Department of Civil and Environmental Engineering

South Dakota State University

Email: luis.duque@sdstate.edu

Phone: (605) 549-5179

1.1 ABSTRACT

This paper is intended to provide the state-of-the-art and of-the-practice on visual inspection, monitoring, and analysis of infrastructure utilizing Unmanned Aerial Vehicles (UAVs). Several researchers have inspected various civil infrastructures, including bridges, buildings, and other structures, by capturing close-up images or recording videos, while operating UAVs. Various image analysis tools, such as the algorithm Morphological Link for Crack (Morpholink-C), were able to conduct precise measurements of crack thickness and length. Corrosion has also been detected using texture and color algorithms to investigate UAV-based images. Other analysis methods include structurally integrated sensors, such as Digital Image Correlation (DIC) equipment, which have helped capture structural behaviors using UAVs. After the literature review was completed, a nationwide survey was distributed to Departments of Transportation (DOTs) to evaluate the current UAV-enabled inspection techniques that different DOTs have used or are planning to use for visual damage assessment for critical transportation infrastructures, especially bridges. Furthermore, a pertinent UAV selection was completed to indicate suitable UAVs for bridge inspection. Primary findings have shown that UAV-enabled infrastructure inspection techniques have been successfully developed to detect a broad variety of damage (including cracks and corruptions), and a few DOTs have used UAVs to inspect bridges as a more economical and versatile tool.

1.2 INTRODUCTION

An Unmanned Aerial Vehicle (UAV), referred to as a drone, is an aircraft without an aviator aboard. A drone has been commonly equipped with a camera capable of capturing high-resolution images and recording videos used to identify structural damage of infrastructures, among other uses (Eschmann et al. 2012; Nebiker et al. 2008). Drone technology has improved in recent years with an increasing number of researchers working to further develop its capabilities. Due to the efficiency and versatility of drone technology with evolving sensor technologies, this has become more appealing to inspectors of infrastructures.

There have been a number of studies on visual-based inspection of infrastructure for an efficient damage identification. (Chan et al. 2015; Chen et al. 2011; Ellenberg et al. 2014b; Hallermann and Morgenthal 2014; Ham et al. 2016a; b; Henriques and Roque 2015; Irizarry and Bastos 2016; Khaloo et al. 2017; Lovelace and Zink 2015; Metni and Hamel 2007; Otero 2015; Rathinam et al. 2008; Roca et al. 2013; Wells and Lovelace 2017; Zhang and Elaksher 2012). For instance, Lovelace and Zink (2015) conducted the demonstration project to identify damage on different bridges in the state of Minnesota (MN). Additionally, a study by Chan et al. (2015) identified an increase in bridge inspection and maintenance backlog due to current time consuming and expensive inspection procedures. The researchers concluded that the drone-based inspection reduced the cost to approximately 1/3 and time significantly as minimal large and heavy equipment needed to be transported and set up at the bridge site.

Further, analytical methods (including mathematical algorithms) have been used to study and quantify damage on different types of infrastructures (Aghaei et al. 2015; Bento et al. 2009; Chanda et al. 2014; Hutchinson and Chen 2010; Jahanshahi et al. 2009; Khaloo et al. 2017; Kim et al. 2017, 2015; McGuire et al. 2016). For example, Kim et al. (2015) developed an algorithm to determine crack thickness and length using images captured by a drone. The researchers determined that when using automated drones and visual imagery, the results were obtained in less time and with high precision. The use of the algorithm to quantify damage using data from drones could be a useful tool in alleviating the complications of direct field crack measurements, especially on inaccessible areas. In the other hand, Jahanshahi et al. (2009) determined the crack length and thickness information using two methods: (1) morphological techniques to gather initial crack location information and (2) edge detection to obtain length, thickness, and inclination information of the crack. Additionally, the incorporation of color and texture algorithms were implemented to identify areas affected by corrosion.

In addition to visual and analytical methods, some researchers have investigated the implementation of incorporated sensors to analyze the infrastructure (Lee and Shinozuka 2006; Mascareñas et al. 2008; Reagan et al. 2017). For instance, Reagan et al. (2017) studied a drone with 3D Digital Image Correlation (DIC) camera assembly to study long-term structural damage such as joint displacements. The use of the joint drone-3D DIC methodology allowed to measure damage on inaccessible areas more efficiently and in less time compared to conventional inspection techniques.

This paper is intended to summarize findings on current drone techniques to inspect and analyze different infrastructures, including bridges, buildings, and other structures. The emphasis of this literature review is to gather the Federal Aviation Administration (FAA) restriction issue to operate UAVs and the research efforts of different investigators on visual-based techniques, analytical algorithms, and incorporated sensors to inspect infrastructure. In addition to the literature review, this work will focus on a better understanding of the practices on drone technology in critical transportation infrastructure (i.e., bridge) throughout an online-based survey. The survey, distributed to state Departments of Transportation (DOTs), was executed to collect practical information regarding their use of drones for bridge inspection. With the information gathered from the survey and literature review, this paper evaluated drone techniques utilized in past DOTs' research projects and capabilities of a variety of drones that have been used for different engineering purposes, in an attempt to recommend suitable drones for bridge inspection.

1.3 FAA REGULATIONS FOR UAVS

Prior to 2016, the FAA regulations had several limitations for the commercial operation of drones (Lovelace and Zink 2015). One of the main limitations included the need for a Section 333 exemption Certificate of Authorization (COA), prior to any commercial drone operation which was only given to pilots representing an organization (FAA 2016). After the newly implemented small UAV part 107 rule on June 2016, the limitations on the operation of UAVs have been alleviated. Although the operation of the drones for business has become accessible to the public, the same core operational limitations still apply: 1) Class G airspace; 2) must keep the aircraft in sight (visual line-of-sight); 3) must fly under

400 feet; 4) must fly during the day; 5) must fly at or below 100 mph; 6) must yield right of way to manned aircraft; 7) must NOT fly over people; and 8) must NOT fly from a moving vehicle. A complete list of operational regulations provided by the FAA can be found in FAA (2016).

1.4 VISUAL INSPECTION OF INFRASTRUCTURES

A number of infrastructures across the United States need to be inspected to ensure appropriate serviceability and sufficient structural integrity. During recent years, many engineers, researchers, and DOTs have used drones to visually assess various infrastructures (Ellenberg et al. 2014b; Moranduzzo and Melgani 2014). Damage on different types of infrastructures has been studied using drones. This section presents significant findings through an extensive literature review of studies made on visual-based techniques to inspect different types of infrastructures, including bridges, buildings, and others.

1.4.1 BRIDGES

Current visual bridge inspection methods with a crane and rope access, are generally unsafe for inspectors due to the high elevation of bridges (Hachem et al. 1991; Koonce et al. 2011). In fact, most large-scale bridges span over water, making close visual inspection a difficult task. In the last decade, state DOTs and other federal organizations such as the United States Department of Agriculture – Forest Service (USDA-FS) began to investigate the capabilities of drones to visually assess bridges for potential damage as a more efficient alternative to current inspection practices (Barfuss et al. 2012; Dye Management Group

2014; Moller 2008; Seo et al. 2017a). Recently, Seo et al. (2017a) inspected a timber bridge near the city of Keystone in South Dakota. The study evaluated the effectiveness of drones as bridge inspection tools for bridges with limited accessibility. During the field inspection, a recommended bridge inspection protocol to aid future generation bridge inspection was developed and applied to the bridge. The findings from Seo et al. (2017a) in comparison to conventional inspection practices demonstrated the ability of the drone to effectively identify damage on the structure.

In 2008, Moller (2008), in a partnership with the California DOT (Caltrans), developed a twin-motor, single duct, electric-powered drone designed to carry video cameras up to 61 m in elevation to enable close inspection of bridges and other elevated structures. The objective of Caltrans was to construct an 'Aerobot' to easily access structural components at high altitudes, such as girders. They studied the use of cameras to closely examine bridge components as a new alternative at the time. The findings were acceptable, but some modifications needed to be made; the technology used back then followed more advanced instruments such as infrared, motion, and modeling sensors seen in recent research (Zhang and Elaksher 2012).

Other state DOTs, such as Florida and Minnesota DOTs, have investigated drone applications to inspect bridges in their states (Otero 2015). Specifically, Otero (2015) investigated different drones in terms of maneuverability, adaptability, software compatibility, payload, size, and user controls to perform bridge inspection. The efficiency of the selected drones, an Ardu Hexa-Copter and a Spider Quadcopter, was tested by

investigating five different types of bridges. The ability of the drone's camera to detect moderate crack thickness ranging from 0.51 mm to 2.03 mm. Additionally, a study of different types of bridges was conducted by (Lovelace and Zink 2015; Wells and Lovelace 2017). Lovelace and Zink (2015), working along with the Minnesota DOT (MnDOT), performed a demonstration project using an Aeyron Skyranger drone to inspect four bridges. During the inspection, damage such as corrosion and missing bolts based on imagery from the drone was observed. The selected bridges included a long single span prestressed concrete bridge, an open spandrel concrete arch bridge, a five-span steel underdeck truss bridge, and an arch truss bridge. At the end of the project, it was recommended that a suitable drone for inspection should have: (1) upward viewing camera and (2) ability to fly without a Global Positioning System (GPS) signal. The Aeyron Skyranger used in the project was deemed not to be the most suitable drone to study a bridge. During Phase II, Well and Lovelace (2017) utilized a more advanced drone, the SenseFly Albris, which costs approximately USD \$45,000 (in 2017 USD). The SenseFly Albris was considered and compared later to other drones in the drone selection section of this paper.

1.4.2 BUILDINGS

Buildings, especially high-rise buildings, have been inspected using drones. Researchers have studied the possibility of using drones to identify damage on the structure (Ellenberg et al. 2014b; Eschmann et al. 2012; Irizarry et al. 2012; Irizarry and Bastos 2016; Jizhou et al. 2004; Morgenthal and Hallermann 2014; Roca et al. 2013). For instance, Morgenthal and Hallermann (2014) using two Falcon drones, one for video and one for

photos, investigated a masonry church and detected critical cracks on a corner of the rooftop. During this study, the pilot was able to approach the structure within 5 m to visually observe the damage and provide high-resolution images. Further, Eschmann et al. (2012) also developed strategies to visualize cracks on buildings. The drone selected for this task was an octocopter, which has a higher payload due to the eight rotors that elevate the platform. Different flight configurations were analyzed by the researchers, but it was determined that the best alternative was to fly horizontally across the building façade and then move to the next story. This flight pattern was determined by considering the needed speed and lens-induced effects (i.e., image distortion due to fish eye lens) for the post-processing requirements of the images.

1.4.3 OTHER STRUCTURES

A variety of structures other than bridges and buildings such as Photovoltaic (PV) fields, dams, High Mast Luminaires (HML), dams, and industrial buildings have been inspected by drones. Such drones are equipped with different sensors and additional attachments, compared to the equipment a drone uses for bridge or building inspection (Aghaei et al. 2015). For example, Aghaei et al. (2015) performed a thermographic assessment using a PLP610 Nimbus drone platform with a FLIR A35 infrared imaging sensor to identify defective panels. Due to the thermal characteristics of the panels, the defective panels are seen as hot spots on the infrared image. This methodology produces a faster inspection of the panels compared to manual visual assessment.

The inspection of HML has been proposed by (Otero 2015). Using a DJI Phantom 2 and a built in-house medium-sized drone, Florida DOT (FDOT) and Florida Institute of Technology (FIT) studied four different HMLs for damage or missing elements. Post-processing software was used to zoom in on the images and remove distortion due to the camera's lens curvature. The conclusions were satisfactory, and the drone effectively identified damage on the HML posts with great detail.

In addition, the study of industrial infrastructures, including industrial plans, chimneys, and dams, was considered by Hallermann and Morgenthal (2013) and Henriques and Roque (2015). Henriques and Roque (2015) from the *Laboratorio Nacional de Engenharia Civil (LNEC)*, or National Civil Engineering Laboratory, in Lisboa, Portugal, investigated the use of drones for dam inspection. They used an Octocopter SKY II drone to better observe cracks on the dam's concrete surface. Previously, surveillance cameras and binoculars were used to observe the damage from the dam's base. Due to poor image quality, the methods were deemed to be ineffective. It was concluded that the drone, in addition to high quality cameras, is considered an efficient mechanism to visually observe the dam due to its capability to obtain detailed images of critical sections located in inaccessible areas.

The industrial applications researched by Hallermann and Morgenthal (2013) consisted of a corrosion level analysis for factors that commonly affect overall structural performance. They inspected a chimney 225 m high. The drone performed the inspection at different altitudes where known damage was located. They concluded that due to the

high-rise of the chimney, a drone would be safer and more efficient compared to a conventional inspection using expensive industrial climbers.

1.5 VISUAL INSPECTION-BASED ANALYTICAL METHODS

The use of directional sensors and computer software allows structural engineers to gather information beyond visual damage assessment alone. Computational algorithms have been studied to quantify damage such as crack thickness and length (Chanda et al. 2014; Ellenberg et al. 2014a). Additionally, the use of laser scanners for 3D virtual modeling has been implemented to study different infrastructure, making drones an adaptable tool for inspection (Bento et al. 2009; Evaraerts 2008; Hallmark et al. 2001; Koch et al. 2014; Zhang and Elaksher 2012). This section presents findings on analytical methods applied to the inspection of different types of infrastructures.

1.5.1 BRIDGES

The development of autonomously flying drones coupled with damage detection algorithms has been of interest for different researchers (Metni and Hamel 2007; Michaelsen and Meidow 2014; Seo et al. 2017a,b,c; Yin 2014). In detail, Metni and Hamel (2007) developed a control algorithm with orientation limits to guide an X4-Flyer drone. The concept is based on computer vision to navigate an unknown 3D environment and saturation functions to maintain the object in the camera's field of view. During the feasibility experiment, the drone was able to obtain high-quality data to be analyzed by inspectors. Additionally, with some image post-processing treatment, cracks with a small thickness of 0.1 mm were observed. A different approach was used by Michaelsen and

Meidow (2014). A structural pattern recognition system with an autonomously flying drone was used. The crack measurements were achieved with statistical analysis and sufficient data to cover a representative inspection area.

Moreover, the use of photogrammetric processing of images have aided researchers in creating 3D virtual models of bridges for their inspection (Khaloo et al. 2017). Khaloo et al. (2017), in partnership with the USDA – FS region 10, University of Alaska Fairbanks, and George Mason University, inspected an existing pedestrian timber truss bridge using a drone in Alaska. In detail, the researchers used a hexacopter drone named “Ptarmigan” built based on a DJI S800 airframe with Gyrostabilized Sony Nex7 and GoPro cameras. The drone was able to identify damage on the bridge components (i.e., gaps between the end of kerf plate and sawn kerf in the brace). The 3D virtual model of the bridge in a dense 3D point cloud was created using the software PhotoScan which was informed by the imagery data from the drone.

The ability to detect and measure concrete crack thickness and length using drones has been widely researched (Chanda et al. 2014; Chen et al. 2011; Duque et al. 2017a,b; Ellenberg et al. 2014a; Eschmann et al. 2013; Jahanshahi et al. 2009; Kim et al. 2015). Duque et al. (2017a) developed a drone-image-based bridge damage quantification protocol. The protocol included image quality assessment techniques using image quality parameters such as sharpness and entropy in addition to damage quantification methods including pixel-based and photogrammetric-based measurements. Further, Duque et al. (2017a) applied the proposed protocol to a timber arch bridge and were able to measure

crack length and thickness and rust staining on the structure. Moreover, Kim et al. (2015) used the specially designed Morphological Link for Crack (Morpholink-C) algorithm and were able to measure the crack thickness of 0.1 mm and greater. Additionally, Ellenberg et al. (2014) from the University of Drexel, Philadelphia, studied the effectiveness of drones to detect cracks in terms of the distance to the structure. The conclusions from the study demonstrated that with a high-resolution camera it is possible to detect a crack thickness of 0.75 mm at a distance of 3 m.

A critical challenge with drone-enabled damage identification and measurement is the image sharpness or clarity. Researchers have studied the effects of environmental conditions (e.g., wind) (Hallermann and Morgenthal 2014; Morgenthal and Hallermann 2014). Morgenthal and Hallermann (2014) used a computer-vision (CV) based crack detection algorithm to compare the accuracy of crack measurements from blurry and clear images. To solve this problem, a probability of detection (POD) was generated from different parameters (i.e. drone properties and wind) and then the parameters were reorganized to obtain the desired image quality.

Other research efforts to investigate bridge inspection results during windy conditions have been made by Guerrero and Bestaoui (2013). Guerrero et al. (2013) used three different approaches: (1) Zermelo-Traveling Salesman Problem (TSP), (2) Meshing techniques with Zermelo-TSP, and (3) Zermelo-Vehicle Routing Problem (VRP). Zermelo-TSP computed the most effective route the drone can take to inspect the structure. The Meshing techniques combined with Zermelo-TSP method created interest points along

the structure using a meshing algorithm, and then the Zermelo-TSP determined the most time efficient order to inspect all the points. Finally, the Zermelo-VRP works similarly to the Zermelo-TSP method, but it considers the energy limitations of the drone.

1.5.2 BUILDINGS

Buildings have been reconstructed in 3D virtual models using computer programs to identify damage (Daftry et al. 2015; Ellenberg et al. 2014b; Jizhou et al. 2004; Püschel et al. 2008; Roca et al. 2013; Zhang et al. 2011; Zischinsky et al. 2000). Using drones and terrestrial images, Püschel et al. (2008) reconstructed Castle Landenberg using photogrammetric processing of images. To create the 3D virtual model, the use of photomodeler software helped the researchers to recreate the structure in detail. Other equipment, such as high-resolution directional sensors or laser sensors, have also been used. The accuracy of 3D virtual models relies on the quality of the gathered images. The greater the image pixel count, the more detail can be observed to inspect buildings. In some cases, a high-resolution image is not required. For example, when only general façade dimensions are desired, a laser sensor could be more suitable in terms of cost. Roca et al. (2013) from the University of Vigo, Spain, performed an analysis using a low-cost drone with a Microsoft Kinect sensor to compare it to a laser scanner in terms of image quality. They concluded that the model obtained with the Microsoft Kinect was of good quality and the results were comparable to those of a laser scanner.

The generation of 3D virtual models of buildings can also provide the engineer with supplementary information of critical roof section, severe weather building exposure, and

general location of structural components (Eschmann et al. 2013). In fact, Eschmann et al. (2013) from the Fraunhofer institute for non-destructive testing, have investigated the use of drones for building inspection and monitoring. Using an octocopter with a high-resolution camera, the researchers inspected a building for damage. The process was based on taking digital images at close intervals to recreate the structure with the help of a photogrammetry computer program. Due to the size of the building a visual inspection from a 2D virtual model was ideal, the virtual image was separated into several small sections for ease of damage observation.

Additionally, crack detection can be complicated in buildings, especially in light-colored ones, but with the help of an image processing software, Eschmann et al. (2013) enhanced the color of the crack using two methods: (1) adding additional color value and (2) edge detection. The additional color value analyzes the image and determines if the individual pixels need either more black or more white to produce black crack areas. On the other hand, the edge detection methodology searches for a sudden change in color, commonly seen in cracks.

1.5.3 OTHER STRUCTURES

Analytical methods have been applied to other structures such as pipelines and highways (Rathinam et al. 2008). The study performed by Rathinam et al. (2008) was based on a directional logarithm inputted into the single wing Sig Rascal drone. To demonstrate the feasibility of this inspection, they performed a study of a 700-meter-long canal and demonstrated that the drone can autonomously follow the canal path. Some of the benefits

include the rapid inspection and monitoring of important pipelines, such as the Alaska oil pipeline system, where a shutdown could cost about 1 million dollars per hour (in 2008 USD). Additional benefits of the study include a reduced cost to inspect structures with large distances and the ability to perform the monitoring process faster than a human visual inspection.

Further studies (Remondino et al. 2012; Siebert and Teizer 2014; Turner et al. 2012) also suggest the use of drones for inspection of construction zones as conducted by Rathinam et al. (2008). For instance, Siebert and Teizer (2014) investigated the use of drones to perform surveying related work. The drone, a customized Mikrokopter Quad XL, was able to produce a 3D model of construction zones and determine places along the road where fills and cuts were needed to level the surface. They calculated the volume of fills and areas to be covered using Agisoft professional, PhotoScan software. A similar approach was followed and performed by Remondino et al. (2012) by using a micro drone called MD4-200 for mapping extensive zones. Turner et al. (2012) also used a similar approach by generating a point cloud using an automated drone, in order to investigate extensive areas.

Additional structures such as dams have been reconstructed in a 3D virtual environment. The 3D virtual model was generated from images using the software VisualSFM (Structure From Motion) to inspect the dam surface (Henriques and Roque 2015). In depth, Henriques and Roque (2015) used the software *eCognition* from Trimble, to identify relevant characteristics, including deposits of calcium carbonate due to water

leakages, reddish calcium carbonate deposits, and wet concrete. The researchers concluded that the drone, accompanied with high-quality cameras, was an effective tool to inspect dams because they could obtain close-up images of critical sections or inaccessible areas of the dams.

Finally, other structures investigated using analytical methods include industrial plants and PV fields (Aghaei et al. 2015; Bento et al. 2009; Moranduzzo and Melgani 2014; Tyutyundzhiev et al. 2015). Both Bento et al. (2009) and Moranduzzo and Melgani (2014) investigated corrosion detection. Moranduzzo and Melgani (2014) developed a method which consisted of taking two pictures at two different times and then using a three-step process to (1) align the images, (2) identify damages using a threshold technique, and (3) compare and determine the corrosion size. Aghaei et al. (2015) used binary images to locate the defective solar panels. The images were obtained using a grayscale and a Gaussian filter to detect the defective panels. A more in-depth study of PV fields inspection was conducted by Tyutyundzhiev et al. (2015). Methods such as image and aerial photo-mapping techniques were considered. Additionally, different low-cost camera models (e.g., Canon IXUS 135 IS) were used to gather aerial images and video. It was concluded that the drone was capable of helping reproducing 3D virtual models and that the integrated technology was able to conduct PV inspection.

1.6 INFRASTRUCTURE INSPECTION WITH INTEGRATED SENSORS

Few researchers have investigated the use of drones to analyze different aspects of infrastructure such as deflection of bridges (Lee and Shinozuka 2006; Mascareñas et al.

2008). This technology can aid structural engineers in performing different non-destructive tests such as joint deflection. Although Lee and Shinozuka (2006) did not use a drone for their analysis, the use of a visual approach to determine deflections could potentially be incorporated into drones in the future. The method they conducted utilized image-processing techniques to obtain deflection in real time. Several innovative features, including a high-resolution dynamic measurement, remote sensing, cost-effectiveness, real-time measurement and visualization, ease of installation and operation, and no electromagnetic interferences are implemented to measure the bridge displacement. The deflection is calculated using a sensor located at the desired plane (i.e. girder mid-span) and a video camera shooting at the sensor to gather the measurements. With the use of a target recognition algorithm, the numbers of pixels displaced by the bridge due to external forces can be determined. The researchers concluded that the method can be implemented with a high level of accuracy and will be cost-effective and easy to utilize.

Additionally, Mascareñas et al. (2008) also inspected a bridge using integrated sensors. They used an X-Cell Spectra G drone to transmit microwave energy to a wireless sensor node located at the structure. After the node is charged the drone can receive displacement measurements to be analyzed. During this experiment, the researchers' main goal was to charge the node, and a further study will be performed to obtain actual measurements from piezoelectric sensors located at the bridge. The innovative approach used can aid in structural health monitoring (SHM) applications to assess structures after a natural disaster occurs.

Further, the use of Digital Image Correlation (DIC) cameras integrated with drone technology has aided researchers in monitoring long-term deflections (Reagan et al. 2017). Reagan et al. (2017) have studied the enhancement of the drone's capabilities by introducing an innovative drone - 3D DIC platform for long-term SHM. It was proven that the platform was able to accurately measure the evolution of displacements at a deck joint due to aging. They concluded that the new drone-3D DIC platform can produce more accurate results and better performance when compared to visual inspection techniques.

1.7 UAV SELECTION

After completing the literature review of drone techniques to inspect, monitor and analyze infrastructures, a drone for infrastructure inspection was recommended. While performing the literature review, several researchers have investigated different drones to compare their capabilities in terms of data acquisition. The goal of this paper was to provide a comprehensive summary of drone inspection techniques and pertinent image data investigation tools and relate them to the most suitable drone for infrastructure inspection. Based on the knowledge from the literature review, the following considerations needed to be verified when reasonably selecting the most suitable inspection drone:

- (1) Flying time over 20 min: A relatively long flying time is beneficial for a more efficient structure inspection by limiting the need for additional batteries and allowing for longer inspection times;
- (2) Additional camera on top of drone: A second camera facing straight up to inspect underneath the bridge will allow for its comprehensive inspection;

- (3) Camera resolution with low illumination: Low illumination reduces the image quality as small damage would be challenging to detect. Additional flashlights can be attached to a drone to enhance illumination;
- (4) Video resolution: High-resolution video is required to visually observe details of damage;
- (5) Payload capacity: It would be beneficial for potential attachments that might be required to be carried by a drone;
- (6) Drone lights: Light-Emitting Diode (LED) lights attached to a drone will provide some extra illumination required for efficient damage observation underneath a bridge; and
- (7) Remote range: Some structures might not be relatively close from the pilot location. Long range modules for remote control will allow for inspection of a structure at long distances.

With the required seven considerations, thirteen drones (see **Fig. 1-1**) with a variety of prices, physical sizes, and manufacturers were identified and listed in **Table 1-1**. The drones and each of their capabilities were compared in terms of the aforementioned considerations and rated from 1 (not suitable) to 5 (extremely suitable). From the table, the most appropriate drone is the Sensefly Albris rated “5” (**Fig. 1-11**). This is because 1) the ability to rotate the camera vertically 180 degrees with an integrated flashlight, infrared camera, and wide-angle camera; 2) the different flight modes (e.g., GPS-Mapping and manual) allow the drone to program missions or fly under bridges where GPS signal is unavailable, as many researchers have expressed issues with the low signal of the drones;

and 3) its effectiveness for bridge inspection was previously demonstrated through the MnDOT project. However, the elevated cost of the drone, close to \$45,000 (in 2015 USD), may not be suitable for many inspectors.

Alternatively, options such as the DJI Matrice 100 (**Fig. 1-1c**), DJI S900 (**Fig. 1-1g**), DJI Phantom 3 Pro (**Fig. 1-1d**), and DJI Phantom 4 (**Fig. 1-1e**) were deemed to be suitable at a more affordable price compared to the Sensefly Albris. The DJI Phantom 4 was selected over the others due to its performance and versatility meeting the aforementioned specifications at a reasonable cost. Additional equipment, which is Obstacle Avoidance (OA) technology, of the drone will be beneficial while approaching a structure to prevent damage to both structure and drone components. Another key consideration is the ability to fly without GPS signal. This enables the drone to inspect underneath bridges without the problem of losing satellite connection, as stated before. Some attachments including a flashlight and second camera could be added to the drone to overcome such inspection challenges.



Fig. 1-1. Investigated drones: (a) DJI Inspire 1; (b) Voyager 3; (c) DJI Matrice 100; (d) DJI Phantom 3 Pro; (e) DJI Phantom 4; (f) Yuneec Typhoon H; (g) DJI S900 airframe; (h) Yuneec Typhoon 4K; (i) Blade Chroma; (j) Autel Robotics X-Star Premium; (k) SenseFly eBee; (l) SenseFly Albris; and (m) Topcon Sirius Pro.

Table 1-1. Comparison of Identified Drone Specifications.

Drone	Price (2017 USD)	Approximate Fly Time	Upward camera view	Camera resolution with low illumination	Video Resolution	Payload capacity	Other source of light	Remote range	Satisfactory*
(a) <u>DJI Inspire 1 (DJI 2014a)</u>	\$2,000	18 min	94-degree vertical range	Optional flashlight attachment will improve quality	4k / 1080p	1700 grams	Drone have red LED lights	2000 meters	3
(b) <u>Voyager 3 (Walkera 2015)</u>	\$2,000	25 min	Facing upward at an angle	Optional flashlight attachment will improve quality	1080p	320 grams	Drone have red and blue LED lights	1000 meters	2
(c) <u>DJI Matrice 100 (DJI 2013a)</u>	\$2,800 to \$3,300 +\$750 for camera	40 min	Need to buy camera	Optional flashlight attachment will improve quality	1080p	1000 grams	Drone have green LED lights	5000 meters	4
(d) <u>DJI Phantom 3 Pro (DJI 2013b)</u>	\$1,200 + \$499 for GoPro Camera	23 min	94-degree vertical range**	Optional flashlight attachment will improve quality	4k / 1080p	462 grams	Drone have red and yellow LED lights	5000 meters	4
(e) <u>DJI Phantom 4 (DJI 2016)</u>	\$1,800 + \$499 for GoPro Camera	28 min	94-degree vertical range**	Optional flashlight attachment will improve quality	4k / 1080p	462 grams	Drone have red and yellow LED lights	5000 meters	4
(f) <u>Yuneec Typhoon H (Yuneec 2016)</u>	\$1,600	25 min	Facing upward at an angle	Optional flashlight attachment will improve quality	4k / 1080p	600 grams	Drone have green, red and blue LED lights	1000 meters	3

* Rated 1-5 with 5 being the highest score

**Attachments:

GoPro camera to look straight up USD \$499, total weight approximately 200 grams including mount.

GoPro camera mount to attach to drone (Included with camera or additional mount can be bought for USD \$29.99

Table 1-1. Comparison of Identified Drone Specifications (continued).

Drone	Price (2017 USD)	Approximate Fly Time	Upward camera view	Camera resolution with low illumination	Video Resolution	Payload capacity	Other source of light	Remote range	Satisfactory*
(g) DJI S900 airframe (DJI 2014b)	\$3,000 –\$750 to \$1300 for camera	20 min	Optional attachment	Optional flashlight attachment will improve quality	4k / 1080p	4300 grams	No LED lights	1000 meters	4
(h) Yuneec Typhoon 4K (Yuneec 2015)	\$1,100	25 min	115-degree vertical range	Optional flashlight attachment will improve quality	1080p	600 grams	Drone have red and yellow LED lights	800 meters	3
(i) Blade Chroma (Horizon Hobby 2015)	\$700	30 min	Facing upward at an angle	Optional flashlight attachment will improve quality	4k / 1080p	200 grams	Drone have green, red and blue LED lights	400 meters	2
(j) Autel Robotics X-Star Premium (Autel Robotics 2016)	\$900	25 min	108-degree vertical range	Optional flashlight attachment will improve quality	4k / 1080p	180 grams	No LED lights	2000 meters	2
(k) SenseFly eBee (Sensefly 2016a)	\$25,000	50 min	No	Optional flashlight attachment will improve quality	1080p	NA	No LED lights	3000 meters	1
(l) SenseFly Albris (Sensefly 2016b)	\$45,000	22 mi	Yes	Flashlight included	4K/ 1080p	NA	Drone have green, red and blue LED lights	2000 meters	5
(m) Topcon Sirius Pro (Top Con 2016)	\$53,000	55 min	No	Optional flashlight attachment will improve quality	1080p	NA	No LED lights	3000 meters	1

* Rated 1-5 with 5 being the highest score

1.8 SURVEY

An online survey sent to all 50 DOTs was also conducted to gather additional hands-on information about the use of drones for infrastructure inspection, especially bridge inspection. Nineteen responses to the survey through an online version were received from different DOTs: Idaho, Iowa, Illinois, Missouri, Wyoming, Florida, Delaware, New York, Wisconsin (2), Alaska, Arkansas, Nevada, South Dakota (2), Kentucky, Arizona, and Colorado DOTs along with Alaska USDA – FS. It was specified that seven states, including Florida, Iowa, Idaho, Kentucky, New York, Wisconsin, and Alaska, have used or planned to use drones for bridge inspection. This shows the increasing interest of states to use the drone technology. The summary of the responses for the survey are presented below:

Question 1 of the survey enquired if the state has used or is planning to use any drone for bridge inspection. Also, if they have used or are planning to use drones, it enquired which drone was utilized including attachments. Only one state (Alaska USDA FS), from those who answered Question 1, had used a drone for bridge inspection. The remainder six state DOTs were planning to perform bridge inspection using drones in the near future. A summary of the responses is presented in **Table 1-2**.

Table 1-2. Summary of Responses for Question 1 of Survey.

State	Questions		
	Have your state used or is your state planning to use any drone for bridge inspection or planned?	Specify your drone type	Specify attachments
Alaska DOT	No	-	-
Alaska USDA - FS	Yes, have used	Purpose-built hexacopter (based on DJI S800 airframe)	Gyro-stabilized SONY Nex7 and GoPro unit
Arizona DOT	No	-	-
Arkansas DOT	No	-	-
Colorado DOT	No	-	-
Delaware DOT	No	-	-
Florida DOT	Yes, planning to use	Not specified	-
Idaho DOT	Yes, planning to use	Coaxial Octocopter	-
Illinois DOT	No	-	-
Iowa DOT	Yes, planning to use	Aibotix X6	-
Kentucky DOT	Yes, planning to use	Rotor UAV	GoPro camera
Missouri DOT	No	-	-
Nevada DOT	No	-	-
New York DOT	Yes, planning to use	Not specified	-
South Dakota DOT	No	-	-
Wisconsin DOT	Yes, planning to use	Not specified	-
Wyoming DOT	No	-	-

Note: The presence of “-” indicates Not Applicable.

For Question 2, material regarding drone techniques for bridge inspection was requested from the DOTs. The question asked, “What techniques or data were or will be used to inspect bridges?” All the DOTs that participated in the survey by responding to the first two questions mentioned that images and video are the most relevant information used to detect damage. **Fig. 1-2** shows the relevant data. Eight state DOTs stated that imagery and video data is considered the most effective to identify damage on bridges. Among the eight DOTs, five of them, including Wisconsin (2), Colorado (1), Idaho (1), and Iowa (1) DOTs, specified that data obtained from thermal cameras is the second most important

source for damage detection. Lastly, the response from Colorado DOT stated that displacement sensors will provide critical data necessary for the damage identification. Alaska USDA–FS responded that 3D site reconstruction photogrammetric software (e.g., Structure from Motion (SfM)) was important for detailed damage investigation.

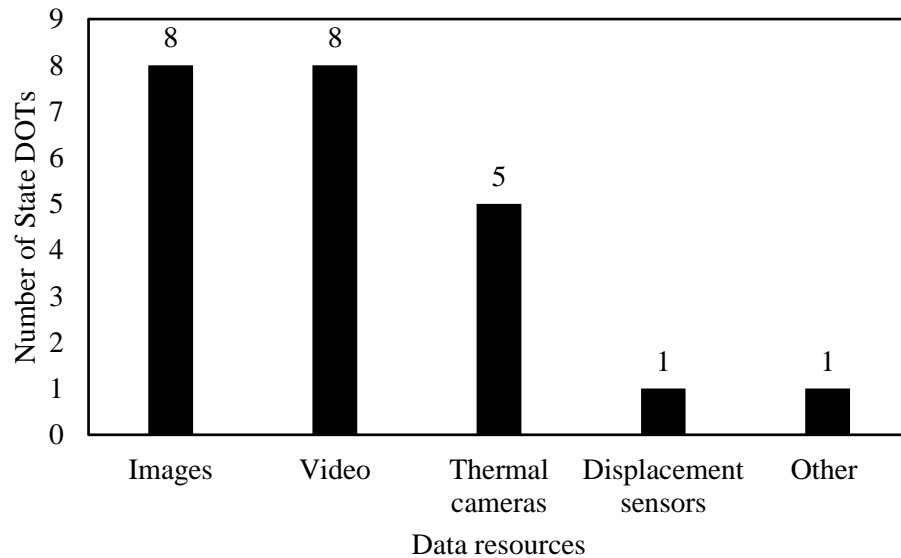


Fig. 1-2. Responses to question 2 of survey.

Question 3 enquired regarding the most necessary data and challenges that drone technology may have for bridge inspection. Numerous challenges were specified regarding the technology by several state DOTs due to relatively new appearance on the market, especially for bridge inspection. The details for answers to Question 3 are listed in **Table 1-3**.

Table 1-3. Summary of Responses For Question 3 of Survey.

State	Questions	
	Necessary Data	Inspection Challenges
Alaska DOT	-	-
Alaska USDA - FS	High-definition imagery along with a replicable inspection pattern/process	Weather/wind, payload limitations, battery life, safe stand-off distances and collision avoidance, lighting conditions for under-bridge viewing
Arizona DOT	-	-
Arkansas DOT	-	-
Colorado DOT	-	-
Delaware DOT	-	-
Florida DOT	Images are the most important; Data from video and thermal cameras may be important; Displacement sensors are probably only useful in rare instances	-
Idaho DOT	-	Issues related to the platform, autonomous control of UAVs, post-processing of acquired data
Illinois DOT	-	-
Iowa DOT	High quality images are necessary	Regulations have been the biggest challenge
Kentucky DOT	Video data would be most necessary	A challenge would be losing signal underneath a bridge
Missouri DOT	-	-
Nevada DOT	-	-
New York DOT	-	-
South Dakota DOT	-	-
Wisconsin DOT	Data will be used to quantify condition and change in condition	FAA rules have been the biggest obstacle
Wyoming DOT	-	-

Note: The presence of “-” indicates Not Applicable.

Question 4 requested that the DOTs detailed their main concerns when inspecting bridges using drones. Safety and regulations concerns were specified by several state DOTs

due to the relatively new appearance of the drone technology, especially for bridge inspection. Some states such as Delaware, Florida, Idaho, Illinois, Iowa, South Dakota, Wisconsin, and Wyoming have express regulations have been the biggest challenge. Other states including Alaska expressed that low-light conditions, upward viewing cameras, and GPS signal could be a challenge specially during underside of deck inspection. Finally, a concern regarding traffic safety was expressed by Arkansas, Colorado, Illinois, Kentucky, and South Dakota.

Question 5 requested information from DOTs having either past or ongoing research projects on UAV inspection techniques. Several state DOTs, including Arkansas, Arizona, Illinois, Missouri, Wyoming, Delaware, and New York DOTs, did not have any ongoing research. The remaining state DOTs provided specifics of their ongoing research. For example, the Alaska USDA-FS specified a demonstration project conducted in 2015 to evaluate the capabilities and limitations of the aerial platform. This study was conducted by (Khaloo et al. 2017) and has been presented in this literature review. Other studies such as the proof of concept study by the Florida DOT lead by (Otero 2015) has also been summarized in this paper. Other states with on-going research include Colorado, Idaho, Iowa, Kentucky, Nevada, and Wisconsin.

Finally, Question 6 requested information regarding future research plans relevant to drone techniques to inspect bridges. Once more, the state DOTs from Question 5, with the addition of South Dakota and Alaska did not mentioned any future research plans on drone techniques. The remaining states including Wisconsin, Kentucky, Iowa, Florida, and

Alaska USDA- FS expressed their intention to evaluate the effectiveness of drones through field studies to determine their applicability for bridge inspection.

The survey results were somewhat as expected with few state DOTs having ongoing research using drones and therefore being very skeptical about this new technology. It was confirmed that the most common data necessary for bridge inspection are images and videos. Nevertheless, several state DOTs mentioned concerns regarding safety, traffic control, privacy, frequent changes in FAA regulations, and others. Hence, these and other concerns should be considered when inspecting infrastructure in the future.

1.9 SUMMARY AND CONCLUSION

Different methods were presented in this state-of-the-art and of-the-practice on drone techniques to inspect, monitor, and analyze infrastructure. The procedures were analyzed under three different categories: (1) visual-based techniques, (2) analytical techniques, and (3) incorporated structural sensors to examine infrastructure. Based on the findings from this literature review, drone selection, and survey the following conclusion, limitations and recommendations can be made to improve the use of drones as infrastructure inspection tools:

1. Visual inspection of infrastructure has been used during the past decade by different departments of transportation and engineers. Bridges, buildings, and other structures such as concrete dams and industrial plants have been studied. The results from recent findings are satisfactory and have lead engineers to visually inspect structures more efficiently and in less time compared to conventional inspection

techniques. Additionally, images obtained from such studies have been utilized to detect cracks, corrosion, and other damages. Also, the results obtained from the drone-enabled inspections have similar or better image quality compared to traditional inspection methodologies. One of the benefits identified by some researchers was the ability to access bridge areas with restricted accessibility for inspectors allowing a more comprehensive infrastructure inspection.

2. Integrated analytical methods have aided visual inspection to detect damage, program flights, and create 3D virtual models. Some of the most relevant features include autonomous flights, crack thickness and length measurement, and corrosion growth analysis. The literature review showed the versatility of drones to detect damage on different structures and materials. Attachments such as multi-sensors, infrared cameras, and laser sensors helped generate different types of images for inspection purposes. Some computer software has been developed to measure crack thickness and length, corrosion, and to create 3D virtual models using photogrammetric processing of images.
3. Integrated structural sensors have not been studied widely, this technique is proposed to be researched further due to the benefits in structural health monitoring and structural analysis. Current methods are limited in equipment and implementation as presented in this review. An innovative method to measure deflection using digital image correlation cameras integrated with drones to measure long term deflections was presented as a promising technique to inspect infrastructure with limited accessibility. This method of integrated digital image correlation cameras and drone technology could potentially be further developed to

study crack propagation and the monitoring of other types of damage such as joint displacement.

4. The results from the survey to state departments of transportation demonstrated the interest of these organizations to conduct research projects on drone technology. Currently, only one state among those who participated in the survey has conducted bridge inspection using a drone. It can be noted that Florida, Iowa, Idaho, Kentucky, New York, and Wisconsin are planning to use drones in a near future showing the increasing interest for this new technology.

1.10 REFERENCES

- Aghaei, M., Grimaccia, F., Gonano, C. A., and Leva, S. (2015). “Innovative Automated Control System for PV Fields Inspection and Remote Control.” *IEEE Transactions on Industrial Electronics*, 62(11), 7287–7296. doi: 10.1109/TIE.2015.2475235
- Autel Robotics. (2016). “Autel Robotics X-Star Premium.”
 <<https://www.autelrobotics.com/x-star-premium-tech-specs/>> (Jul. 25, 2016).
- Barfuss, S. L., Jensen, A., and Clemens, S. (2012). *Evaluation and Development of Unmanned Aircraft (UAV) for UDOT Needs*. Utah Department of Transportation, Salt Lake City, UT.
- Bento, M. P., S de Medeiros, F. N., de Paula Jr, I. C., and B Ramalho, G. L. (2009). “Image processing techniques applied for corrosion damage analysis.” *Proceedings of the XXII Brazilian Symposium on Computer Graphics and Image Processing*, DBLP, Rio de Janeiro, Brazil.
- Chan, B., Guan, H., Jo, J., and Blumenstein, M. (2015). “Towards UAV-Based Bridge Inspection Systems: A Review and an Application Perspective.” *Structural Monitoring and Maintenance*, 2(3), 283–300. doi: 10.12989/smm.2015.2.3.283
- Chanda, S., Bu, G., Guan, H., Jo, J., Pal, U., Loo, Y.-C., and Blumenstein, M. (2014). “Automatic bridge crack detection – a texture analysis-based approach.” *IAPR Workshop on Artificial Neural Networks in Pattern Recognition*, Springer International Publishing, Ulm, Germany, 193–203. doi: 10.1007/978-3-319-11656-3_18

- Chen, S., Rice, C., Boyle, C., and Hauser, E. (2011). "Small-Format Aerial Photography for Highway-Bridge Monitoring." *Journal of Performance of Constructed Facilities*, 25(4), 105–112. doi: 10.1061/(ASCE)CF.1943-5509.0000145.
- Daftry, S., Hoppe, C., and Bischof, H. (2015). "Building with drones: accurate 3D facade reconstruction using MAVs." *Proceedings - IEEE International Conference on Robotics and Automation*, IEEE, Seattle, WA, 3487–3494. doi: 10.1109/ICRA.2015.7139681.
- DJI. (2013a). "DJI Matrice 100." <<http://www.dji.com/product/matrice100/info#specs>> (Jul. 25, 2016).
- DJI. (2013b). "DJI Phantom 3." <<http://www.dji.com/product/phantom-3-pro/info#specs>> (Jul. 25, 2016).
- DJI. (2014a). "DJI Inspire 1." <<http://www.dji.com/product/inspire-1/info#specs>> (Jul. 25, 2016).
- DJI. (2014b). "DJI S900." <<http://www.dji.com/product/spreading-wings-s900/info#specs>> (Jul. 25, 2016).
- DJI. (2016). "DJI Phantom 4." <<http://www.dji.com/product/phantom-4/info#specs>> (Jul. 25, 2016).
- Duque, L., Seo, J., Wacker, J. (2017a) "Bridge Damage Quantification Methodology using UAV platform" *ASCE Journal of Bridge Engineering*, In review.
- Duque, L., Seo, J., Wacker, J. (2017b) "Timber Bridge Inspection using UAV" 2018

ASCE Structures Congress, In press.

Dye Management Group, I. (2014). *Monitoring Highway Assets with Remote Technology*

MDOT Research Project Number : OR10-030 MDOT Report Number : RC- 1607.

The Michigan Department of Transportation (MDOT), Lansing, MI.

Ellenberg, A., Branco, L., Krick, A., Bartoli, I., and Kontsos, A. (2014a). “Use of

Unmanned Aerial Vehicle for Quantitative Infrastructure Evaluation.” *Journal of*

Infrastructure Systems, 21(3), 4014054. doi: 10.1061/(ASCE)IS.1943-

555X.0000246.

Ellenberg, A., Kontsos, A., Bartoli, I., and Pradhan, A. (2014b). “Masonry crack

detection application of an unmanned aerial vehicle.” In *2014 Conference in*

Computing on Civil and Building Engineering, ASCE, Reston, VA, 1788–1795. doi:

10.1061/9780784413616.222.

Eschmann, C., Kuo, C.-M., and Boller, C. (2012). “Unmanned aircraft systems for

remote building inspection and monitoring.” *Proceedings of the 6th European*

Workshop on Structural Health Monitoring. July 3-6, 2012, Dresden, Germany, 2,

1–8.

Eschmann, C., Kuo, C.-M., Kuo, C.-H., and Boller, C. (2013). “High-Resolution

Multisensor Infrastructure Inspection With Unmanned Aircraft Systems.” *ISPRS -*

International Archives of the Photogrammetry, Remote Sensing and Spatial

Information Sciences, XL-1/W2(11), 125–129. doi: 10.5194/isprsarchives-XL-1-

W2-125-2013.

- Evaraerts, J. (2008). "The Use of Unmanned Aerial Vehicles (UAVs) for Remote Sensing and Mapping." *The International Archives of the Photogrammetry, Remote Sensing and Spatial Information Sciences*, XXXVII (Part B1), 1187–1192.
- Guerrero, J. A., and Bestaoui, Y. (2013). "UAV Path Planning for Structure Inspection in Windy Environments." *Journal of Intelligent and Robotic Systems: Theory and Applications*, 69(1–4), 297–311. doi: 10.1007/s10846-012-9778-2.
- Hachem, Y., Zografos, K., and Soltani, M. (1991). "Bridge Inspection Strategies." *ASCE: Journal of performance of constructed facilities*, 5(1), 37–56.
- Hallermann, N., and Morgenthal, G. (2013). "Unmanned aerial vehicles (UAV) for the assessment of existing structures." *International Association for Bridge and Structural Engineering*, IABSE, Zurich, Switzerland, 1–8. doi: 10.2749/222137813808627172.
- Hallermann, N., and Morgenthal, G. (2014). "Visual inspection strategies for large bridges using unmanned aerial vehicles (UAV)." *7th International Conference on Bridge Maintenance, Safety and Management*, Transportation Research Board (TRB), Washington, DC. doi: 10.1201/b17063-96.
- Hallmark, S. L., Mantravadi, K., Veneziano, D., and Souleyrette, R. R. (2001). *Evaluating Remotely Sensed Images for use in Inventorying Roadway Infrastructure Features*. National Consortium on Remote Sensing in Transportation for Infrastructure, Santa Brabara, CA.
- Ham, Y., Han, K. K., Lin, J. J., and Golparvar-Fard, M. (2011). "Visual Monitoring of

- Civil Infrastructure Systems via Camera-Equipped Unmanned Aerial Vehicles (UAVs): A Review of Related Works.” *Visualization in Engineering*, 4(1), 1–8. doi: 10.1186/s40327-015-0029-z.
- Henriques, M., and Roque, D. (2015). “Unmanned aerial vehicles (UAV) as a support to visual inspections of concrete dams.” *Second International Dam World Conference*, LNEC, Lisbon, Portugal, 1–12.
- Horizon Hobby. (2015). “Blade Chroma.”
<<http://www.horizonhobby.com/product/multirotor/multirotor-aircraft/ready-to-fly-15086--1/chroma-w-st-10-and-c-go3-blh8675>> (Jul. 25, 2016).
- Hutchinson, T. C., and Chen, Z. (2010). “Image-Based Framework for Concrete Surface Crack Monitoring and Quantification.” *Advances in Civil Engineering*, 2010(215295), 1-18 doi: 10.1155/2010/215295.
- Irizarry, J., and Bastos, D. (2016). “Exploratory Study of Potential Applications of Unmanned Aerial Systems for Construction Management Tasks.” *J. Manage. Eng.*, 32(3). doi: 10.1061/(ASCE)ME.1943-5479.0000422.
- Irizarry, J., Gheisari, M., and Walker, B. N. (2012). “Usability Assessment of Drone Technology as Safety Inspection Tools.” *Journal of Information Technology in Construction (ITcon)*, 17, 194–212.
- Jahanshahi, M. R., Kelly, J. S., Masri, S. F., and Sukhatme, G. S. (2009). “A Survey and Evaluation of Promising Approaches for Automatic Image-Based Defect Detection of Bridge Structures.” *Structure and Infrastructure Engineering*, 5(6), 455–486. doi:

10.1080/15732470801945930.

Jizhou, W., Zongjian, L., and Chengming, L. (2004). "Reconstruction of buildings from a single uav image." In *International Society for Photogrammetry and Remote Sensing Congress*, A. Gruen, S. Murai, T. Fuse, and F. Remondino, eds., ISPRS, Pitsanulok, Thailand, 100–103.

Khaloo, A., Lattanzi, D., Cunningham, K., Dell'Andrea, R., and Riley, M. (2017).

"Unmanned Aerial Vehicle Inspection of the Placer River Trail Bridge Through Image-Based 3D Modeling." *Structure and Infrastructure Engineering*, 1–13. doi: 10.1080/15732479.2017.1330891.

Kim, H., Lee, J., Ahn, E., Cho, S., Shin, M., and Sim, S.-H. (2017). "Concrete Crack Identification using a UAV Incorporating Hybrid Image Processing." *Sensors*, 17(9). doi: 10.3390/s17092052.

Kim, J., Kim, S., Park, J., & Nam, J. (2015). "Development of Crack Detection System with Unmanned Aerial Vehicles and Digital Image Processing." *Advances in Structure Engineering and Mechanics*.

Koch, C., Paal, S. G., Rashidi, A., Zhu, Z., König, M., Brilakis, I., and German Paal, S. (2014). "Achievements and Challenges in Machine Vision-Based Inspection of Large Concrete Structures." *Advances in Structural Engineering*, 17(3), 303–318.

Koonce, J., Demski, T., Rowe, M., and Morriss, N. (2011). *Bridge Inspection Access to Minimize Operational Impacts*. Collins Engineering Inc, Chicago, IL.

- Lee, J. J., and Shinozuka, M. (2006). "A Vision-Based System for Remote Sensing of Bridge Displacement." *NDT & E International*, 39(5), 425–431. doi: 10.1016/j.ndteint.2005.12.003.
- Lovelace, B., and Zink, J. (2015). *Unmanned Aerial Vehicle Bridge Inspection Demonstration Project Report No. MN/RC 2015-40*. Minnesota Department of Transportation Research Services & Library, St. Paul, MN.
- Mascareñas, D., Flynn, E., Todd, M., and San, C. (2008). "Wireless Sensor Technologies for Monitoring Civil Structures." *Sound and Vibration*, (4), 16–20.
- McGuire, B., Atadero, R., Clevenger, C., and Ozbek, M. (2016). "Bridge Information Modeling for Inspection and Evaluation." *Journal of Bridge Engineering*, 21(4), 4015076.
- Metni, N., and Hamel, T. (2007). "A UAV for Bridge Inspection: Visual Servoing Control Law with Orientation Limits." *Automation in Construction*, 17(1), 3–10.
- Michaelsen, E., and Meidow, J. (2014). "Stochastic Reasoning for Structural Pattern Recognition: An Example from Image-Based UAV Navigation." *Pattern Recognition*, 47(8), 2732–2744. doi: 10.1016/j.autcon.2006.12.010.
- Moller, P. (2008). *CALTRANS Bridge Inspection Aerial Robot Report No. CA08-0182*. Office of Transportation Management Final Report Federal Highway Administration, Washington, DC.
- Moranduzzo, T., and Melgani, F. (2014). "Monitoring structural damages in big

industrial plants with UAV images.” *International Geoscience and Remote Sensing Symposium (IGARSS)*, IEEE, Trento, Italy, 4950–4953. doi: 10.1109/IGARSS.2014.6947606.

Morgenthal, G., and Hallermann, N. (2014). “Quality Assessment of Unmanned Aerial Vehicle (UAV) Based Visual Inspection of Structures.” *Advances in Structure Engineering*, 17(3).

Nebiker, S., Annen, A., Scherrer, M., and Oesch, D. (2008). “A Light-Weight Multispectral Sensor for Micro UAV – Opportunities for very High Resolution Airborne Remote Sensing.” *The International Archives of the Photogrammetry, Remote Sensing and Spatial Information Sciences*, XXXVII, 1193–1200.

Otero, L. D. (2015). *Proof of Concept for using Unmanned Aerial Vehicles for High Mast Pole and Bridge Inspections, Final Report*. Florida Department of Transportation, Melbourne, FL.

Püschel, H., Sauerbier, M., and Eisenbeiss, H. (2008). “A 3D Model of Castle Landenberg (CH) from Combined Photogrammetric Processing of Terrestrial and UAV Based Images.” *Int. Arch. Photogramm. Remote Sens. Spat. Inf. Sci.*, 37, 93–98.

Rathinam, S., Kim, Z. W., and Sengupta, R. (2008). “Vision-Based Monitoring of Locally Linear Structures Using an Unmanned Aerial Vehicle.” *Journal of Information Technology in Construction (ITcon)*, 14(1), 52–63.

Reagan, D., Sabato, A., and Niezrecki, C. (2017). “Unmanned aerial vehicle acquisition

of three - dimensional digital image correlation measurements for structural health monitoring of bridges.” In *SPIE Smart Structures and Materials and Nondestructive Evaluation and Health Monitoring*, SPIE, Portland, OR. doi: 10.1117/12.2259985.

Remondino, F., Barazzetti, L., Nex, F., Scaioni, M., and Sarazzi, D. (2012). “UAV Photogrammetry for Mapping and 3D Modeling – Current Status and Future Perspectives.” *ISPRS - International Archives of the Photogrammetry, Remote Sensing and Spatial Information Sciences*, XXXVIII-1/, 25–31. doi: 10.5194/isprsarchives-XXXVIII-1-C22-25-2011.

Roca, D., Laguela, Diaz-Vilariño, L., Armesto, J., Arias, P., Lagüela, S., Díaz-Vilariño, L., Armesto, J., and Arias, P. (2013). “Low-Cost Aerial Unit for Outdoor Inspection of Building Facades.” *Automation in Construction*, 36, 128–135. doi: 10.1016/j.autcon.2013.08.020.

Sensefly. (2016a). “Sensefly Ebee.” <<https://www.sensefly.com/drones/ebee.html>> (Jul. 25, 2016).

Sensefly. (2016b). “Sensefly Albris.” <<https://www.sensefly.com/drones/albris.html>> (Jul. 25, 2016).

Siebert, S., and Teizer, J. (2014). “Mobile 3D Mapping for Surveying Earthwork Projects Using an Unmanned Aerial Vehicle (UAV) System.” *Automation in Construction*, 41, 1–14. doi: 10.1016/j.autcon.2014.01.004.

Seo, J., Duque, L., and Wacker, J. (2018a). “Bridge Inspection Protocol using Drone Technology.” *Automation in Construction*. In review.

Seo, J., Duque, L., and Wacker, J. (2018b). "Field Application of UAS-Based Bridge Inspection." *Transportation Research Board 97th Annual Meeting*. In press.

Seo, J., Wacker, J., and Duque, L. (2018c). Evaluation of Unmanned Aircraft Systems as a Bridge Inspection Tool. Madison, WI: U.S. Department of Agriculture, Forest Service, Forest Products Laboratory.

Top Con. (2016). "Top Con Sirius Pro."

<https://www.topconpositioning.com/sites/default/files/product_files/sirius_solutions_catalog_7010_2162_revb_sm_0.pdf> (Jul. 25, 2016).

Turner, D., Lucieer, A., and Watson, C. (2012). "An Automated Technique for Generating Georectified Mosaics from Ultra-High Resolution Unmanned Aerial Vehicle (UAV) Imagery, Based on Structure from Motion (SFM) Point Clouds." *Remote Sensing*, 4(5), 1392–1410. doi: 10.3390/rs4051392.

Tyutyundzhiev, N., Lovchinov, K., Martínez-Moreno, F., Leloux, J., and Narvarte, L. (2015). "Advanced PV modules inspection using multirotor UAV." In *31st European Photovoltaic Solar Energy Conference and Exhibition Proceedings*, Universidad Politecnica Madrid, Madrid, Spain.

Walkera. (2015). "Walkera Voyager 3."

<<http://www.walkera.com/index.php/Goods/canshu/id/25.html>> (Jul. 25, 2016).

Wells, J., and Lovelace, B. (2017). *Unmanned Aircraft System Bridge Inspection Demonstration Project Phase II Report No. MN/RC 2017-18*. Minnesota Department of Transportation Research Services & Library, St. Paul, MN.

- Yin, Z. (2014). *A Quadcopter with Heterogeneous Sensors for Autonomous Bridge Inspection Report # MATC-MS&T: 197 Final Report*. U.S. Department of Transportation-Research, Innovation and Technology Innovation Administration, Washington, DC.
- Yuneec. (2015). “Yuneec Typhoon 4K.”
<https://yuneec.com/en_US/products/typhoon/q500-4k/specs.html> (Jul. 25, 2016).
- Yuneec. (2016). “Yuneec Typhoon H.”
<https://yuneec.com/en_US/products/typhoon/h/specs.html> (Jul. 25, 2016).
- Zhang, C., and Elaksher, A. (2012). “An Unmanned Aerial Vehicle-Based Imaging System for 3D Measurement of Unpaved Road Surface Distresses.” *Computer-Aided Civil and Infrastructure Engineering*, 27(2), 118–129. doi: 10.1111/j.1467-8667.2011.00727.x.
- Zhang, Y., Xiong, J., and Hao, L. (2011). “Photogrammetric Processing of Low-Altitude Images Acquired by Unpiloted Aerial Vehicles.” *Photogrammetric Record*, 26(134), 190–211. doi: 10.1111/j.1477-9730.2011.00641.x.
- Zischinsky, T., Dorffner, L., and Rottensteiner, F. (2000). “Application of a New Model Helicopter System in Architectural Photogrammetry.” *International Archives of Photogrammetry. Remote Sensing and Spatial Information Sciences*, 33, 177–183.

CHAPTER 2: BRIDGE INSPECTION PROTOCOL USING DRONE TECHNOLOGY

Luis Duque, EIT, S.M. ASCE, S.M SEI

Graduate Research Assistant

Department of Civil and Environmental Engineering

South Dakota State University

Brookings, SD 57007

Phone: (305) 965 - 1363

luis.duque@sdstate.edu

2.1 ABSTRACT

The field of Civil Engineering has recently gained interest in Unmanned Aerial Vehicles (UAV), commonly referred to as drones. Due to an increase of deteriorating bridges, according to the report released by the American Society of Civil Engineers (ASCE), a more efficient and cost-effective alternative for bridge inspection is required. The goal of this paper was to analyze the effectiveness of drones as supplemental bridge inspection tools. In pursuit of this goal, the selected bridge to perform the inspection was a three-span glued-laminated timber girder with a composite concrete deck located near the city of Keystone in the state of South Dakota (SD). A drone, a Dà-Jiāng Innovations (DJI) Phantom 4, was utilized for this study. An extensive literature review to gain knowledge on current bridge inspection techniques using drones was conducted. The findings from the literature review served as the basis for the development of a five-stage drone-enabled bridge inspection protocol. A field inspection utilizing the drone was performed following the protocol stages, and the findings were compared to current historical inspection reports provided by SD Department of Transportation (SDDOT). This study detailed drone-enabled inspection principles and relevant considerations to obtain optimum data acquisition. The field investigation of the bridge demonstrated the image quality and damage identification capabilities the drone possesses to perform bridge inspection at a lower cost when compared to traditional methods.

2.2 INTRODUCTION

The American Society of Civil Engineers (ASCE) has regularly studied the structural performance of the nation's infrastructure, including bridges. The most recent ASCE report card for America's infrastructure, released in December 2016, specified that approximately 9.1% of the nation's bridges were classified as structurally deficient for a letter grade of C⁺ (ASCE 2016). Although the number of deficient bridges has declined from 11% to 9.1% in the last three years (ASCE 2013), there is a need for a more efficient and affordable technique to visually inspect bridges (Koonce et al. 2011). In fact, the use of drones has become more attractive to bridge owners, researchers and stakeholder due to the drone ability to gather critical information in less time and at a lower cost in comparison to traditional inspection techniques.

Numerous research efforts (Chan et al. 2015; Hallermann and Morgenthal 2014; Koch et al. 2014) have been made to develop new techniques to monitor and inspect infrastructure. Drone technology have shed light on how to overcome time consuming, risky, and relatively expensive bridge inspection practices. For instance, Chan et al. (2015) conducted a study on drone-based inspection compared to conventional inspection practices. To complete the study, several considerations were made concerning drone capabilities for bridge inspection, inspection requirements, cost-benefit analysis, and challenges of aerial platforms. It was concluded that drones have some advantages over conventional inspection practices including cost, time, reduced risk for inspectors, and inspection quality. A more in-depth study of structure inspection was conducted by Koch et al. (2014). During this study, the authors performed an analysis of large concrete

structures, including bridge columns. To conduct the analysis, different inspection techniques such as 3D surface reconstruction were implemented to identify damage. The authors concluded that the drone-enabled inspection coupled with vision-based technology has potential to serve as a more economical and safe alternative to conventional inspection practices. It can be seen that drone technology has helped inspectors conduct visual assessment of infrastructure at a low cost and with less injury risk when compared to conventional inspection methods.

The primary goal of this research was to evaluate the capabilities of drone technology as a supplemental bridge inspection tool to support conventional bridge inspections that are legally mandated. To that end, a selected bridge located near Keystone, South Dakota (SD) was inspected following state and federal regulations (i.e., SD Department of Transportation (SDDOT) and Federal Aviation Administration (FAA)). This paper is subdivided into five sections, including this section. The second section presents the selected drone and bridge for this study. The third section details the developed bridge inspection protocol, while the fourth section deals with the application of the protocol to the selected bridge in accordance with the state and federal regulations. The fifth section presented a comparison of results between drone-based and conventional bridge inspection. The final section provides conclusions and challenges during bridge inspection using drone technology.

2.3 DRONE AND BRIDGE SELECTION

This section is dedicated to the discussion of the drone and bridge selection; thus, the results of the selection process are presented in the following subsections.

2.3.1 *SELECTED DRONE*

The drone to conduct this study was chosen based upon different considerations including flight time, upward viewing camera, camera resolution, video resolution, and others. A number of researchers have utilized and studied a variety of drones to determine their proficiencies in terms of data gathering for bridge inspection. A total of 13 different drones were investigated to efficiently select a suitable drone for bridge inspection. To efficiently select a drone, the following seven considerations were studied:

- (1) **Flying time over 20 min:** Longer inspection time allows for a more efficient and comprehensive bridge inspection as it minimizes interruptions to change the drone batteries;
- (2) **Additional camera on top of drone:** The ability to observe directly under the deck permits a more detailed inspection;
- (3) **Camera resolution with low illumination:** Due to lack of illumination under the deck, the drone camera must be able to capture high-resolution images under low illumination. It can be noted that the illumination can be enhanced by additional flashlights either attached to the drone or from the ground;
- (4) **Video resolution:** Aside from still images, the drone must be able to record high-definition videos to perform video-based inspection as needed;
- (5) **Payload capacity:** Payload is important as it allows the drone to carry additional attachments such as flashlights or cameras if needed;

- (6) **Drone lights:** The drone Light-Emitting Diode (LED) lights included in some drones serve as a source of illumination and should be considered to provide extra illumination required for efficient damage observation underneath a bridge; and
- (7) **Remote range:** Some structures are located over water or are not accessible by inspectors, therefore, a long range remote control is required to inspect such structures.

Considering the aforementioned specifications, a total of four drones were deemed suitable for bridge inspection. The selected drones include the DJI Matrice 100, DJI S900, DJI Phantom 3 pro, and DJI Phantom 4. Among the suitable drones, the DJI Phantom 4 (see **Fig. 2-1**) was selected over the others due to its performance and versatility meeting the considered requirements at a reasonable cost. The intent of selecting an affordable drone was to provide a viable and cost-efficient alternative to current inspection practices that can be implemented by county-level administrations. Additional technology, which is Obstacle Avoidance (OA), allows the drone to avoid harm to both bridge and drone components along with persons and property. Another consideration is the ability to fly in manual mode to avoid Global Positioning System (GPS) signal under the bridge, as mentioned in the past literature (Lovelace and Zink 2015). It should be noted that drone technologies have rapidly grown in recent years; thus, their costs and features will be quickly changed over time.



Fig. 2-1. Image of the DJI Phantom 4 (taken by Junwon Seo).

2.3.2 SELECTED BRIDGE

A glued-laminated girder bridge with a composite concrete deck was selected as seen in **Fig. 2-2**. The bridge is located on US16 to US16A Highway, near the city of Keystone in Pennington County, SD. The bridge has three simply supported spans with four girders spaced at 2.3 m (7.5 ft.) on center (o.c.) and a clear width of 7.9 m (26 ft.). The bridge is horizontally curved at an estimated radius of 116.4 m (881.97 ft.) and is a 51.8 m (170 ft.) long with steel guardrails along the edges of the superstructure.



Fig. 2-2. Glulam timber girder bridge overview taken by the drone (taken by Luis Duque).

2.4 BRIDGE INSPECTION PROTOCOL

Due to a lack of systematic damage identification and drone inspection procedures, a five-stage bridge inspection protocol that allowed for an efficient drone-enabled bridge inspection (see **Fig. 2-3**) was developed. The protocol was based on holistic information related to drone limitations, drone operation conditions, and data acquisition methodology. State and federal regulations were also considered. The protocol is detailed below:

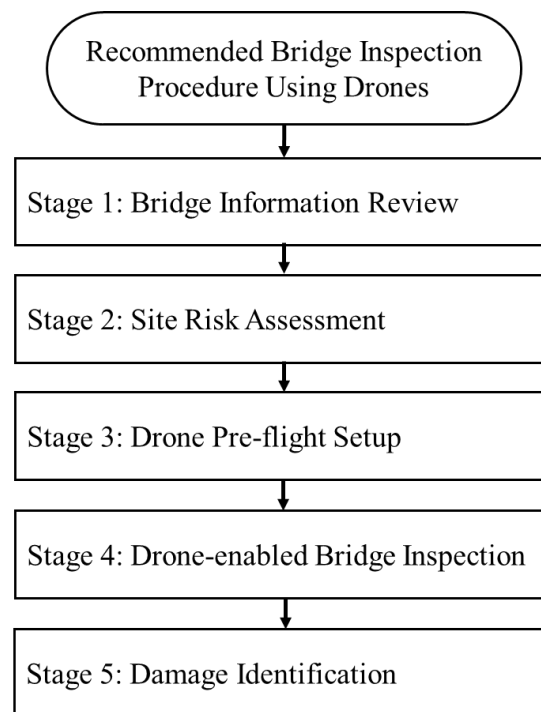


Fig. 2-3. Recommended five-stage bridge inspection protocol using a drone.

Stage 1 is to complete the *Bridge Information Review*. Information such as as-built plans, historical inspection reports, and other applicable documents should be studied in this stage to ensure a complete inspection of the bridge structure. For instance, the review of the inspection reports allows a pilot to identify critical inspection locations (e.g., deck or girders) prior to the drone-enabled inspection. The information gained during this stage

permits the pilot to develop flight strategies under limited bridge approachability conditions, identify current damage, and monitor or update critical damage such as concrete cracks on the target bridge.

Stage 2 is to perform a thorough *Site Risk Assessment* of the bridge's surrounding areas. This stage is intended to identify potential risks such as near trees or traffic lanes to safely proceed with the drone-enabled inspection. Other benefits of performing a site risk assessment prior to conducting the inspection include identification of safe landing/take off zones, safe bridge approaching areas, and pilot risk minimization. Additionally, state and federal regulations should be accounted for prior to establishing a flying strategy. Regulations vary from location to location; it is advised to confirm with DOTs and FAA to identify potential applicable restrictions for the bridge location. Finally, to ensure pilot safety, traffic control mechanisms such as warning signs near the pilot should be implemented.

Stage 3 is to perform the *Drone Pre-flight Setup*. It is recommended, by both the FAA and drone manufacturers, to conduct a thorough inspection of the drone prior to the first flight of the day. Inspections of all the software and hardware including, but not limited to, propellers and rotors inspection, full charging of all instruments (e.g., a remote controller, storage batteries, and a monitor), remote controller adjustments, gimbal inspection, and firmware updates should be conducted. A compass calibration must be performed prior to flying at a new location to prevent GPS signal loss during a flight.

Stage 4 is to complete the *Drone-Enabled Bridge Inspection*. Once all the preliminary information has been gathered during the previous stages, the inspection using the drone can be conducted. During the operation of the drone, it is necessary to consider weather conditions such as wind as it can negatively affect the performance of the drone. Aside from weather condition, the inspection plan should be performed as planned to avoid delays or damage to both the structure and the drone. It is recommended to capture the overall sections of the bridge, and then gather close-up or detailed information of each structural and non-structural component. It can be noted that current regulation does not allow drone operation over traffic, thus, the inspection of some sections (i.e., location over roadway) should be conducted from afar. Finally, per FAA regulations, the Pilot-in-Command (PIC) should be continuously assisted by an observer to avoid distractions and possible accidents.

Stage 5 is to complete the *Damage Identification*. For a successful drone-based bridge inspection, the damage should be easily identified from the gathered information. The images captured using the drone serve as the basis for further computational analysis including photogrammetry based inspection. The use of 3D photogrammetric virtual models serves as an overview of the damage compared to conventional 2D images. The reconstruction of 3D virtual models could be completed in a computer software such as PhotoScan. To build up the 3D virtual model, PhotoScan will need images taken by the drone that can represent points enabling a 3D view of the target structure. Then, using a triangulation technique to connect the points, PhotoScan can generate the surface for a more detailed view and make a texture and color correction. This process is able to provide a visual representation of the target structure in a 3D virtual space.

2.5 APPLICATION OF INSPECTION PROTOCOL TO TIMBER GIRDER BRIDGE

The following section presents the inspection conducted on the selected bridge in accordance with the proposed five-stage bridge inspection protocol.

2.5.1 STAGE 1

During the *Bridge Information Review*, critical information regarding the bridge structure was determined. Based upon the inspection report provided by the SDDOT, it was found that the deck joints were the most critical component due to water leakage coming from the deck surface. After determining the critical inspection zones, the study of the as-built plans was completed. The information regarding the location and dimension of the bridge components, allowed for a more efficient inspection of the bridge components. During the inspection, the component numbering was followed based on the plans as seen in **Fig. 2-4**. After the review of all the documentation, an inspection plan was developed to inspect the bridge using the drone. To complete the inspection, it was established that a general bridge view should be first inspected first, and then more detailed structural components such as girders, columns, and underside of deck can be captured for a more comprehensive data gathering.

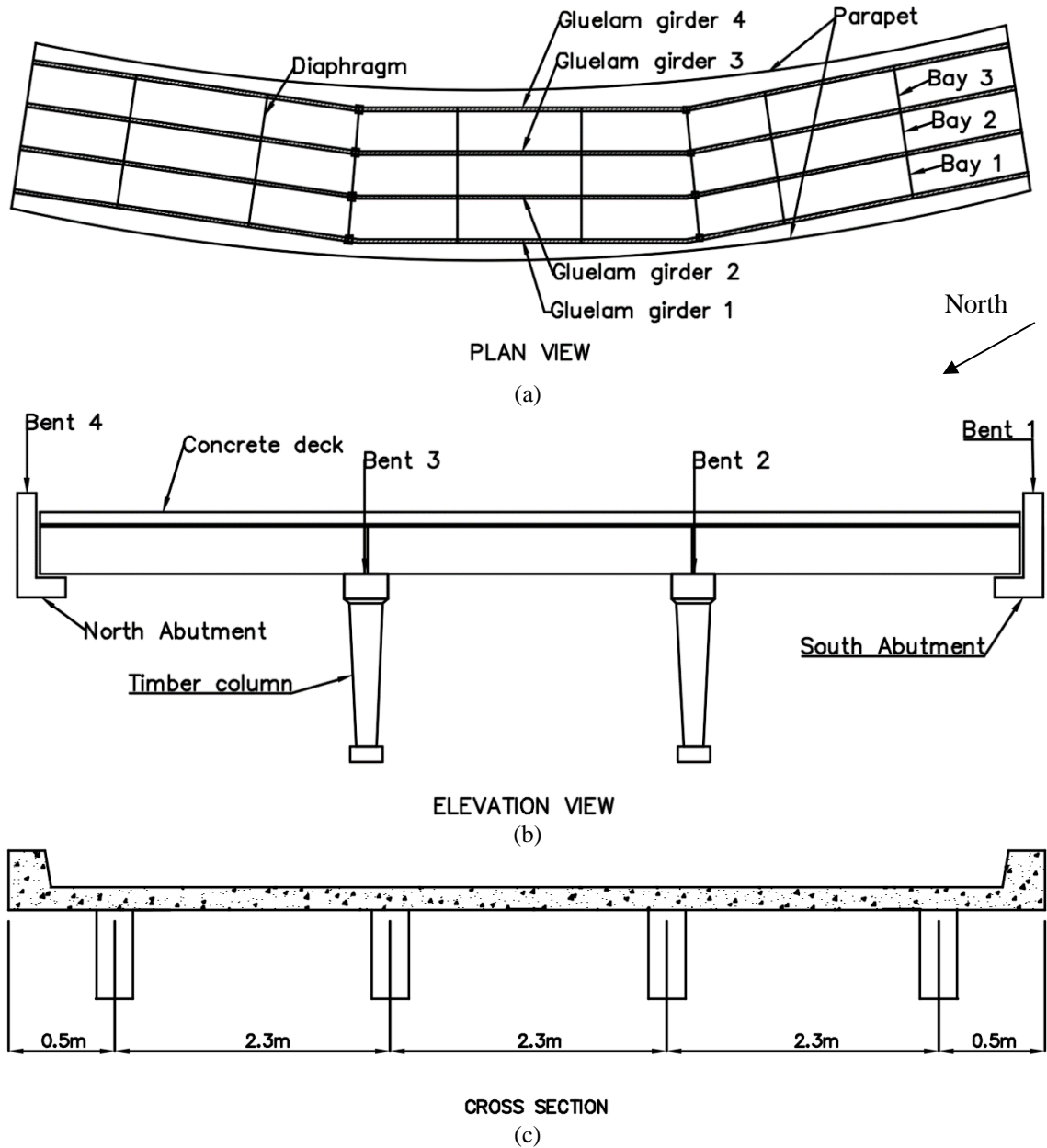


Fig. 2-4. Glulam timber girder bridge components numbering: (a) component numbering on plan view; (b) component numbering on elevation view; and (c) cross-section view.

2.5.2 STAGE 2

A comprehensive *Site Risk Assessment* of the surrounding and bridge were conducted to determine potential risk zones for the operation of the drone. Two potential critical inspection areas were identified based on the geometry of the bridge and adjacent structures as seen in **Fig. 2-5**. The identified critical inspection areas were defined as the location of

restricted access for the operation of the drone to obtain overview and close-up views of the bridge caused by the adjacent bridge and trees. Fortunately, the bridge was not located in a high-risk zone, despite limited operation space in the identified critical inspection areas, as there were not many trees near or over the bridge.

The SDDOT mentioned that no drone operation over the deck is allowed. Other recommendations from SDDOT included traffic control warning signs near inspectors and liability insurance (i.e., Verifly) to protect both the drone and the bridge structure in case of an accidental flyaway. Further, FAA specific regulations, such as flying within five miles of an airport, did not apply to this bridge location. In detail, general FAA part 107 regulations for drone operation include the following (Federal Aviation Administration (FAA) 2016): 1) no restriction for Class G airspace, need air traffic control tower permission otherwise; 2) must keep the aircraft in sight (visual line-of-sight); 3) must fly under 400 ft.; 4) must fly during the day; 5) must fly at or below 100 mph; 6) must yield right of way to manned aircraft; 7) must not fly over people; and 8) must not fly from a moving vehicle.

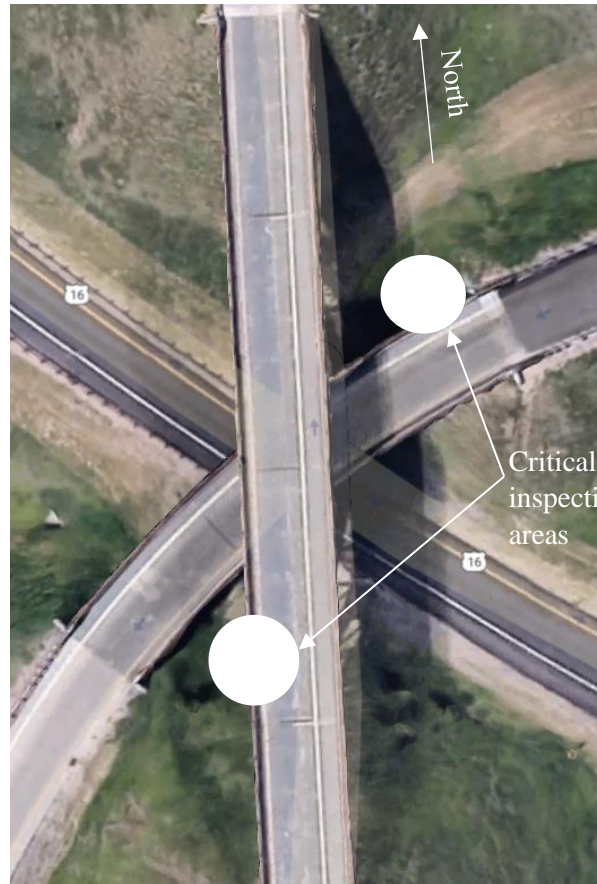


Fig. 2-5. Critical bridge inspection areas (extracted from Google Maps).

2.5.3 STAGE 3

Prior to the inspection of the bridge, a *Drone Pre-Flight Setup* must be completed. As previously mentioned, the DJI Phantom 4 was selected. It is recommended by both the FAA and DJI to perform a thorough inspection of the platform prior to the first flight of the day. To conduct the drone's inspection, all the components and software were inspected including rotors, propellers, batteries, iPad, remote controller, gimbal, and software updates to ensure flight safety. The components were found to be in excellent condition, minimizing potential failure during the inspection. Finally, the compass of the drone was calibrated to ensure full GPS support during the flight. The calibration is performed using two drone rotation movements, first it is rotated counter clockwise while being held

horizontally shown in **Fig. 2-6a**. Then, the same rotation is executed with the drone vertically and the camera facing down as seen in **Fig. 2-6b**.

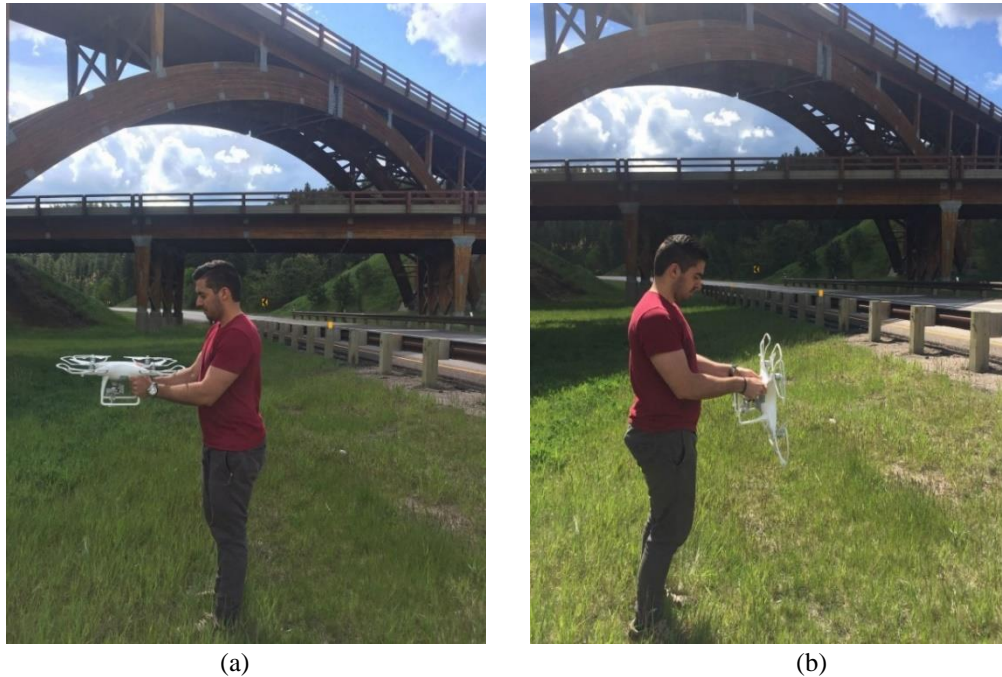


Fig. 2-6. DJI Phantom 4 compass calibration demonstration: (a) drone camera horizontally rotating counterclockwise and (b) drone camera facing down rotating counterclockwise (taken by Callie Duque using digital camera).

2.5.4 STAGE 4

The *Drone-Enabled Bridge Inspection* was completed after all the precautionary actions detailed in Stages 1 through 3 were considered. To perform the inspection, the preplanned scheme of capturing general views of the bridge first and then obtaining close-up views was followed as demonstrated in **Fig. 2-7a** and **2-7b**. The inspection of the bridge was conducted over the course of two days. The weather conditions were favorable during the first day of inspection, with wind speeds under 10 mph. The favorable weather conditions allowed the inspectors to capture details of structural components to identify damage such as concrete cracks and corrosion. On the other hand, during the second day

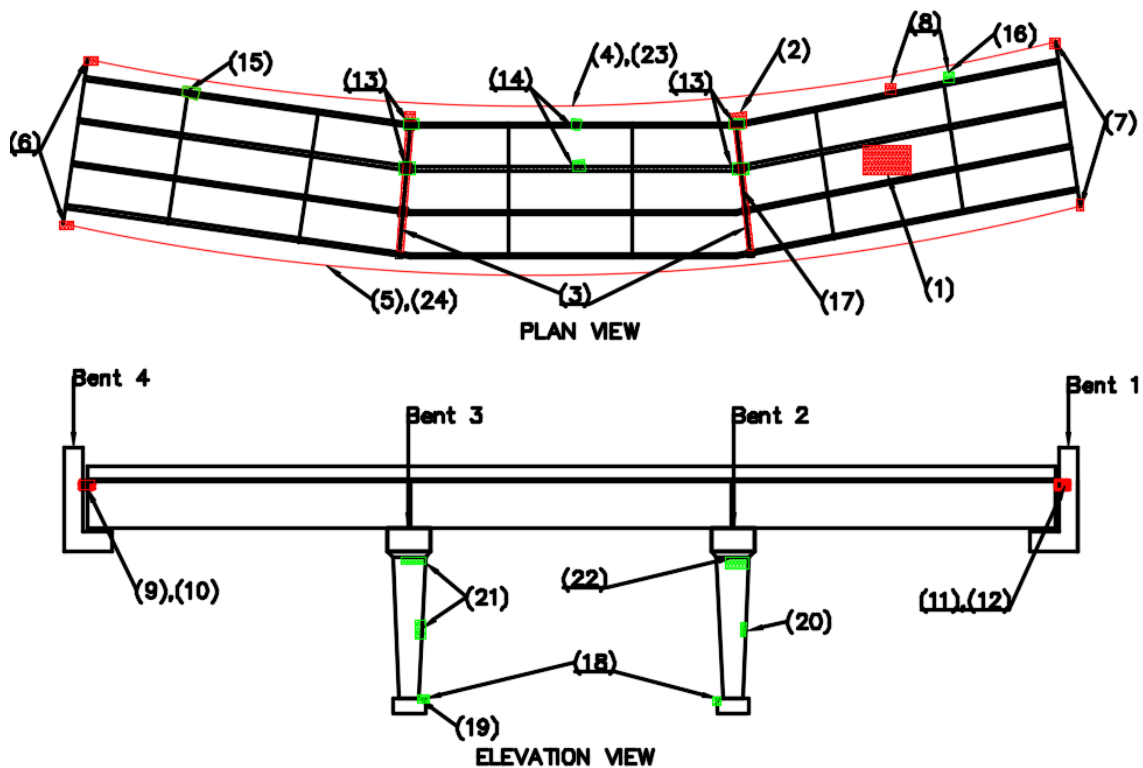
of inspection, the weather conditions were not as favorable with wind speeds of 15 mph and wind gust of over 25 mph. Due to the high wind speeds, a video-based data acquisition approach was considered to minimize distractions from the picture-taking process. Further, the PIC was continuously assisted by an observer, especially during the second day when the flying conditions were not ideal. After concluding the inspection, it was established that the video-based data acquisition, with additional post-processing to gather still images, could potentially reduce the risk of drone crashing and simplify damage identification.



Fig. 2-7. Sample images obtained from the timber girder bridge inspection: (a) glulam girder bridge overview (taken by Junwon Seo using drone); (b) damage on timber girder bridge (taken by Luis Duque using drone); and (c) drone flying near girder (taken by Junwon Seo using digital camera).

2.5.5 STAGE 5

The final stage for the drone-enabled bridge inspection is to conduct the *Damage Identification*. Sample results for the Underside of Deck, Abutment, and Girder damage are presented to demonstrate the quality of data obtained using the drone. Using a photogrammetric computer software, PhotoScan, the structural components were recreated in 3D virtual space to observe the damage from different angles. The schematic shown in **Fig. 2-8**, shows all the identified damage on the bridge using the drone.



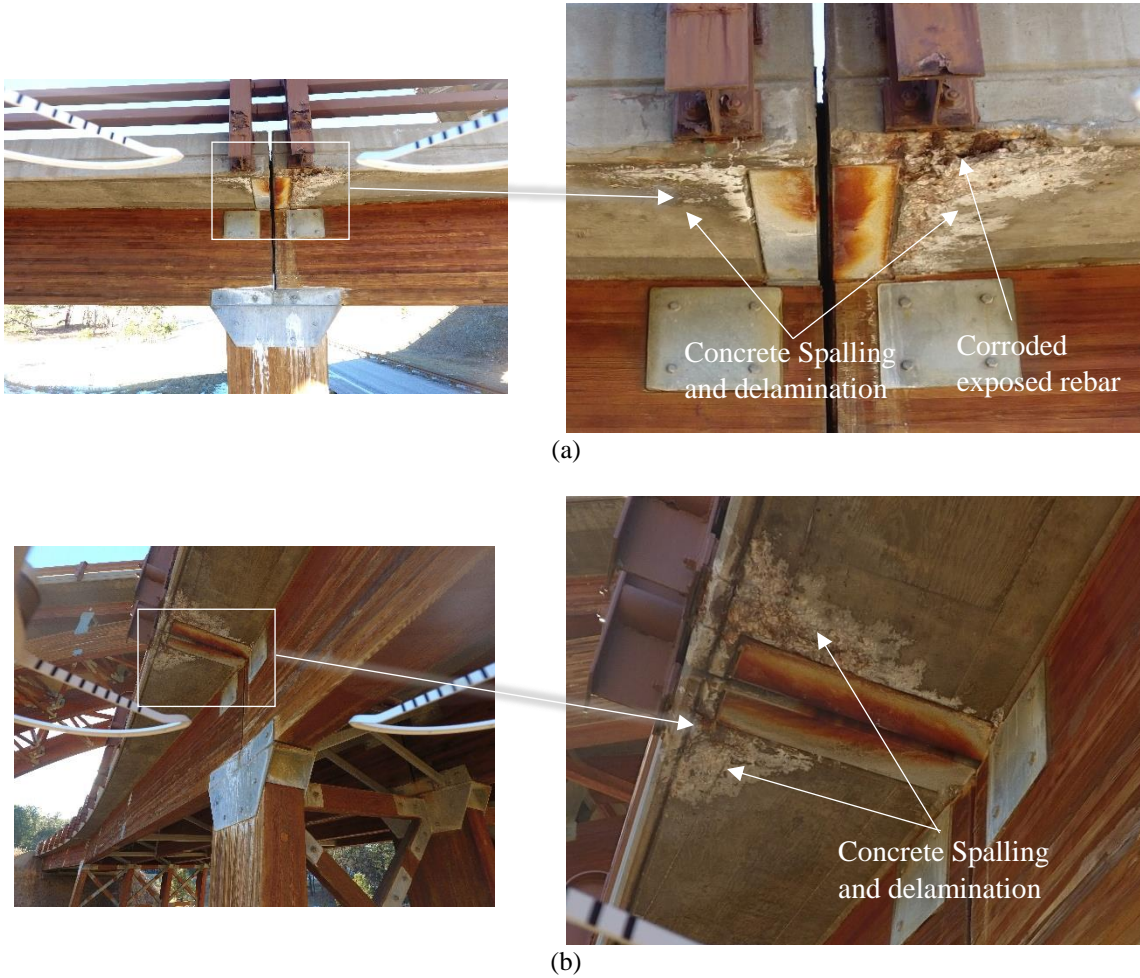
Note: red marks in plan and elevation views indicate concrete damage, green marks represent timber damage. Also, red lines in plan view denote minor cracks along the parapet and rusting in railing in a longitudinal direction.

Fig. 2-8. Timber girder bridge layout with identified damage.

2.5.5.1 Underside of Deck

In general, the inspected deck had the deck had numerous moisture-related damage at the joints (see **Fig. 2-9a** and **2-9b**) as expected from the historical inspection reports. **Fig.**

2-9a shows concrete spalling and exposed rebar near Girder 4 at Joint 2 and **Fig. 2-9b** presents concrete spalling and delaminations near Girder 4 at Joint 3. Further, a representation of the damage near Girder 4 at Joint 2 was created using PhotoScan to create a 3D virtual model in order to better visualize it in 3D virtual space as seen in **Fig. 2-9c**.



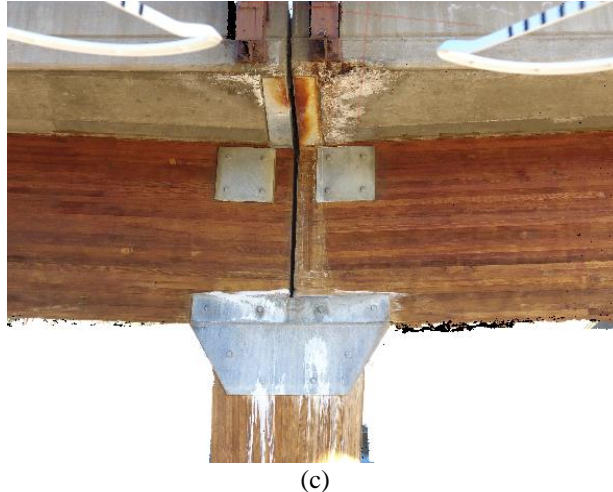
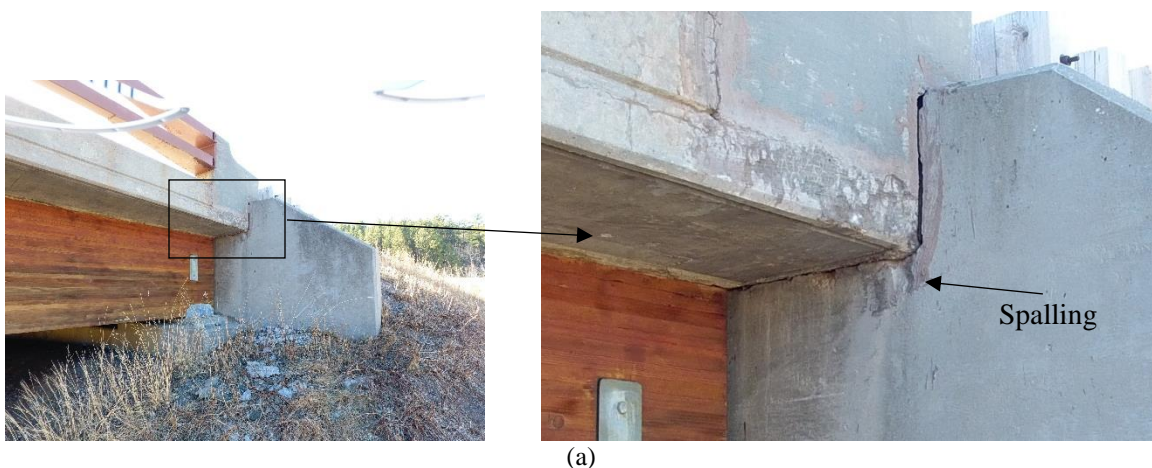


Fig. 2-9. Underside of deck sample damage gathered using drone (taken by Junwon Seo): (a) concrete spalling and corrosion with exposed rebar near Girder 4 at Joint 1; (b) concrete spalling near Girder 4 at Joint 3; and (c) 3D virtual model of Joint 2 near Girder 4 using PhotoScan.

2.5.5.2 Abutment

The abutments were identified as being in overall good condition. Only minor damage such as cracking and discoloration was observed during the drone-enabled inspection as seen in **Fig. 2-10a** and **2-10b**. **Fig. 2-10a** shows spalling on the South Abutment near Girder 1 and **Fig 2-10b** displays spalling, efflorescence, and moisture on the North Abutment near Girder 4. Additionally, using PhotoScan, the damage on the South Abutment near Girder 1 was successfully recreated in 3D virtual space as seen in **Fig. 2-10c**



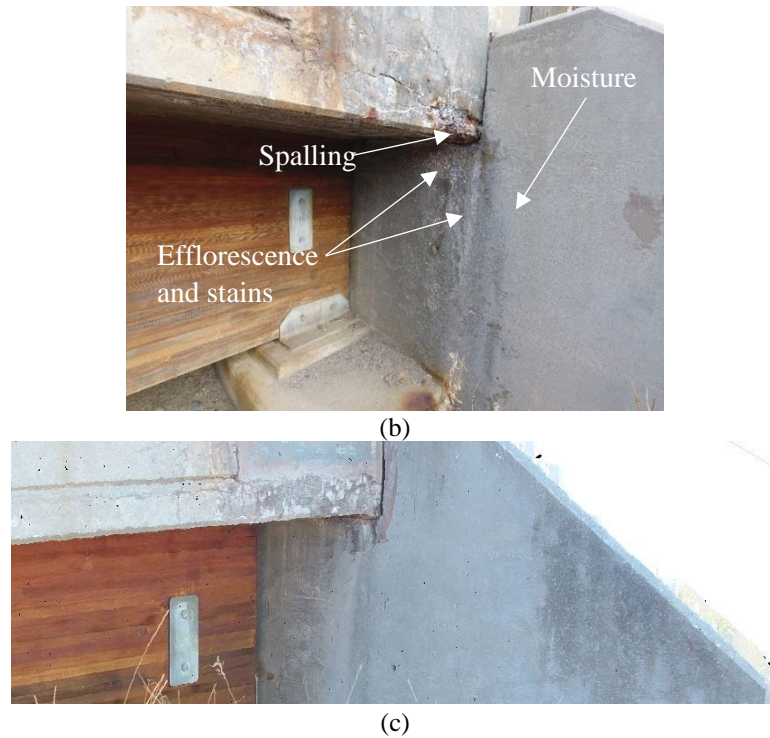


Fig. 2-10. Sample abutment damage detected using drone (taken by Luis Duque): (a) Spalling on South Abutment near Girder 1; (b) spalling and discoloration of concrete caused by moisture at North Abutment near Girder 4; and (c) 3D virtual representation of South Abutment near Girder 1.

2.5.5.3 Girders

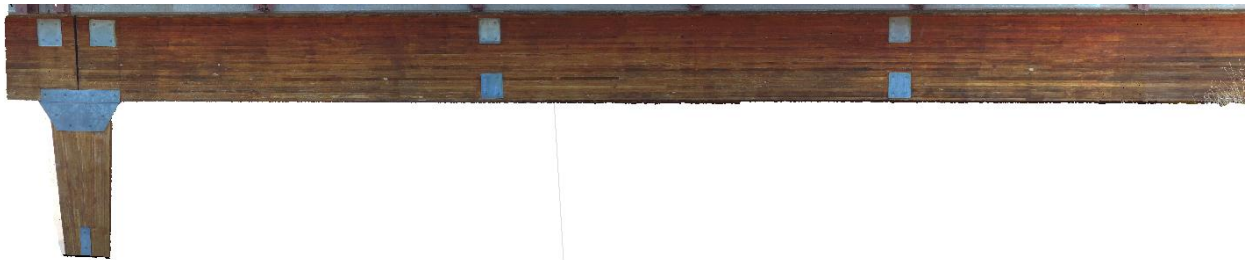
Overall, the girders were in good condition despite some minor water damage caused by water coming from the deck. In detail, the ends of the girders presented some stains and discoloration possibly caused by calcium deposits from the chemical reaction between salt, water, concrete, and steel, especially during the winter season. Sample images of the sample identified damage can be seen in **Fig. 2-11a** and **2-12b**. **Fig. 2-11a** shows high moisture on Girder 4 between Joints 3 and 4 and **Fig. 2-11b** illustrates stains due to water leakage from the deck. With the aid of PhotoScan, the Girder 4 between Joints 3 and 4 was successfully recreated in 3D virtual environment.



(a)



(b)



(c)

Fig. 2-11. Sample girder damage detected using the drone (Taken by Luis Duque): (a) moisture damage on the side of Girder 4 between Joints 3 and 4; (b) stains on the side of Girder 3 at Joint 3; and (c) 3D virtual representation.

2.6 COMPARISON TO CONVENTIONAL INSPECTION METHODS

After all the damage was identified, a side-by-side comparison between the drone-enabled bridge inspection and conventional inspection techniques was performed. The schematic presented in **Fig. 2-8**, accompanied by the side-by-side comparison of each identified damage on **Table 2-2**, aimed to provide a simplified and detailed comparison between the two methods. Images obtained using the drone for the sample structural components, including underside of deck, abutments, and girders, are also compared to images images provided by SDDOT for a visual comparison.

Table 2-2. Comparison of SDDOT Inspection Report and Drone-Enabled Inspection Report for Timber Girder Bridge.

Structural component	SDDOT inspection report	Drone-enabled inspection report	Comparison
Underside of deck	Near Stringer 1 at Joint 2: cracking delamination, and discoloration	(1) Bay 2 between Joints 1 and 2: white efflorescence	There are no major differences between the damage reported by SDDOT and the drone-enabled inspection report. Minor differences include water damage between spans captured using the drone and not reported by SDDOT.
	Bays 2 and 3 at Joint 2: joint cracking and minor scaling	(2) Near Girder 4 at Joint 2: corroded exposed rebar, spalling	
	Bays 2 and 3 at Joint 3: joint scaling, cracking, and delamination	(3) Along Joints 2 and 3: corrosion, spalling, delamination	
	Near Girder 1 parapet along entire deck: has cracking and discoloration	(4) Near Girder 4 Parapet along entire deck: minor cracks and discoloration especially near railings	
	Near Girder 4 parapet along entire deck: scaling, cracking, delamination, and efflorescence	(5) Near Girder 1 Parapet along entire deck: minor cracks and spalling especially near railings	
	Near Girder 4 at Joint 4: spalling and exposed rebar	(6) Near Girders 1 and 4 at Joint 4: concrete cracking, spalling, exposed rebar, discoloration, and water damage	
	Near Girder 4 at Joint 1: cracking, discoloration, and efflorescence	(7) Near Girders 1 and 4 at Joint 1: cracking and discoloration	
	Bay 2 at Joint 4: Scaling, delamination and efflorescence in Bay 2	(8) Near Girder 4 between Joints 1 and 2: water leakage	
	North Abutment near Girder 1: is spalled off and has exposed rebar	(9) North Abutment near Girder 1: spalling and corroded exposed rebar	
	North Abutment near Girder 1: spalling	(10) North Abutment near Girder 4: cracking, efflorescence and water damage	
Abutment	South Abutment near Girder 4: efflorescence, scaling, and spalling	(11) South Abutment near Girders 1 and 4: spalling, efflorescence, and moisture	There are no major differences between the damage reported by SDDOT and the drone-enabled inspection report.
	South Abutment on Bays 1 and 2: scaling and spalling	(12) South Abutment on Bays 1 and 2: concrete spalling	
Girder	At supports at Joints 2 and 3: bottom of girders has discoloration and decay due to trapped water and debris	(13) Girders 3 and 4 at Joints 2 and 3: bottom surface on both girders has discoloration and stains due to water leakage	Moisture damage between bents was identified using the drone but not reported by SDDOT.
	Girder 3 at Joint 3: surface scratch	(14) Girders 3 and 4 between Joints 2 and 3: stains at bottom of both girders	
	N/A	(15) Girder 4 between Joints 3 and 4: some moisture	
	N/A	(16) Girder 4 between Joints 1 and 2: some moisture	
	Diaphragms have slight discoloration where water has been present	(17) No major issues were found apart from minor discoloration near joints due to water leakage	
	Pedestals at Bent 2: horizontal crack along Bay 2 pedestal wall and crack along top of left side of Column 3 pedestal	(18) Column 4 Pedestal at Bents 2 and 3: minor spalling, cracking, and efflorescence	
Column	Pedestals at Bent 3: spalling with expose rebar on right side of pedestal and vertical cracks at top left side of Column 3 and left side of Column 4	(19) Column 1 Pedestal at Bent 3: minor spalling and exposed rebar	No major differences other than minor cracks observed on the columns which were not included in the SDDOT report.
	Column 4 pedestal at Bent 2: horizontal crack	(20) Columns 2, 3, and 4 at Bent 2: minor cracks	
	Pedestal wall Bay 2 at Bent 2: longitudinal crack on top	(21) Column 4 at Bent 3: minor cracks and stains on top	
	N/A	(22) Column 4 at Bent 2: stains on top	
Railing	Paint is peeling due to heavy rust in locations throughout, especially on the Railing near Girder 4.	(23) Heavy rusting on Railing at different sections near Girder 4	No difference.
		(24) Mild rusting on Railing near Girder 1	

Note: numbering of drone-enabled inspection report corresponds to damage location in Fig. 2-8 and N/A indicates Not Applicable.

2.6.1 UNDERSIDE OF DECK

The inspection report developed based on the drone-enabled bridge inspection findings coincided with the damage reported by the SDDOT. As expected, damage such as concrete spalling, corrosion, and exposed rebar was observed near joints due to water leakage from the surface of the deck. A visual comparison of images provided by the SDDOT to those gathered using the drone can be seen in **Fig. 2-12**. The image provided by the SDDOT is shown in **Fig. 2-12a** to provide a visual comparison to those taken using the drone as seen in **Fig. 2-12c** and **Fig. 2-12d**. It is evident that the images are of similar quality, and for the underside of deck, the drone was able to capture a closer view.

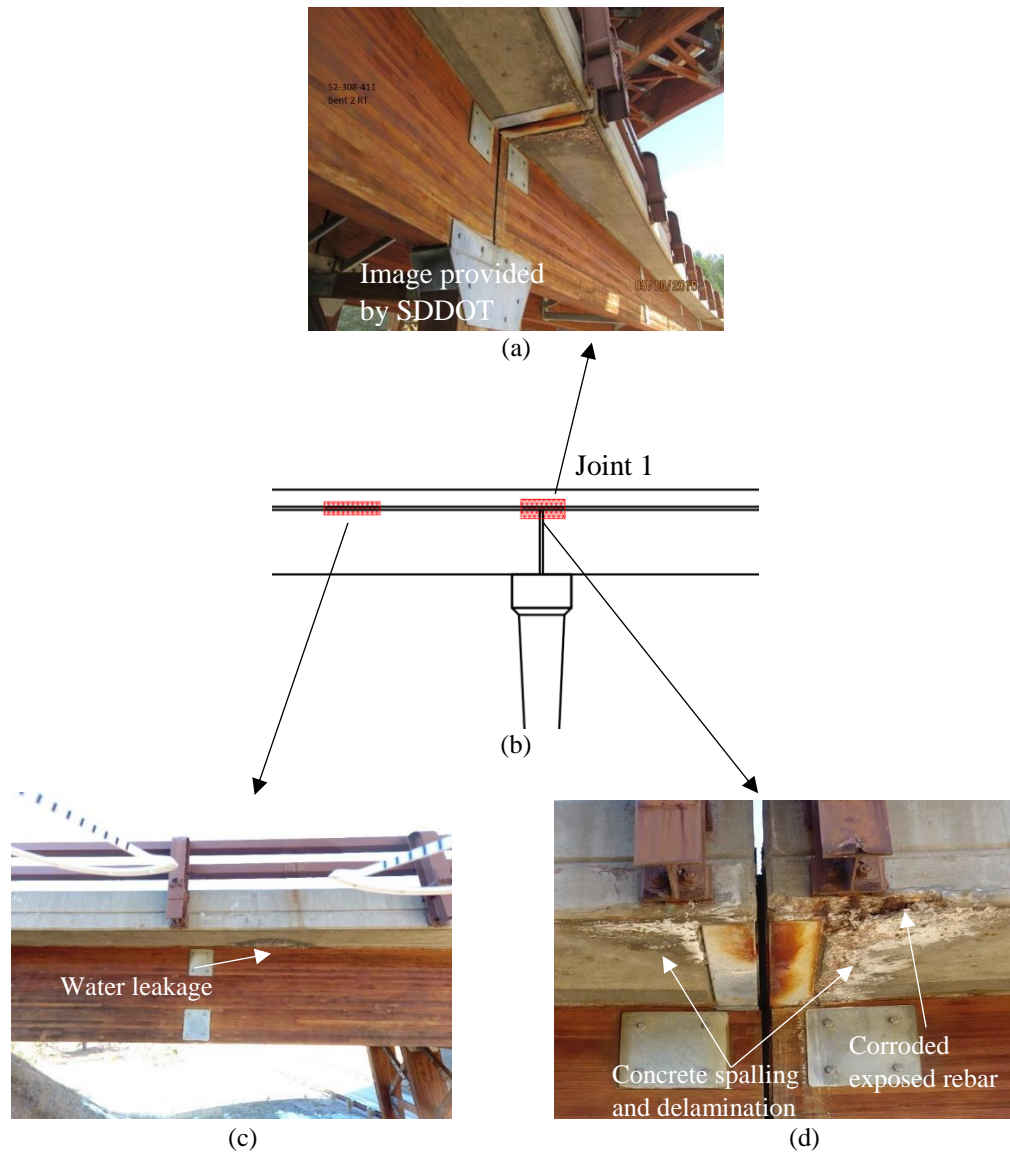


Fig. 2-12. Comparison of results between drone-enabled and conventional inspections: (a) image provided by SDDOT; (b) damage locations; (c) water leakage under deck between South Abutment and Joint 1 (taken by Luis Duque using drone); and (d) concrete spalling and corrosion with exposed rebar near Girder 4 at Joint 1 (taken by Luis Duque using drone).

2.6.2 ABUTMENTS

Overall, the abutments were in good condition and the identified damage (see **Fig. 2-13a**) coincided with the inspection report provided by SDDOT. No major damage was observed other than some minor damage such as cracking, spalling, and discoloration on the South Abutment (see **Fig. 2-13b**) and discoloration and water leakage on the North

Abutment (see **Fig. 2-13c**). It can be noted that there were no images provided by the SDDOT to be compared for the abutments.

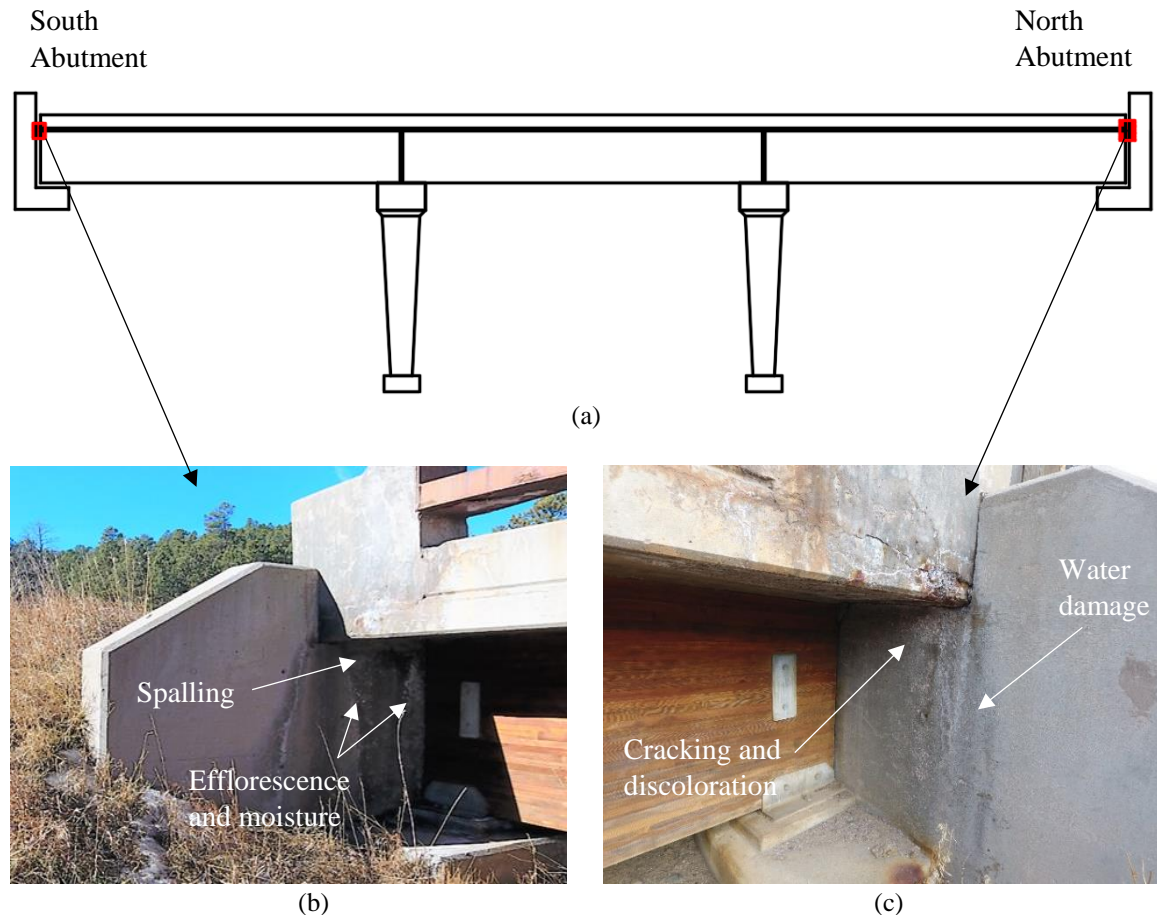


Fig. 2-13. Sample damage on Abutment: (a) schematic of damage location on abutment; (b) damage on South Abutment near Girder 4 (taken by Luis Duque using drone); and (c) damage on North Abutment near Girder 4 (taken by Junwon Seo using drone).

2.6.3 GIRDERS

The identified damage on the girders reported by SDDOT was observed using the drone. **Fig. 2-14a** shows an image provided by the SDDOT to be compared to drone-enabled images (see **Fig. 2-14c** and **2-14d**). The images gathered using the drone are of comparable quality to the one provided by SDDOT, confirming the ability of the drone to

obtain high-quality data for damage identification. Note that some damage, such as moisture on Girder 4 between Joints 1 and 2 and Girder 4 between Joints 3 and 4, were not specified by the SDDOT. This damage must have been recent and demonstrated the importance of frequent routine inspections using drones to evaluate the damage and prevent unreparable structure failure.

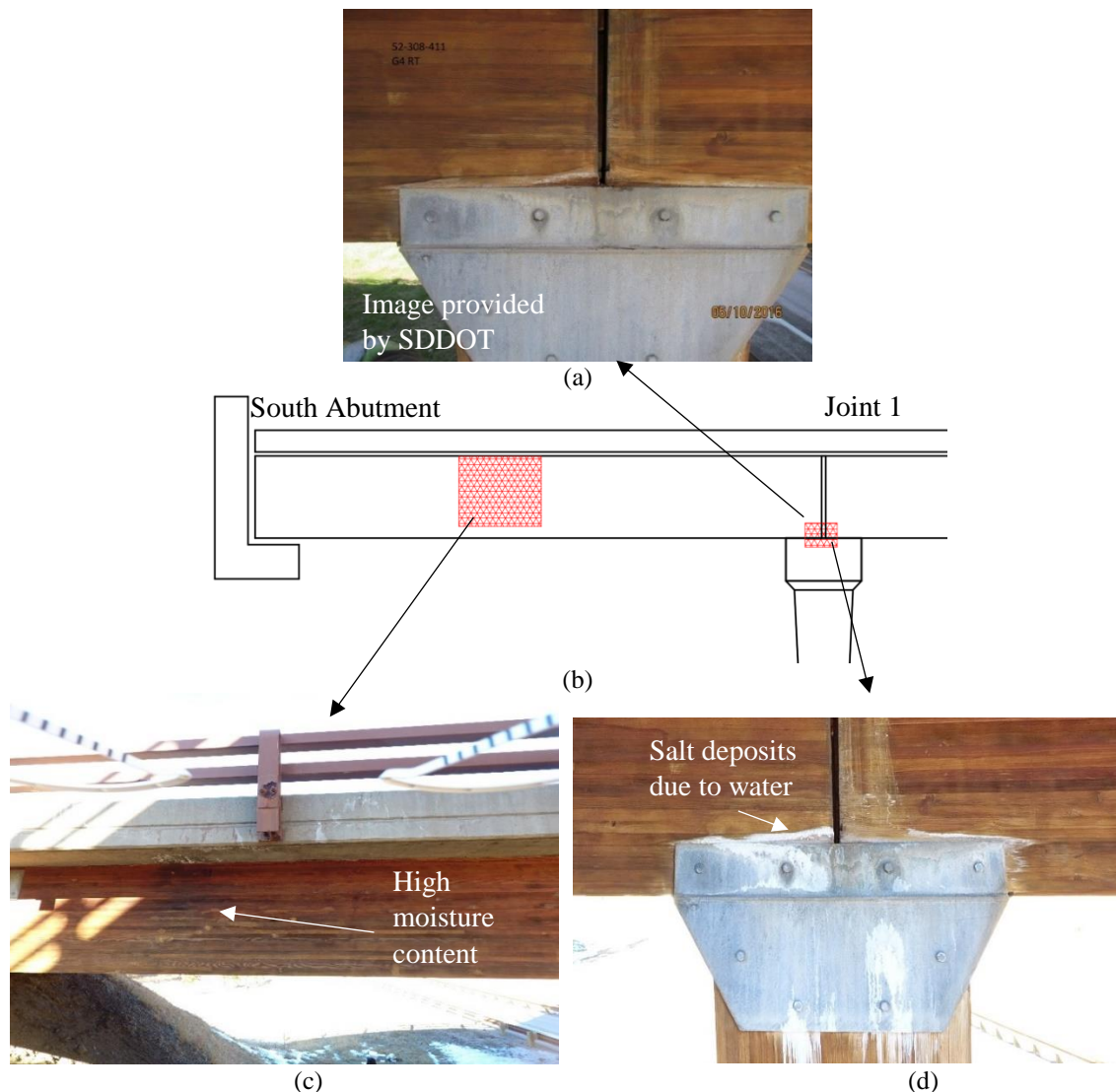


Fig. 2-14. Comparison of identified damage on girder: (a) image provided by SDDOT; (b) damage location; (c) damage on Girder 4 between South Abutment and Joint 1 (taken by Junwon Seo using drone); and (d) salt deposits due to water coming from deck at support of Girder 4 at Joint 1 (taken by Junwon Seo using drone).

2.7 CONCLUSIONS AND CHALLENGES

This study aimed to investigate the capabilities of the drone to conduct bridge inspection related activities. To complete this study, the inspection of an in-service timber girder bridge structures was completed using the DJI Phantom 4 aerial platform. In addition, the five-stage recommended drone-enabled bridge inspection protocol was developed for a more efficient inspection procedure and to aid next generation bridge inspections. The drone's capabilities to complete bridge inspection tasks were studied in terms of image quality and damage identification. A side-by-side comparison of the damage detected using the drone and inspection reports provided by SDDOT was conducted. Based on the results obtained, the following conclusion can be drawn from this study.

1. High resolution cameras of the drone, combined with image processing software such as PhotoScan, proved to be an efficient tool to identify damage on different structural components of the bridge. The use of the photogrammetry software allowed for a more comprehensive and detailed view of damage.
2. During the inspection of the bridge, the drone performs appropriately while flying under the deck despite concerns regarding GPS signal failure. It is noteworthy that the strong GPS signal helps keep the drone stable even at a high wind speed. In addition, the inspection of underside of the deck was completed without issues with the camera tilted up at an angle of 35 degrees. It can be noted that the DJI Phantom 4 has the camera under the main body which initially caused concerns for damage observation above the platform.

3. The drone was able to identify a variety of damage including cracking, spalling, corrosion, and moisture on the bridge. The identified damage was observed on timber, concrete, and steel, demonstrating the versatility of the drone to identify a wide range of damage on different materials.
4. The side-by-side comparison between the drone-enabled bridge inspection report and the results obtained from the inspection reports provided by the SDDOT further established the efficiency of the drone to identify damage on the bridge.
5. The proposed protocol can be implemented in routine inspection to access areas of the bridge otherwise not visible for inspectors. It is worthwhile to note that inspectors should be guided to conduct preliminary drone inspection work under different weather conditions, including low or moderate wind and sunny or cloudy days, prior to the protocol implementation.

During the conduction of the study, some limitations were largely identified caused by unfavorable weather conditions affecting the performance of the aerial platform. The identified limitations include, but are not limited to: (1) high wind speeds, (2) camera overexposure due to sun or snow, (3) low-illumination under the deck, (4) limitations on where the drone can operate due to DOT and FAA rules, and (5) flight challenges due to obstacles in an enclosed section (e.g., between closely spaced girders. Despite the challenges, the drone has great potential to supplement conventional bridge inspection methods and proved to be efficient in identifying different types of damage on specific components of the target bridge.

2.8 ACKNOWLEDGMENTS

Funding for this study was provided by the United State Department of Agriculture – Forest Products Laboratory (USDA-FPL). The assistance and cooperation of the SDDOT is gratefully acknowledged. The results in this paper do not reflect the views of the USDA-FPL.

2.9 REFERENCES

ASCE. (2013). *ASCE 2013 Report Card for America's Infrastructure*. ASCE, Reston, VA.

ASCE. (2016). *ASCE 2017 Report Card for America's Infrastructure*. ASCE, Reston, VA.

Autel Robotics. (2016). "Autel Robotics X-Star Premium."
<<https://www.autelrobotics.com/x-star-premium-tech-specs/>> (Jul. 25, 2016).

Chan, B., Guan, H., Jo, J., and Blumenstein, M. (2015). "Towards UAV-Based Bridge Inspection Systems: A Review and an Application Perspective." *Structural Monitoring and Maintenance*, 2(3), 283–300.

DJI. (2013a). "DJI Matrice 100."
<<http://www.dji.com/product/matrice100/info#specs>> (Jul. 25, 2016).

DJI. (2013b). "DJI Phantom 3." <<http://www.dji.com/product/phantom-3-pro/info#specs>> (Jul. 25, 2016).

DJI. (2014a). "DJI Inspire 1." <<http://www.dji.com/product/inspire-1/info#specs>> (Jul. 25, 2016).

DJI. (2014b). "DJI S900." <<http://www.dji.com/product/spreading-wings-s900/info#specs>> (Jul. 25, 2016).

DJI. (2016). "DJI Phantom 4." <<http://www.dji.com/product/phantom-4/info#specs>> (Jul. 25, 2016).

Federal Aviation Administration (FAA). (2016). *Code of Federal Regulations (14 CFR) part 107*. Washington, DC.

Hallermann, N., and Morgenthal, G. (2014). “Visual inspection strategies for large bridges using unmanned aerial vehicles (UAV).” *7th International Conference on Bridge Maintenance, Safety and Management*, Transportation Research Board (TRB), Washington, DC.

Horizon Hobby. (2015). “Blade Chroma.”
<<http://www.horizonhobby.com/product/multicopter/multicopter-aircraft/ready-to-fly-15086--1/chroma-w-st-10-and-c-go3-blh8675>> (Jul. 25, 2016).

Koch, C., Paal, S. G., Rashidi, A., Zhu, Z., König, M., Brilakis, I., and German Paal, S. (2014). “Achievements and Challenges in Machine Vision-Based Inspection of Large Concrete Structures.” *Advances in Structural Engineering*, 17(3), 303–318.

Koonce, J., Demski, T., Rowe, M., and Morriss, N. (2011). *Bridge Inspection Access to Minimize Operational Impacts*. Chicago, IL.

Lovelace, B., and Zink, J. (2015). *Unmanned Aerial Vehicle Bridge Inspection Demonstration Project Report No. MN/RC 2015-40*. St. Paul, MN.

Sensefly. (2016a). “Sensefly Ebee.” <<https://www.sensefly.com/drones/ebee.html>> (Jul. 25, 2016).

Sensefly. (2016b). “Sensefly Albris.” <<https://www.sensefly.com/drones/albris.html>> (Jul. 25, 2016).

Top Con. (2016). "Top Con Sirius Pro."
<https://www.topconpositioning.com/sites/default/files/product_files/sirius_solutions_catalog_7010_2162_revb_sm_0.pdf> (Jul. 25, 2016).

Walkera. (2015). "Walkera Voyager 3."
<<http://www.walkera.com/index.php/Goods/canshu/id/25.html>> (Jul. 25, 2016).

Yuneeec. (2015). "Yuneeec Typhoon 4K."
<https://yuneeec.com/en_US/products/typhoon/q500-4k/specs.html> (Jul. 25, 2016).

Yuneeec. (2016). "Yuneeec Typhoon H."
<https://yuneeec.com/en_US/products/typhoon/h/specs.html> (Jul. 25, 2016).

CHAPTER 3: BRIDGE DAMAGE QUANTIFICATION PROTOCOL USING UAV

Luis Duque, EIT, S.M. ASCE, S.M SEI

Graduate Research Assistant

Department of Civil and Environmental Engineering

South Dakota State University

Brookings, SD 57007

Phone: (305) 965 - 1363

luis.duque@sdstate.edu

3.1 ABSTRACT

This paper focuses on evaluating the effectiveness of an Unmanned Aerial Vehicle (UAV) as a supplementary bridge damage quantification tool. For this study, a glued-laminated timber arch bridge in South Dakota (SD) was selected and an UAV, the Dà-Jiāng Innovations (DJI) Phantom 4, was utilized for the bridge damage quantification. A recommended four-stage UAV-enabled bridge damage quantification protocol involving image quality assessment and image-based damage quantification was developed. A field application using the UAV to measure crack lengths, thicknesses, and rust stain areas of the selected bridge was conducted following the recommended protocol. The image quality parameters including sharpness and entropy were used to determine the quality of the captured images. The pixel- and photogrammetry-based measurements using the high-quality images were conducted to quantify the bridge damage, and the damage was compared to those from field measurements. Once the damage information was gathered, the UAV image-based damage level classification was established based on the damage levels defined by the American Association of State Highway and Transportation Officials (AASHTO) Bridge Elements Inspection Manual. The findings confirmed the accuracy of the recommended protocol with results within 3.5%, 7.9%, and 14.9% difference for crack length, thickness, and rust stain area, respectively, when compared with the field measurements.

3.2 INTRODUCTION

The use of Unmanned Aerial Vehicles (UAVs) has lately gained interest among structure or bridge inspectors due to costly and inefficient current bridge inspection practices. UAVs provide unique capabilities including the ability to fly near limited accessibility bridge locations and carry high-resolution cameras and sensors to overcome current bridge inspection limitations (Guerrero and Bestaoui 2013). In 2013, a study was conducted to evaluate the current bridge inspection backlog due to an increasing number of deficient bridges (Kirk and Mallett 2013). Kirk and Mallet (2013) prepared a report to provide information on the conditions of the structural integrity of highway bridges. It was reported that based on the total projected investment on bridge rehabilitation from 2008, the Federal Highway Administration (FHWA) could reduce the amount of inspection backlog by 11% by the year 2028. The UAV technology has the potential to alleviate the cost and supplement current bridge inspection procedures to provide safer bridges for future generations.

Different researchers have made significant efforts to detect damage using UAVs (Ellenberg et al. 2016; Hutchinson and Chen 2010; Khaloo et al. 2017; Kim et al. 2017, 2015). For instance, Khaloo et al. (2017) inspected a bridge by developing a 3D virtual model in order to observe damage on the bridge. The identified damage included missing bolts, damaged truss connections, and defective truss chords. It was reported that by conducting the 3D virtual model generation, inspectors were able to observe damage in less time and without risk of injury as only an UAV was needed to gather all the

information. It was also mentioned that the generation of 3D virtual models during the life-cycle of the bridge could allow for the analysis of long-term damage such as camber sag.

Further, Chen and Hutchinson (2010) and Kim et al. (2015) developed innovative alternatives to quantify concrete cracks using UAVs. Kim et al. (2015) developed a crack measurement algorithm known as Morphological Link for Crack (MorphLink-C) to analyze images gathered using an UAV. The algorithm executes a 14-step process to determine the crack area, length and thickness. The researchers performed a verification test to validate the accuracy of the algorithm. Findings revealed that the proposed algorithm obtained results within 0.08 mm difference when compared to direct measurements.

Most recently, Kim et al. (2017) developed a hybrid image processing method to obtain crack length and thickness measurements from images captured by an UAV. To complete the measurements, a camera, an ultrasonic displacement sensor, and a WIFI module were utilized. Then, the implementation of a binarization method (i.e., use of white and black pixels to identify crack boundaries) permitted the estimation of the crack length and thickness. Kim et al. (2017) determined that the method produced accurate results for cracks with thickness greater than 0.1 mm. It was concluded that the maximum percent error was of 7.3% for the crack length, confirming the accuracy of the proposed hybrid method. Although significant findings have been obtained by a number of researchers to quantify damage on bridges, a comprehensive UAV-enabled bridge inspection and damage quantification procedure has not been fully developed to date.

The main objective of this study was to develop an UAV-image-based damage quantification protocol to facilitate both future bridge inspection and damage quantification procedures. This paper is divided into five different sections, including this section. The second section includes a description of the selected UAV and bridge to conduct the study. The third and fourth sections detail the four-stage damage quantification protocol and its application to the selected bridge, respectively. Finally, the fifth section presents conclusions drawn from this study and future work.

3.3 UAV AND BRIDGE SELECTION

Prior to beginning the study, an UAV and bridge selection was required. An UAV capable of capturing high resolution images to capture the damage on the bridge was needed, and a bridge structure, which is suitable for the application of the protocol, was required to perform the damage quantification evaluation. Details of the UAV and bridge selection can be seen in the following subsections.

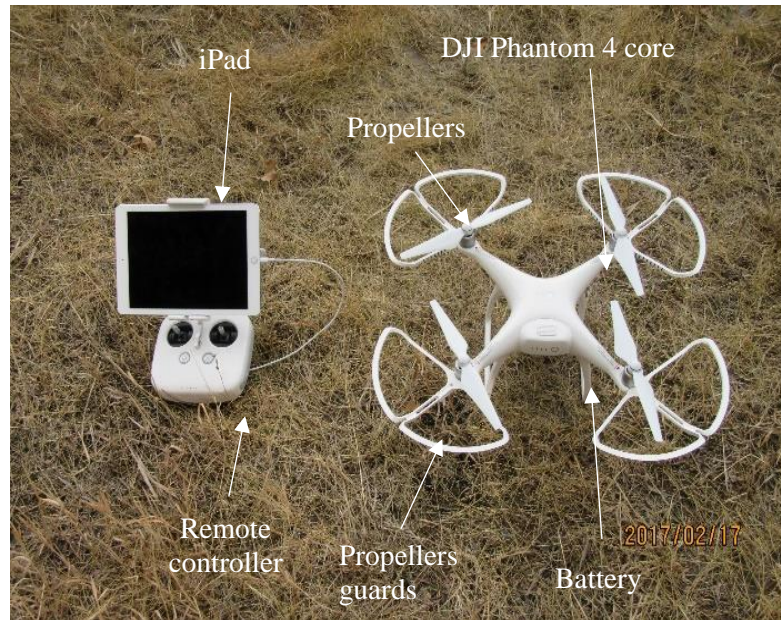
3.3.1 UAV SELECTION

For the selection of the UAV, a comprehensive comparison between thirteen different UAVs from seven different manufacturers was conducted. When selecting the appropriate UAV for the damage quantification, different considerations, including flight time, camera location, image resolution, video resolution, payload capacity, UAV lights, and remote range, were considered. Considering these specifications and analyzing the advantages and disadvantages for each UAV, a Dà-Jiāng Innovations (DJI) Phantom 4 was selected (see **Figs. 3-1a** and **3-1b**). The cost-performance ratio provided a high-end UAV with

appropriate technology suitable for bridge inspection at an affordable price. In particular, the technology of the DJI Phantom 4 includes the ability to avoid obstacles with sensors at the front and the bottom; thus, the UAV pilot can be allowed to fly between complicated sections near the bridge. Other relevant specifications, such as the ability to fly without Global Positioning System (GPS) signal, high-resolution camera, and 135-degree camera vertical rotation, allow the UAV to efficiently inspect a bridge. Details on the selection of UAVs can be found in past work done by Duque et al. (2017).



(a)



(b)

Fig. 3-1. DJI Phantom 4: (a) UAV flying near a bridge and (b) UAV set up prior to inspection (captured by Junwon Seo using digital camera).

3.3.2 BRIDGE SELECTION

A bridge located within the Black Hills National Forest in the state of South Dakota (SD) was selected for the damage quantification study in conjunction with the UAV (see **Figs. 3-2a** and **3-2b**). The selected bridge was the Keystone Wye timber arch bridge, which has three continuous spans with a total length of 19.20 m (63 ft.) near the end approaches, and a symmetrical set of four continuous spans with a length of 24.69 m (81 ft.) over both sides of the arch hinge. Three sets of glued-laminated timber stringers spaced at 3.12 m (10.25 ft.) on center (o.c.) support a reinforced concrete deck having a total width of 7.92 m (26 ft.). The bridge has a 49 m (161 ft.) arch span length, a total length of 88.4 m (290 ft.), and guardrails along the edge of the superstructure.



(a)



(b)

Fig. 3-2. Selected Keystone Wye timber arch bridge: (a) overview of bridge (captured by Luis Duque using UAV) and (b) view from under the arch (captured by Luis Duque using digital camera).

3.4 UAV-IMAGE-BASED BRIDGE DAMAGE QUANTIFICATION PROTOCOL

To efficiently identify and quantify damage on the bridge using the UAV, a recommended four-stage damage quantification protocol was developed as seen in **Fig. 3-3**. It is believed that the protocol is capable of providing a more systematic procedure for

future generation bridge damage quantification using UAVs. A description of the recommended protocol stages is presented below:

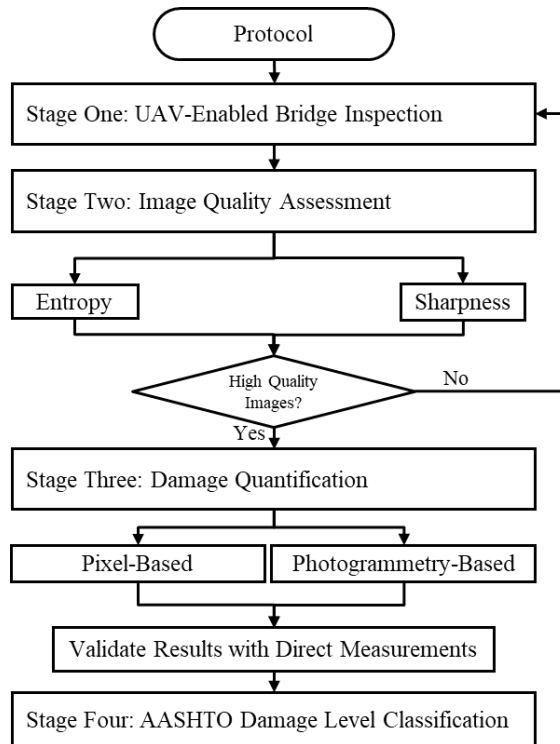


Fig. 3-3. UAV-image-based bridge damage quantification protocol.

Stage One is to conduct the *UAV-enabled bridge inspection*. The inspection of the bridge using the UAV must first consider all safety and regulatory regulations from both the state and federal organizations. For example, state Departments of Transportation (DOTs) regulations including no flying over people and Federal Aviation Administration (FAA) airspace restrictions must be followed. It is recommended that the inspection considers the following four sub-steps: (1) bridge documentation review; (2) bridge surroundings observation; (3) UAV-preflight check; and (4) conduct the UAV-enabled bridge inspection. These steps allow for a safe bridge inspection and efficient flight plan development to identify and quantify damage on the bridge. During the inspection of the

bridge, weather conditions must be considered to avoid unexpected wind gusts while flying near the structure. It is anticipated that wind speeds of 24.1 km/h (15 mph) or higher are unsatisfactory for the operation of the UAV due to instability issues of the UAV. Finally, the UAV operator, or Pilot-in-Command (PIC) should be continuously assisted by an observer per FAA regulations.

Stage Two is to perform the *image quality assessment*. After the inspection has been completed and all the necessary images are obtained, the image quality assessment can be conducted. During this stage, image quality parameters such as entropy and sharpness can be implemented to determine the quality of individual images. To efficiently identify high-quality images, the values for entropy and sharpness per image are compared to the average value for the entire image set. High quality images can be identified by: (1) a significant increase in sharpness without a variation in entropy or (2) a significant increase in both parameters due to sufficient illumination.

Benefits of conducting the image quality assessment include the removal of low-quality images not suitable for damage quantification; thus, a reduced number of high-quality images are used for a more efficient damage quantification. It can be noted that once the image quality assessment is completed, the images identified as low-quality should be reviewed to confirm they are unsatisfactory for damage quantification. In detail, the cause of low quality can be produced by blurriness from adjacent objects such as moving trees or crossing traffic and not by low-quality of the entire image. Finally, a decision considering the number of identified high-quality images should be made. If the number of

images gathered is not sufficient for damage quantification, it is recommended that the inspection be repeated to gather more high-quality images for a satisfactory damage quantification.

Stage Three is to conduct the *damage quantification*. After all the high-quality images are selected, the damage quantification can be performed. The use of image analysis software coupled with mathematical algorithms can facilitate the measurement of damage on the bridge. For instance, the use of pixel- and photogrammetry-based methods can be implemented for damage quantification practices. The pixel-based method can be executed utilizing the commercially available image analysis software ImageJ (Rasband 1997). To conduct the measurements, a scale must be defined first by the user. The scale is assigned by identifying a known distance on the image (e.g., girder depth). Then, using the line tool, the software determines the number of pixels along the known distance and provides a scale in pixels/cm. The distance unit is defined by the user (i.e., units can also be in m or mm). After the scale is identified, different measurements such as length and area can be conducted using the available measuring tool to quantify damage.

On the other hand, the photogrammetry-based quantification method, using the PhotoScan software, utilizes the imported geo-referenced data from the GPS of the UAV to determine the scale (Agisoft PhotoScan 2016). Once the images are imported, PhotoScan identifies unique features from each image and scans the entire image set to align the unique features and produce a sparse point cloud. Then, it creates a dense point cloud and surface in order to obtain the measurements directly on the model. The surface (also known

as mesh) is created using a triangulation method by connect points in a triangular manner, in order to produce a solid surface. Finally, a texture and color correction are applied based on the information from the imported images to generate a closer representation of the target structure in 3D virtual space. Once the 3D virtual model is completed, the measurements can be conducted using the ruler tool available in PhotoScan. Both methods can be validated by comparing the UAV-image-based results to the direct measurements.

Stage Four is to determine a *damage level classification* according, to the American Association of State Highway and Transportation Officials (AASHTO) Bridge Element Inspection Manual (AASHTO 2013). Specifically, during this stage a damage level classification was assigned, in an attempt to provide a quantitative value rather than the descriptive damage states provided by the AASHTO. The use of damage quantification methods could be implemented in an attempt to provide an objective structural integrity assessment to minimize inconsistencies in the designation of damage states by bridge inspectors.

3.5 APPLICATION OF PROTOCOL TO KEYSTONE WYE BRIDGE DAMAGE

The following section includes the application of the identified UAV-image-based bridge damage quantification protocol to the selected Keystone Wye Bridge. The findings are presented as follows, subdivided into the aforementioned stages.

3.5.1 STAGE ONE

To complete an efficient UAV-enabled bridge inspection, the recommended four steps were followed. During the first step, the PIC reviewed the bridge plans and inspection reports provided by the South Dakota DOT (SDDOT). From the bridge plans, the schematic of Keystone Wye Bridge was plotted as seen in **Fig. 3-4**. The component numbering on **Fig. 3-4** was assigned to effectively locate the damage gathered during the UAV-enabled bridge inspection. Moreover, the inspection reports revealed the poor condition of several components including the abutments and deck due to severe cracking and water damage. The information from the inspection reports allowed the PIC to identify critical sections for efficient inspection of the bridge.

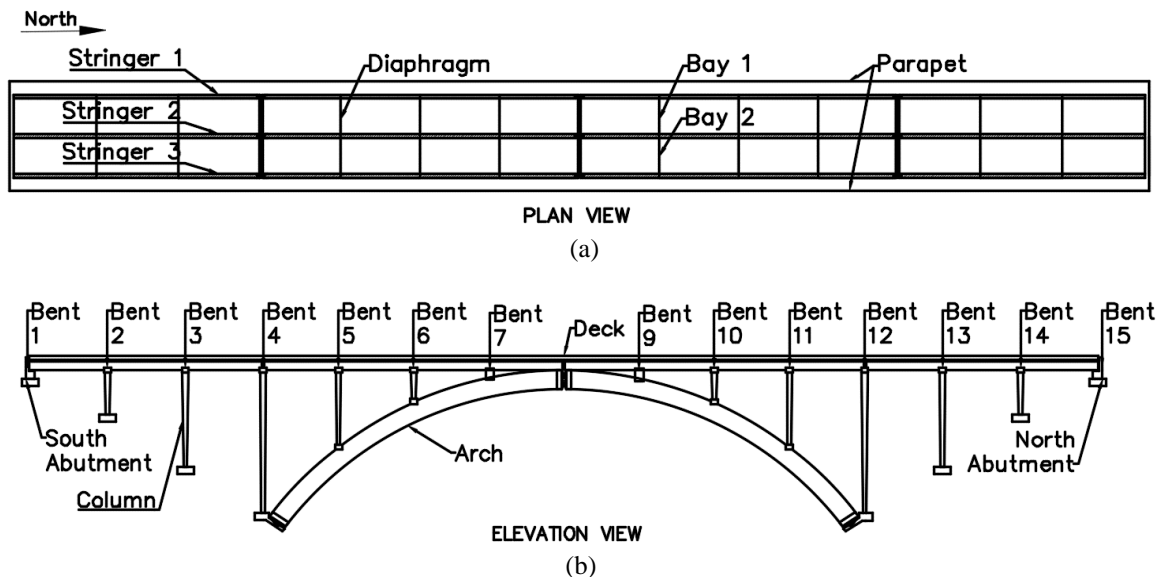


Fig. 3-4. Keystone Wye Bridge with structural component numbering: (a) component numbering on plan view and (b) component numbering on elevation view.

The second step of Stage One was to conduct the observation of the bridge surroundings. During this process, no significant high-risk zones were identified as there were no large trees or structures nearby that may have affected the flight safety. The

restrictions from both the SDDOT and FAA were considered prior to take off. The SDDOT specified that the operation of the UAV above the bridge deck and highway was prohibited. Further, there were no specific airspace limitations per the FAA regulations as the bridge site was located in class G airspace, but other regulations pertinent to the operation of the UAV were considered (FAA 2016).

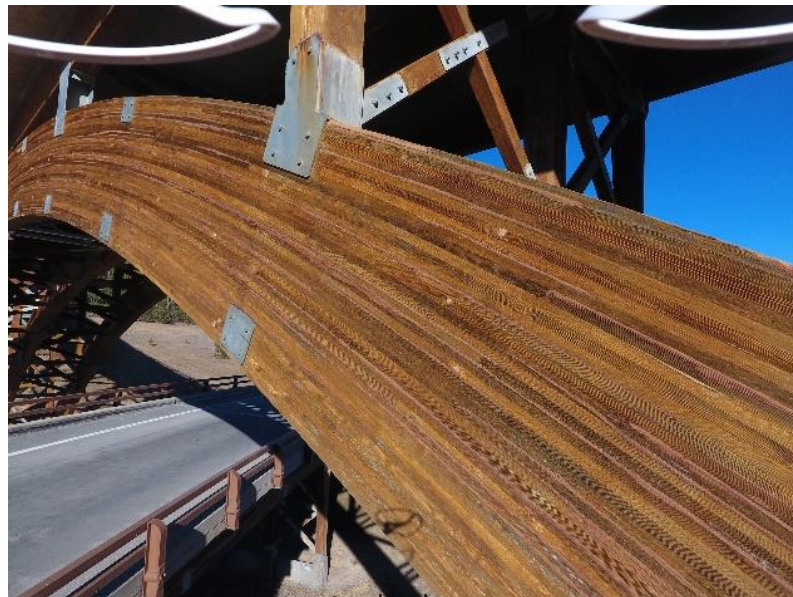
For the third step, the UAV pre-flight check was conducted. Following both the manufacturers and FAA requirements, the DJI Phantom 4 was inspected thoroughly. Individual components, including rotors, propellers, batteries, iPad, remote controller, gimbal, and software updates were tested to ensure safety during the flight. The compass was calibrated to guarantee a strong GPS signal while flying near the bridge. To complete the calibration, the UAV was rotated counterclockwise with the camera facing down. Then, the same procedure was followed with the camera facing forward. There were no issues found during the pre-flight check that could have potentially affected the performance of the UAV.

The last step was to conduct the UAV-enabled bridge inspection. During the inspection of the bridge, all regulatory limitations imparted by the SDDOT and FAA were considered. The information gathered from the bridge plans and inspection reports was carefully applied to identify damage on the structure. The deck and other structural components were successfully inspected following the preplanned scheme despite relatively high-wind speeds of 24.1 km/h (15mph). The structural components were inspected by obtaining overall views first and then proceeding with detail view of the damage as seen in **Fig. 3-5**.

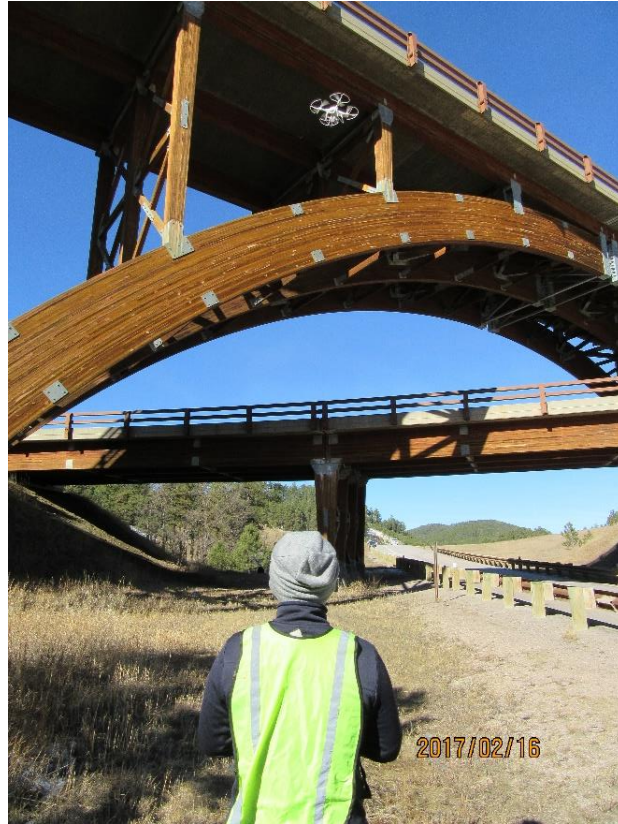
Fig. 3-5a shows the elevation view of one half of the bridge and **Fig. 3-5b** shows a detail view of the arch. A sample image of the operation of the UAV can be seen in **Fig. 3-5c**. A complete UAV-enable bridge inspection procedure can be seen in Seo et al. (2017).



(a)



(b)



(c)

Fig. 3-5. Sample images obtained from the inspection of the Keystone Wye Bridge: (a) overall view of the bridge; (b) detail view of arch; and (c) UAV flying near Keystone Wye Bridge (images captured by Luis Duque).

3.5.2 STAGE TWO

This section presents a description of the image quality method and its application to the Keystone Wye Bridge.

3.5.2.1 Image Quality Assessment Method

The image quality assessment method utilized two image quality parameters, including entropy and sharpness, in order to obtain information on the quality of the images captured from the UAV. In this method, an entropy-sharpness relationship was used to evaluate the quality of individual images. A fictitious image with entropy and sharpness values equal to the average values of the entire set was used as a reference image for the analysis. It is

noteworthy that for the efficient damage quantification process, it is important to analyze the high-quality images identified from the proposed method. Details on each image quality parameter and their relationship to determine high-quality images are presented in the subsections below.

3.5.2.1.1 Entropy Definition

Entropy can be conventionally defined as the sum of the standard deviation of every color pixel based on a grayscale image. A grayscale image has pixel values from 0 (Black) to 255 (white) representing the pixel color in a grayscale. To provide a single entropy value per image, a mathematical function (as shown in Eq. 3-1) available in MATLAB to calculate the entropy of each image was applied (MATLAB 2017). The function measures the sum of pixel color from the histogram counts (range of grayscale pixel values) and then determines the standard deviation of color from pixel to pixel.

$$E = Entropy(I) = -sum(p.* log2(p)) \quad (Eq. 3-1)$$

where E = scalar value of entropy, *Entropy* (MATLAB function to determine entropy); I = input image in a grayscale; and p = normalized histogram pixel values for grayscale images. A sample image in a grayscale is presented in **Fig. 3-6** with sample grayscale pixel values for a small portion of the image as a visual representation of the input for the entropy function. **Fig. 3-6a** shows a sample image in a grayscale. **Fig. 3-6b** shows a small portion of the image with visible pixels and **Fig. 3-6c** shows grayscale pixel values corresponding to each pixel within the image.

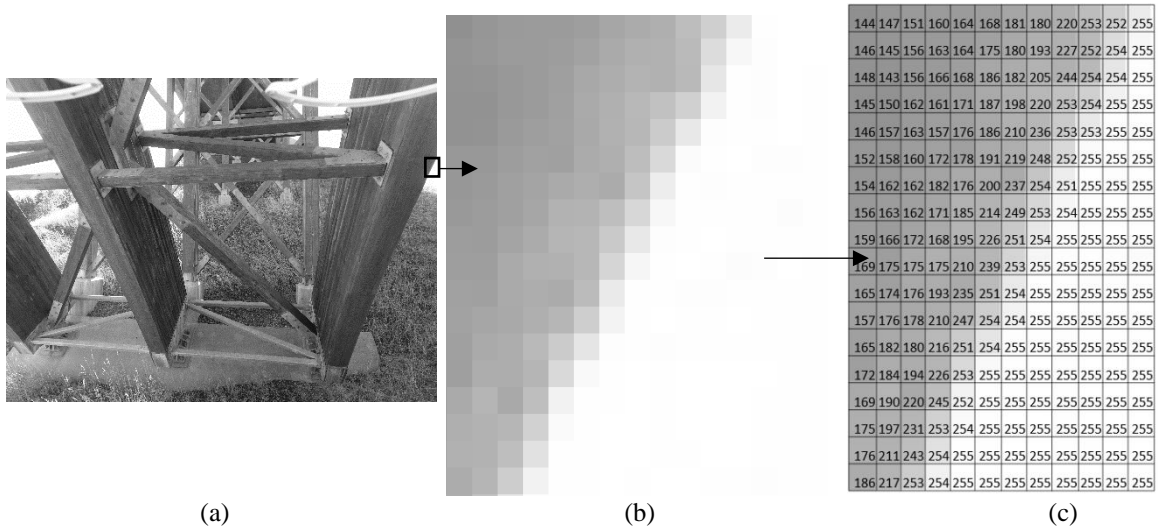


Fig. 3-6. Sample pixel values for an image in grayscale: (a) image in grayscale; (b) small portion of image with visible pixels; and (c) grayscale pixel values for small portion of image.

3.5.2.1.2 Sharpness Definition

Sharpness is defined as the transition gradient at pixel color boundaries. For instance, if a color boundary transitions from white to black, the sharpness value is greater than a transition from white to light gray. To conduct the analysis, a sharpness estimation algorithm developed by Birdal (2011) was implemented. The mathematical process converts the original image into a grayscale to obtain the grayscale pixel boundary gradient. If the transition between pixels was gradual, it was considered blurry, and if that was not the case, it was deemed as sharp. A single quantifiable value was obtained by dividing the sum of all the gradient norms (or magnitude of vectors along grayscale pixel boundaries) by the number of pixels on the picture as seen in Eq. 3-2.

$$S = \frac{\sum(\sum G)}{P} \quad (\text{Eq. 3-2})$$

where S = sharpness; G = gradient vector of pixel in x and y direction; and P = total pixels on the image.

3.5.2.1.3 Entropy-Sharpness Relationship

To estimate the quality of the image set obtained from the bridge inspection, a proposed entropy-sharpness relationship was developed. The proposed method calculated both entropy and sharpness along each of the images. Then, the average values for both entropy and sharpness were calculated to establish a fictitious reference image to analyze the captured images in terms of change in sharpness (ΔS) and change in entropy (ΔE). A high-quality image can be determined based upon the variation in the values of the image quality parameters for each image in comparison to the average values in two ways: (1) positive ΔS with negative ΔE and (2) a positive value for both ΔS and ΔE due to sufficient illumination and good image exposure. A low-quality image can be identified by a positive ΔE and a negative ΔS . Finally, a negative value for both ΔS and ΔE requires a visual observation from the inspector to determine if the image has high- or low-quality.

3.5.2.2 *High Quality Image Determination*

To conduct the image quality assessment, the proposed entropy-sharpness relationship was applied to the 110 images (including different bridge components) gathered during the inspection of the bridge. Specifically, the number of images per component was divided into: 25 for the bridge overview, 30 for the arch, 36 for the underside of deck, 32 for the

stringers, 11 for the abutments, and 21 for the columns. It should be noted that more than one component was observed per image. The entropy and sharpness functions were applied to each image to determine their individual values. Then, the average values for the entropy and sharpness were determined to produce a fictitious reference image for comparison. Once all the image quality values per image were gathered, the ΔE and ΔS were determined by comparing the entropy and sharpness of each image to the reference image. A graphical representation of the results obtained can be seen in **Fig. 3-7**. In **Fig. 3-7**, the green area can be considered the high-quality image region, the red area shows low-quality images, and the yellow section present images that require further review by the inspector to determine the image quality.

Seven sample images are presented in **Fig. 3-7** numbered from one to seven to validate the results obtained. It can be seen that images one through three are high-quality images as their entropy and sharpness are higher than the reference image reflected by either a positive ΔS and ΔE or a positive ΔS and a negative ΔE . Images number four and five are identified as low-quality images as their ΔE is positive and the ΔS is negative. Similarly, images number six and seven are classified as images that require visual assessment by the inspector as both the ΔS and ΔE are negative when compared to the reference image.

From the sample images presented in the yellow area, it is evident that image five is not suitable to identify damage as the arch is underexposed and no damage could be observed. On the other hand, image six would allow the inspector to observe damage on the structure as it is evenly exposed, and all the bridge components are clearly visible. The

comparison of images number five and six demonstrated the need to review the images that fall within the yellow area. Following this method, a total of 29 images were considered low-quality images not suitable for damage identification; therefore, they were removed prior to the damage quantification process. It was concluded that the image set presented sufficient number of high-quality images to conduct the damage quantification in Stage Three.

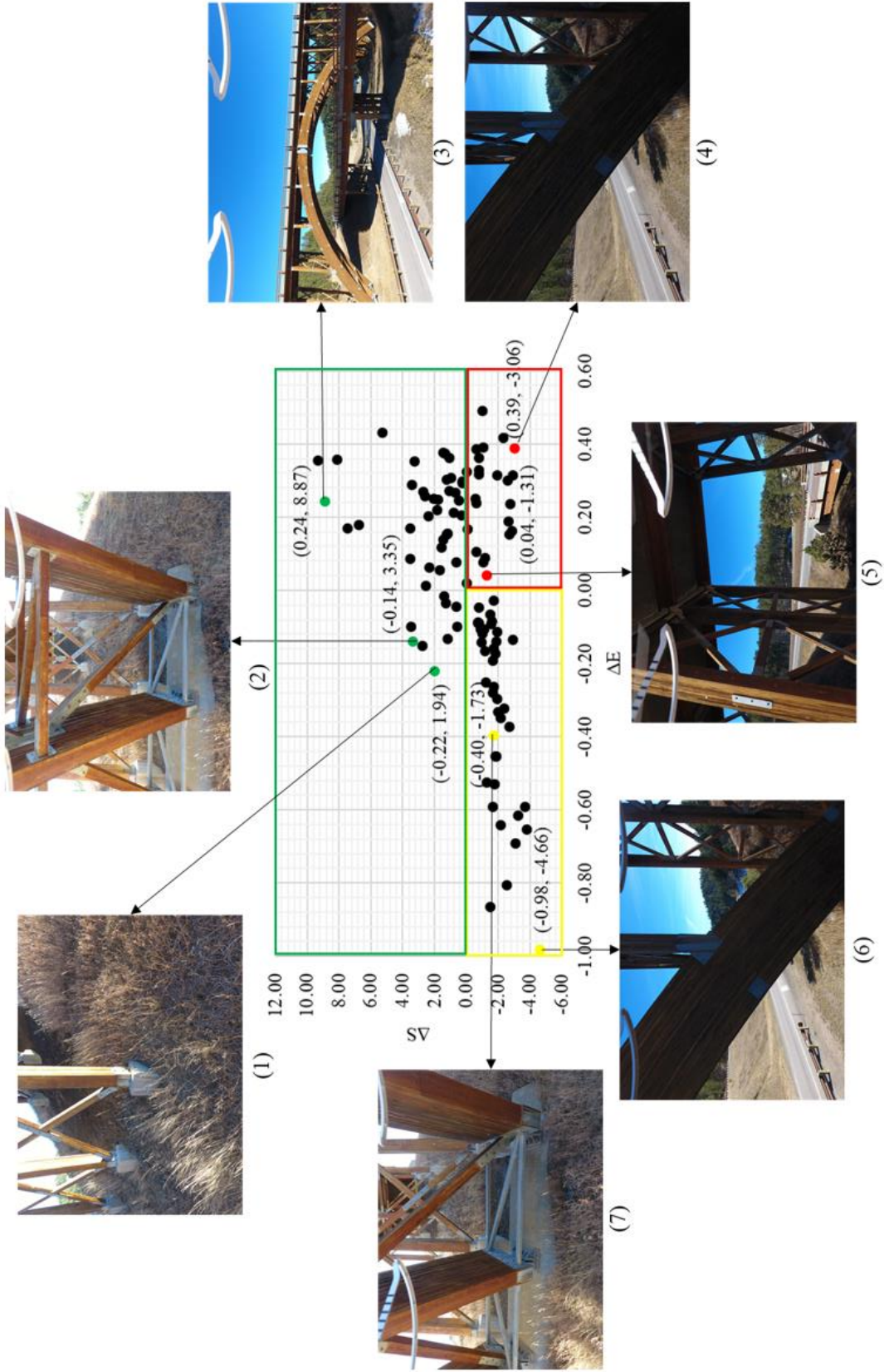


Fig. 3-7. Graphical representation of entropy-sharpness relationship results with sample images.

3.5.3 STAGE THREE

The selected high-quality images were utilized to conduct the damage quantification. The proposed methods including the pixel- and photogrammetry-based measurements were applied to a damage on the bridge to assess their accuracy in more detail. The selected damage was chosen based on physical accessibility to perform the direct measurements which were compared to those obtained using the UAV. The following subsections present the results of the pixel- and photogrammetry-based measurements in comparison to the field measurements.

3.5.3.1 Pixel-Based Measurements Results

For the field study of the pixel-based method, a set of two images were gathered from two different angles to evaluate the effect of image distortion on the measurements accuracy. The selected camera rotation was chosen as one of the recommended camera rotations seen in Zhuolei et al. (2009) to produce image distortion. The first image was obtained by taking a picture aligned to the damage. A graphical representation can be seen in **Fig. 3-8a**, where the solid line represents the field of view for the camera, and the red dashed line the damage position. For this case, both the field of view and the damage location are aligned; thus, there is not image distortion. A second image to the side of the damage was taken as seen in **Fig. 3-8b**. This case shows how the solid line representing the field of view for the camera does not match the red dashed line showing the damage location; therefore, some image distortion is observed. The study of these two images was considered necessary to evaluate the accuracy of the pixel-based method considering image distortion.

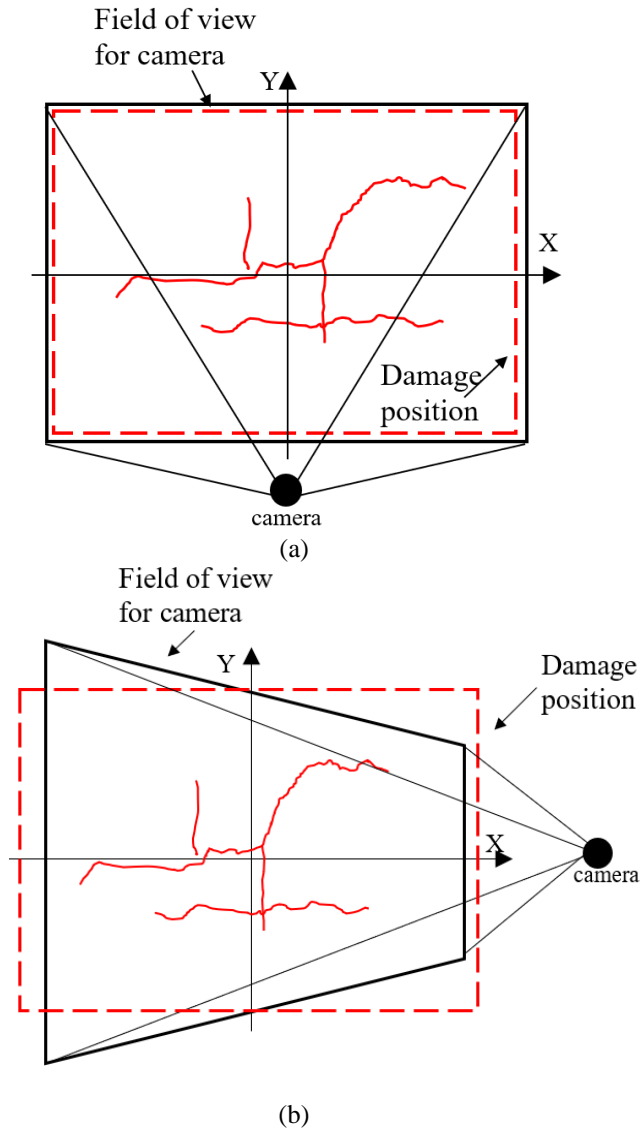


Fig. 3-8. Image comparison for different camera position: (a) camera aligned to damage and (b) camera to the side of damage.

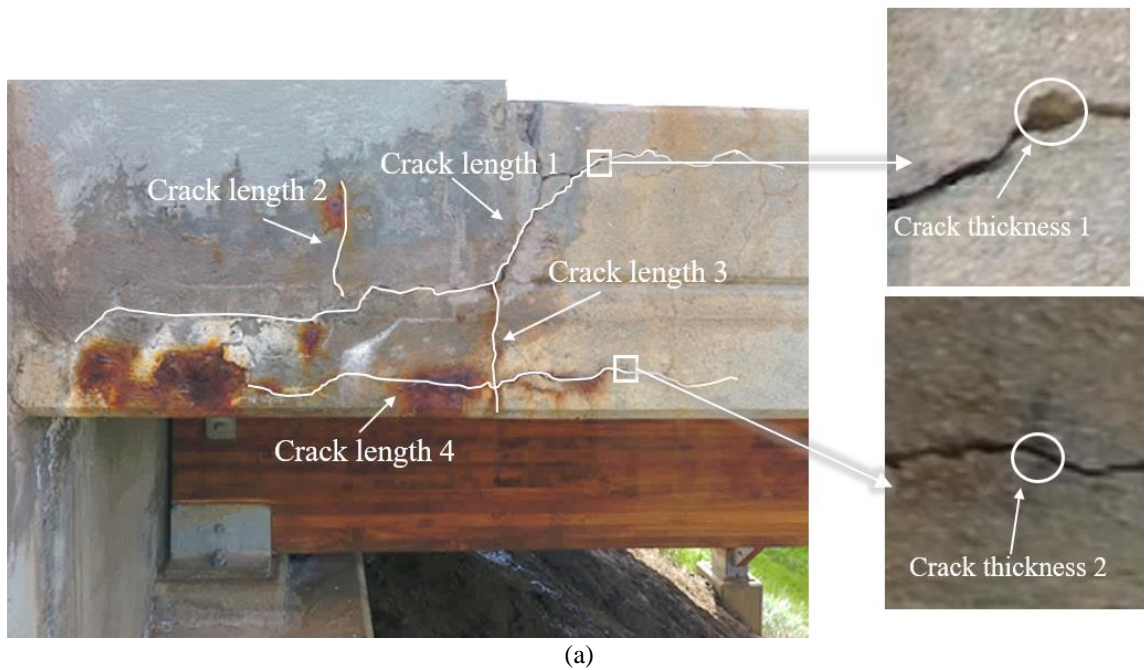
The field study of the pixel-based method was completed by capturing images from two different angles as seen in **Figs. 3-9a** and **3-9b**. Using this method, the results were obtained in less than five minutes due to its simple user interface. To measure the damage, a scale of 22.7 pixels/cm for the image aligned to damage and 28.2 pixels/cm for the image to the side of the damage, based upon the depth of the parapet, was assigned. It can be

noted that the scale must be determined for every image analyzed using ImageJ. The results of the cracks lengths and thicknesses measurements using ImageJ are presented in **Table 3-1**. After completing the measurements of the image aligned to the damage (see **Fig. 3-9a**), the results were compared to the field measurements. The field measurements were completed using a measuring tape. As expected, the results obtained using the pixel-based method were accurate with percent difference within 2.7% and 7.9% for the crack length and thickness, respectively.

Contrary to the results for the image aligned to the damage, the analysis for the image taken to the side of the damage presented percent difference within 8.7% and 21.9% for the cracks lengths and thicknesses, respectively, showing a significant decrease in accuracy. The decrease in accuracy can be attributed to image distortion caused by obtaining the picture to the side of the damage. It was identified that there is an inverse relationship between the accuracy of measurements and the angle between the field of view for the camera and the damage location. The complete set of results for the crack measurements with image distortion are also presented in **Table 3-1**.

For the identified rust stained areas, an approximate area was calculated for the direct measurement. To achieve the measurement, linear segments along the edges of the rust stained area were directly measured using a measuring tape. Then, using AutoCAD, the simplified irregular shape area was determined. In ImageJ, the available area function was used based on the predetermined scale to calculate the pixel-based area measurements and compare them to field measurements. ImageJ utilizes the scale information and the number

of pixels inside the bounded area to complete the measurement. Due to the approximation for the direct measurements, the results were not as accurate as expected with percent difference of 11.9% for the image aligned to the damage as seen in **Fig. 3-9c**. The study of the rust stained area on the image to the side of the damage was conducted as seen in **Fig. 3-9d**. As expected, a lower accuracy with percent difference of 47.1% when compared to field measurements was observed. The comprehensive results for the study of the rust stained areas are also included in **Table 3-1**.



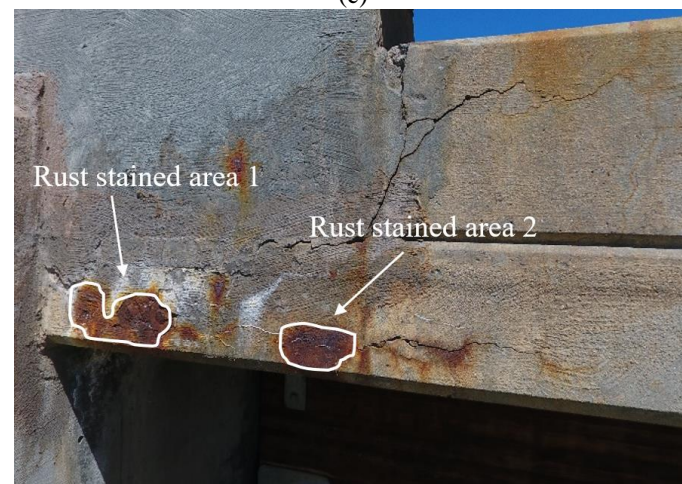
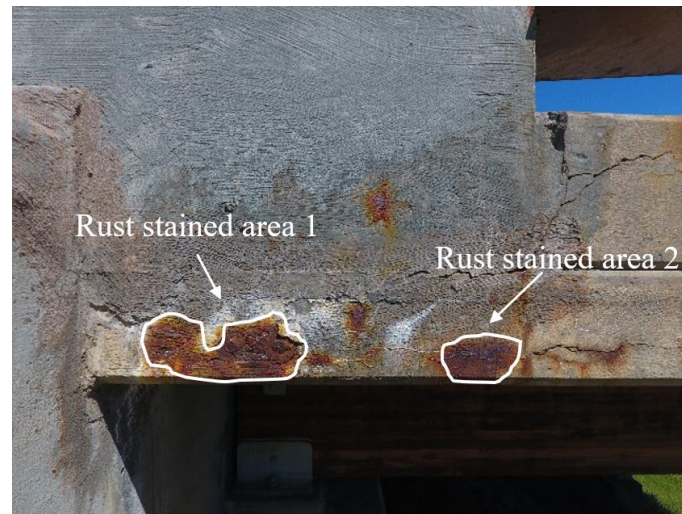
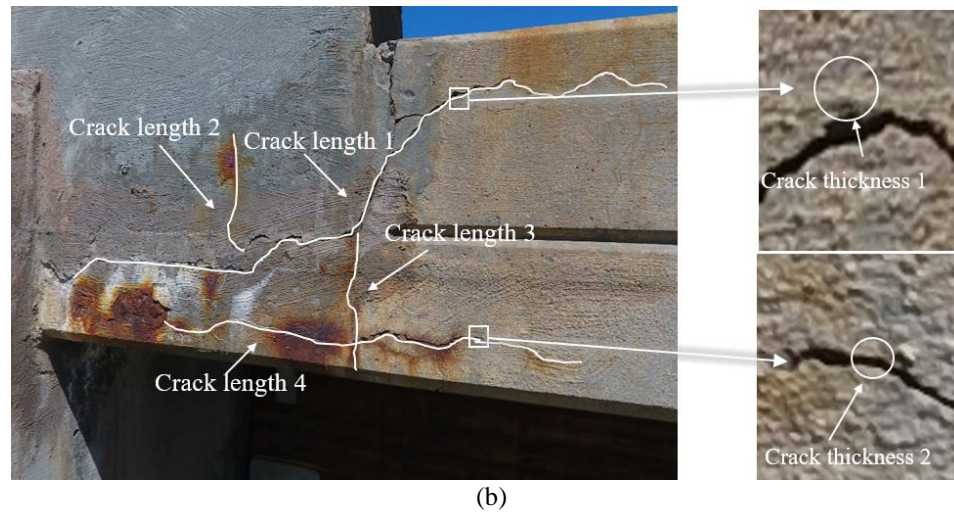


Fig. 3-9. Pixel-based damage quantification of damage near abutment of the Keystone Wye Bridge: (a) image aligned with damage; (b) image to the side of damage; (c) identified rust stained areas for image aligned to damage; and (d) identified rust stained areas for the image to the side of damage.

Table 3-1. Results from Measurements Obtained Using ImageJ.

Damage Type	Identified damage	Pixel-Based Measurement aligned to damage	Pixel-Based Measurement to side of damage	Field Measurement	Measurement Difference (%)	
					Aligned to damage	To side of damage
Crack Length cm (in.)	1	127.3 (50.1)	121.7 (47.9)	126.4 (49.75)	0.7	3.8
	2	18.8 (7.4)	17.3 (6.8)	18.3 (7.2)	2.7	5.6
	3	20.2 (7.97)	20.1 (7.9)	20.3 (8 in)	0.5	1.0
	4	82.8 (33)	75.7 (29.8)	82.6 (32.5)	0.2	8.7
Crack thickness cm (in.)	1	0.66 (0.26)	0.76 (0.3)	0.61 (0.24)	7.9	21.9
	2	0.14 (0.054)	0.15 (0.06)	0.13 (0.051)	7.4	14.3
Rust stained area cm ² (in ²)	1	226.5 (35.1)	156.1 (24.2)	252.3 (39.1)	10.8	47.1
	2	91.0(14.1)	67.7(10.5)	102.6(15.9)	11.9	40.1

3.5.3.2 Photogrammetry-Based Measurements Results

A 3D virtual model based on the aforementioned photogrammetry-based procedure was generated. The 3D virtual model was completed in approximately 40 minutes (8 times longer than the pixel-based method) using the same computer as the pixel-based method. The computer used to complete the damage quantification had a core i7 processor with 16 Gigabytes (GB) of Random Access Memory (RAM) and a Central Processing Unit (CPU) of 2.6 Hertz (Hz). It should be noted that the generation time is depending on the size of the 3D virtual model. In contrast to the analysis of the pixel-based measurements, only one 3D virtual model was developed as seen in **Fig. 3-10**. It is worth mentioning that the image distortion determined during the pixel-based method was introduced by an attempt to capture a 3D object using a 2D image. For that reason, the measurements using the photogrammetry-based method did not present any image distortion as they were conducted directly on the 3D virtual model.

To conduct the measurements, a scale to geo-reference the 3D virtual model was defined. To establish the scale, the GPS location information from the UAV was utilized, in addition to the assignment of known distances on the 3D virtual model. Then, using the ruler tool, the measurements for the same crack lengths and thicknesses were obtained and compared to the field measurements. The results demonstrated the level of accuracy the method was able to obtain with percent differences within 3.5% and 7.4% for the crack lengths and thicknesses, respectively. The details of the results for the crack measurements can be seen in **Table 3-2**.

For the rust stained areas measurements, the desired area was isolated from the rest of the 3D virtual model as seen in **Fig. 3-10**. Then, using the “area and volume” function available in PhotoScan, the measurement was completed. Photoscan estimates the area of the isolated portion of the 3D virtual model by calculating the sum of individual areas for the triangles created to produce the surface of the 3D virtual model. The results were within an acceptable range of difference of 14.9% considering the field measurements were approximated. A summary of the results for the rust stained areas measurements are also included in **Table 3-2**.

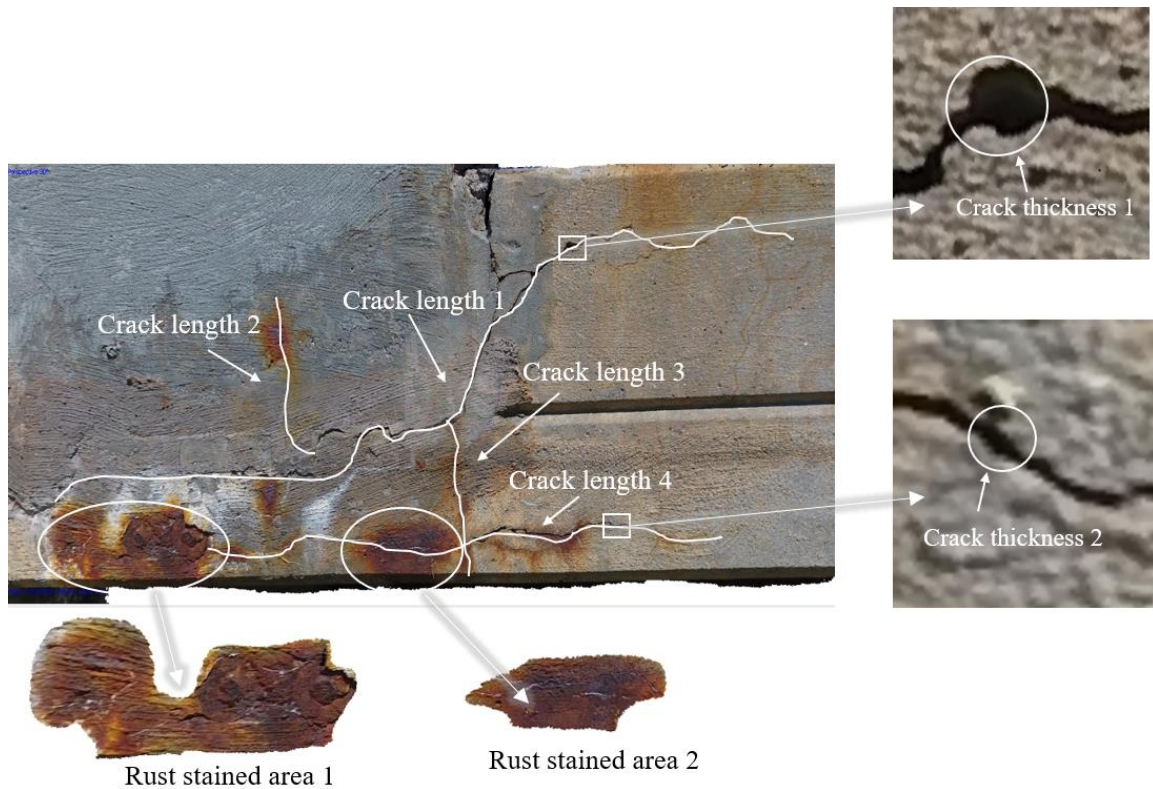


Fig. 3-10. Photogrammetry-based 3D virtual model for damage quantification of damage near abutment of Keystone Wye Bridge.

Table 3-2. Results from Measurements Obtained Using PhotoScan.

Damage Type	Identified damage	Photogrammetry-Based Measurement	Field Measurement	Measurement difference (%)
Crack Length cm (in.)	1	126.0 (49.6)	126.4 (49.8)	0.3
	2	18.8 (7.4)	18.3 (7.2)	2.7
	3	19.6 (7.7)	20.3 (8.0)	3.5
	4	80.2 (31.2)	82.6 (32.5)	2.9
Crack thickness cm (in.)	1	0.64 (0.25)	0.61 (0.24)	4.8
	2	0.14 (0.055)	0.13 (0.051)	7.4
Rust stained area cm ² (in ²)	1	228.4 (35.4)	252.3 (39.1)	9.9
	2	88.4 (13.7)	102.6 (15.9)	14.9

3.5.4 STAGE FOUR

The final stage of the proposed UAV-image-based bridge damage quantification protocol was to establish the damage level following the AASHTO Bridge Element Inspection Manual as seen in **Table 3-3** (AASHTO 2013). A summary of the identified damage level per damage is presented in **Table 3-4**. The damage was assigned following

both the pixel- and photogrammetry-based results. It was determined that the results between the pixel- and photogrammetry-based methods presented an acceptable percent difference of less than 4%; therefore, the damage level following the AASHTO manual was assigned based on the average value of the results as shown in **Table 3-4**. It is worth mentioning that the AASHTO manual does not include a quantifiable value for the rust stained areas but rather a descriptive damage state is presented. Therefore, the damage level was assigned based on the image data (see **Fig. 3-9** and quantified value). Specific damage level for the crack length was not included in the AASHTO manual. It is worthwhile to note that the damage would be subjective due to the lack of quantifiable values in the AASHTO.

Table 3-3
Damage Level Classification Adopted from the AASHTO (2013).

Defects	Condition States			
	1 Good	2 Fair	3 Poor	4 Severe
Efflorescence/Rusting Staining	None	Surface white without build up or leaching without rust staining.	Heavy build up with rust staining.	The condition warrants a structural review to determine the effect on strength or serviceability of the element or bridge; OR a structural review has been completed and the defects impact strength or serviceability of the element or bridge.
Cracking (RC and Others)	Insignificant cracks or moderate width cracks that have been sealed.	Unsealed moderate width cracks or unsealed moderate pattern (map) cracking. Cracks from 0.03 cm (0.012 in) to 0.13 cm (0.05 in) wide.	Wide cracks or heavy pattern (map) cracking. Cracks greater than 0.13 cm (0.05 in) wide.	

Table 3-4. Summary of Results for Quantification Methods and Damage Level Classification.

Damage Type	Identified Damage	Photogrammetry-Based Measurement	Pixel-Based Measurement Aligned to Damage	Measurement Difference (%)	Average Value	AASHTO Damage Level
Crack Length cm (in.)	1	126.0 (49.6)	127.3 (50.1)	1.03	126.65 (49.8)	-
	2	18.8 (7.4)	18.8 (7.4)	0	18.8 (7.4)	-
	3	19.6 (7.7)	20.2 (7.97)	3.02	19.9 (7.8)	-
	4	80.2 (31.6)	82.8 (32.6)	3.4	81.5 (32.1)	-
Crack thickness cm (in.)	1	0.64 (0.25)	0.66 (0.26)	3.1	0.65 (0.26)	Poor or more
	2	0.14 (0.055)	0.14 (0.054)	0	0.14 (0.1)	Poor
Rust stained area cm ² (in ²)	1	228.4 (35.4)	226.5 (35.1)	0.84	227.45 (35.3)	Poor
	2	88.4 (13.7)	91.0 (14.1)	2.9	89.7 (13.9)	Poor

Note: the presence of “-” indicates damage level is not available.

3.6 CONCLUSIONS

This study aimed to propose a UAV-image-based damage quantification protocol to facilitate bridge inspection and structural integrity evaluation procedures for future generations. The study was completed by executing the proposed protocol to quantify the damage on the Keystone Wye Bridge. Based on the results observed, the following conclusions were made:

1. The UAV operation presented some limitations caused mainly by unfavorable weather conditions, including wind speed, limited illumination, and image over and underexposure. Despite the aforementioned limitations, the UAV was able to capture high-quality imagery for the damage quantification process.
2. The proposed entropy-sharpness-based image quality assessment method enabled an efficient selection of high-quality imagery to be used in the damage quantification process. The use of a fictitious reference image to determine the variation of the entropy and sharpness per image allowed for an effective detection

of unsatisfactory images. During this process, a total of 81 out of 110 images were identified as high-quality images based upon the proposed entropy-sharpness relationship.

3. The pixel-based method was efficient to obtain measurements as the results were obtained within five minutes from a single image. The accuracy of the method was reflected on the results for the image aligned to the damage with results within 12% when compared to the direct measurements. Some of the disadvantages of this methods include the inability to obtain accurate results when the camera is not aligned to the damage as shown with the results for the image to the side of the damage.
4. The photogrammetry-based method was accurate when conducting the crack length, thickness, and rust stained area measurements with results falling within 3.5%, 7.4%, and 14.9% difference, respectively, when compared to direct measurements. A drawback of this method is the amount of time it takes for the computer software to generate the 3D virtual model. For the 3D virtual model recreated in this study, the generation time was approximately 40 minutes. Approximately 8 times longer when compared to the pixel-based method.
5. The use of quantifiable values could provide a more systematic and straightforward determination of the damage level if they are integrated within the AASHTO manual. It is hoped that measurable values for the damage state could allow for a rational structural integrity assessment of the bridge. Finally, it is expected that the quantifiable values for the damage level classification will minimize the discrepancies for the damage level designation by inspectors.

It is recommended that future research be conducted to verify the efficiency of the proposed UAV-image-based method in terms of time, expenses, and safety risk reduction. The study of other bridge types including concrete and steel should be conducted to verify the applicability of the recommended damage quantification protocol. The pixel- and photogrammetry-based methods were accurate when compared to field measurements. However, the study of more efficient photogrammetry-based methods in terms of 3D virtual model generation time should be investigated. On the other hand, effective methods to minimize the effect of distortion should be studied further for more accurate pixel-based measurements when the images are not aligned to the damage.

3.7 ACKNOWLEDGEMENTS

Financial support for this research was provided by the Federal Highway Administration through the Forest Products Laboratory (USDA-Forest Service). The assistance and cooperation of the SDDOT is gratefully acknowledged.

3.8 REFERENCES

- ASHTO. (2013). *AASHTO Bridge Element Inspection Guide Manual*. Washington, DC.
- Agisoft PhotoScan. (2016). "Professional Edition." Agisoft LLC, St. Petersburg, Russia.
- Birdal, T. (2011). "Sharpness Estimation from Image Gradients." *MathWorks File Exchange*.
- Duque, L., Seo, J., Wacker, J., (2017). "Synthesis of Unmanned Aerial Vehicle Applications for Infrastructures." *Journal of Performance and Constructed Facilities*. In review
- Ellenberg, A., Kontsos, A., Moon, F., and Bartoli, I. (2016). "Bridge related damage quantification using unmanned aerial vehicle imagery." *Structural Control and Health Monitoring*, 23(9), 1168–1179.
- FAA. (2016). *Code of Federal Regulations (14 CFR) part 107*. Washington, DC.
- Guerrero, J. A., and Bestaoui, Y. (2013). "UAV Path Planning for Structure Inspection in Windy Environments." *Journal of Intelligent and Robotic Systems: Theory and Applications*, 69(1–4), 297–311.
- Hutchinson, T. C., and Chen, Z. (2010). "Image-based framework for concrete surface crack monitoring and quantification." *Advances in Civil Engineering*, Hindawi Publishing Corporation, 2010, 1–18.
- Khaloo, A., Lattanzi, D., Cunningham, K., Dell'Andrea, R., and Riley, M. (2017). "Unmanned Aerial Vehicle Inspection of the Placer River Trail Bridge Through Image-Based 3D Modeling." *Structure and Infrastructure Engineering*, 1–13.
- Kim, H., Lee, J., Ahn, E., Cho, S., Shin, M., and Sim, S.-H. (2017). "Concrete Crack Identification using a UAV Incorporating Hybrid Image Processing." *Sensors*, 17(9).

- Kim, J., Kim, S., Park, J., and Nam, J. (2015). "Development of crack detection system with unmanned aerial vehicles and digital image processing." *Advances in Structure Engineering and Mechanics*, IASEM, Incheon, Korea.
- Kirk, R. S., and Mallett, W. J. (2013). *Highway Bridge Conditions: Issues for Congress Specialist in Transportation Policy Specialist in Transportation Policy*.
- MATLAB. (2017). "Entropy." *MathWorks documentation*,
<<https://www.mathworks.com/help/images/ref/entropy.html>> (Oct. 18, 2017).
- Rasband, W. (1997). "ImageJ." National Institute of Health, Bethesda, Maryland.
- Seo, J., Duque, L., Wacker, J. (2017). "Bridge Inspection Protocol Using Drone Technology." *Automation in Construction*. In review
- Zhuolei, W., Yanli, X., Yingcheng, L., Lijian, Z., and Lina, Z. (2009). "Analyse on image distortion caused by camera tilting angle in mosaic camera." *International Conference on Geo-spatial Solutions for Emergency Management and the 50th Anniversary of the Chinese Academy of Surveying and Mapping*, Beijing, China.

**CHAPTER 4: UAV DATA-DRIVEN FINITE ELEMENT ANALYSIS
FOR BRIDGE PERFORMANCE EVALUATION**

Luis Duque, EIT, S.M. ASCE, S.M SEI

Graduate Research Assistant

Department of Civil and Environmental Engineering

South Dakota State University

Brookings, SD 57007

Phone: (305) 965 - 1363

luis.duque@sdstate.edu

4.1 ABSTRACT

This paper deals with bridge load-carrying capacity evaluation using an integrated Unmanned Aerial Vehicle (UAV) and Finite Element (FE) analysis, following the American Association of State Highway and Transportation Officials (AASHTO) Manual for Bridge Evaluation. For this study, an UAV, the Dà-Jiāng Innovations (DJI) Phantom 4, and the Keystone Wye Bridge located within the Black Hills National Forest in the state of South Dakota (SD) were selected. The bridge was first inspected using the UAV. Through rigorous analysis of image data gained from the inspection, structural damage per critical bridge component was identified, and each was classified as being good, fair, poor, and severe damage levels specified by the AASHTO Manual. A FE model for the as-built bridge was generated and simulated with the AASHTO design truck loadings and modified reflecting the damage levels. Then, lateral live-load distribution factors (DFs) for both the as-built and damaged FE models were determined using stress quantities from the FE simulations and compared to those determined by the codified formula available in the AASHTO LRFD Bridge Design Specifications. Load rating factors (RFs) for both the models were also determined and compared with each other. Primary findings revealed that the damage on the bridge caused the DFs to increase and the corresponding RFs to decrease when compared to the results from the as-built model. This emphasized the need of taking into account the damage in the FE simulation for a better estimate of the load-carrying capacity of the bridge.

4.2 INTRODUCTION

There has been a rapid growing interest in the use of Unmanned Aerial Vehicles (UAVs) in a wide spectrum of structural engineering applications. This promising technology has been used to inspect different types of structures, including buildings, bridges, and dams, among others (Henriques and Roque 2015, Irizarry and Bastos 2016, Khaloo et al. 2017). Due to the increasing costs and limited accessibility of bridges with current inspection techniques, the use of remote-controlled UAVs equipped with high-resolution cameras may shed light on efficient and effective bridge inspection.

In fact, more than 56,007 bridges in the United States are classified as structurally deficient according to the infrastructure report card provided by the American Society of Civil Engineers (ASCE) (ASCE 2016). To inspect the number of structurally deficient bridges, UAV-enabled bridge inspection as a more efficient and cost-effective alternative is needed. Along with damage information from image analysis of the UAV-based inspection data, a Finite Element (FE) model of a bridge should be updated for a better estimate of its load-carrying capacity.

To determine structural damage and performance in terms of load ratings, damage information determined by UAV-enabled inspection technology and damage levels following the codified procedure from the American Association of State Highway and Transportation Officials (AASHTO) Manual for Bridge Evaluation (AASHTO 2011) can be integrated into a FE modeling technique. This paper is broken down into six major sections, starting with a literature review of relevant techniques and ending with key

findings and recommendations for future work. Section two presents the background on the state-of-art and of-the-practice related to UAV-based bridge inspection and FE modeling and simulation techniques for load-carrying capacity assessment. Section three provides a description of the Keystone Wye Bridge used for this study and relevant modeling and simulation details. Section four is devoted to the UAV selection and comprehensive damage identification specific to structural components of the selected bridge. Section five involves a procedure to modify the finite element model reflecting the damage levels, in order to determine realistic lateral live-load distribution factors (DFs) and load rating factors (RFs). Finally, section six is dedicated to a summary of key findings throughout this study and recommended future work.

4.3 BACKGROUND AND LITERATURE REVIEW

This section contains basic knowledge and recent findings through the literature review on each of the principal sub-topics, focusing on UAV-enabled bridge inspection and FE modeling and simulation for the determination of bridge rating. The work performed in this study can help better understand each topic and complete the overall goal of this study. Details for key findings per topic are presented in the following subsections:

4.3.1 UAV-ENABLED BRIDGE INSPECTION

UAVs is able to capture high resolution images, recording video, and performing infrared-based bridge inspection (Eschmann et al. 2012). The ability of UAVs to carry several attachments such as additional cameras, flashlights, and thermal cameras allow for a wider damage identification capability (Vaghefi et al. 2011). The UAV technology has a

great potential to assist future bridge inspection practices, due to limited accessibility for bridge inspectors.

Research efforts have been made to complete bridge inspection and monitoring using UAVs. In 2008, the California Department of Transportation (Caltrans) conducted an initial assessment of the UAV technology and its capabilities to conduct bridge inspection duties (Moller 2008). Moller (2008) developed a twin-motor, single duct, electric-powered UAV designed to carry video cameras up to 61 m in elevation to enable close inspection of bridges. The use of technology to closely assess structural components triggered new research efforts and further development of UAVs in recent years (Chan et al. 2015, Duque et al. 2017b; c, Kim et al. 2017, Lovelace and Zink 2015, Seo et al. 2017b; c; d, Wells and Lovelace 2017). For example, Seo et al. (2017c) developed a recommended UAV-enabled inspection protocol for the efficient damage identification of in-service bridges. It was reported that the UAV was able to identify damage on different components such as girders, underside of deck, and abutments of the target bridge. The comparison of results from the protocol to those of conventional methods demonstrated the capabilities of the UAV to successfully identify damage on the bridge.

Furthermore, Kim et al. (2017) have measured crack lengths and thicknesses on concrete bridges using an integrated UAV and hybrid image processing method. The method included a binarization (i.e., transformation of pixels into white and black) of the images to identify the crack boundaries and complete the measurements. After the images were transformed into binary images, the use of a camera, an ultrasonic displacement

sensor, and a WIFI module facilitated the measurements. It was found that the method was accurate for crack thickness greater than 0.1mm. Finally, it was determined that the crack length presented a maximum percent error of 7.3%, confirming the accuracy the hybrid method.

4.3.2 FE MODELING AND SIMULATION

FE modeling and simulation approaches have been widely used in structural analysis to determine the response of bridges (Chung and Sotelino 2005, Hou et al. 2015, Kwasniewski et al. 2006). Many researchers (Cai 2005, Hodson 2011, Huo and Wassermann 2004, Schlune et al. 2009, Seo et al. 2013) have applied the FE approach to predict the results from either experimental and field testing, in order to determine the DFs and RFs. Due to the high cost of experimental equipment and difficulties to collect relevant information to consider the response of a bridge, there is an increasing number of studies conducted on a variety of FE approaches (Huseynov et al. 2017, Seo et al. 2017d, Yan et al. 2017)

Determination of the DFs using FE approaches is a key component for either designing or rating different types of girder bridges (Seo and Hu 2014, Seo et al. 2014a; b, Seo et al. 2015b, Seo et al. 2017a; d, Gheitasi and Harris 2015a). DF equations available in the AASHTO (2014) Load and Resistance Factor Design (LRFD) Bridge Design Specifications have been in common use to determine DFs for designing and rating such bridges. The number of FE-based DF studies for concrete (Eamon et al. 2016, Semendary (2017), steel (Fatemi et al. 2016, Seo et al. 2014a; b), and timber bridges (Fanous et al.

2011, Seo et al. 2015b; 2017d) have been made. For example, Seo et al. (2017d) developed and calibrate the FE approach for existing timber bridges with data resulting from their field tests. Then, the DFs gained from the FE simulation and field work were also compared to those from the AASHTO DFs which were, in most cases, conservative.

A number of research efforts have focused on performing FE-based determination of RFs (Gheitasi and Harris 2015b, Jauregui 2010, Ju et al. 2015, Seo et al. 2013a; 2015a; 2016, Yost et al. 2005). For instance, Seo et al. (2013a) initiated the research on load rating determination of an in-service bridge subjected to unknown trucks using FE models calibrated with field data, and then Seo et al. (2015a) integrated the field data with multi-regression models to evaluate the RFs of the bridge. It was reported that the use of multi-regression models efficiently predicted the RFs resulting from unknown truck loadings. Another method to determine FE-based RFs conducted by Jauregui (2010) has been applied to existing bridges. The researchers concluded that the RFs determined using the codified values found in the AASHTO LRFD Bridge Design Specifications were more conservative when compared to those found using the FE-based approach.

4.3.3 SUMMARY

Based on the literature review, a number of studies have attempted to identify the issues by each of the aforementioned topics. However, there has been no study to date integrating UAV-informed damage on FE models, in an attempt to determine DFs and RFs that can be in use to help estimate loading-carrying capacity of bridges.

4.4 STUDIED BRIDGE DESCRIPTION AND MODELING

This section presents a description of the selected bridge and FE model to conduct the load-carrying capacity evaluation, involving DFs and RFs. The details are presented in the following subsections.

4.4.1 BRIDGE DESCRIPTION

A glued-laminated timber arch bridge with a composite concrete deck was selected for this study as seen in **Fig. 4-1**. The bridge, known as the Keystone Wye Bridge, is located at the US Highway 16 connection to US Highway 16A near the city of Keystone in the Black Hills National Forest, in South Dakota (SD). The bridge has three sets of stringers spaced at 3.12 m on center (o.c.) connected with galvanized C12x20.7 channel diaphragms and a clear width of 7.92 m. The stringers are 19.20 m long with three spans continuous near the approaches and 24.69 m long with four spans continuous over both sides of the arch hinge. The bridge has an arch length of 49 m and a total length of 88.4 m with steel guardrails along the edge of the superstructure. The overview of the bridge can be seen in **Fig. 4-1a**, the detailed plan view in **Fig. 4-1b**, the elevation view in **Fig. 4-1c**, and the cross section is shown in **Fig. 4-1d**.



(a)

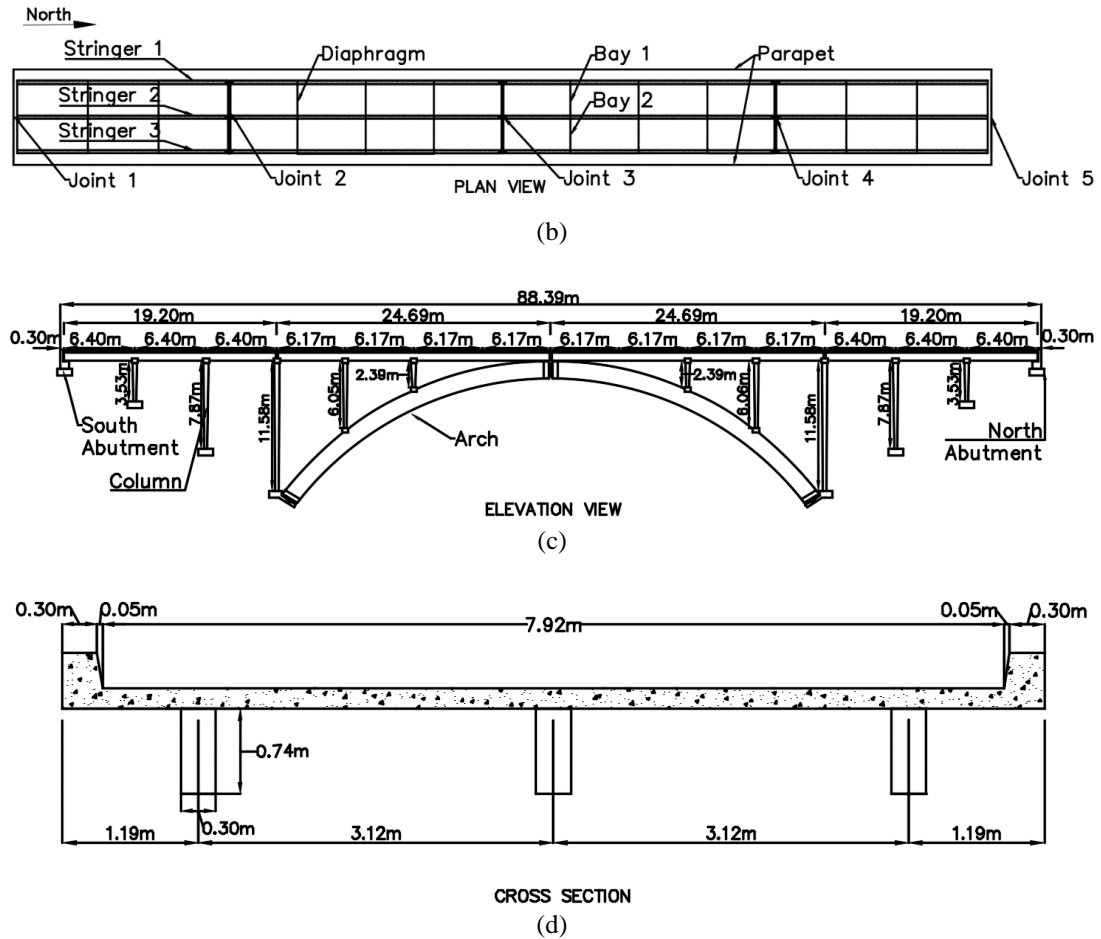


Fig. 4-1. Keystone Wye glue-lam arch bridge drawings: (a) overview image of bridge; (b) plan view; (c) elevation view; and (d) superstructure cross section.

4.4.2 FE MODELING

Using the commercially available SAP2000 FE modeling software, a model for the Keystone Wye Bridge was generated as shown in **Fig. 4-2**. The design loads (including HL-93 truck) stipulated by the AASHTO LRFD Bridge Design Specifications (AASHTO 2014) were applied to the bridge to determine its DFs and RFs. The FE model generation was conducted following a recommended procedure found in Seo et al. (2017d) and Fanous et al. (2011). The model consisted of frame elements for the stringers, quadrilateral shell elements for the deck, and translational springs for the abutments along with frame

elements for the bridge substructure system. The substructure system included columns, cross-frames, and arch. It should be noted that the modeling of the substructure was deemed necessary to develop a complete FE model. Specifically, the shell element found in the software (Computer and Structures Inc. 2017a) is in use to model membrane and plate-bending behavior to simulate a bridge deck system. The use of shell elements has been used to model the concrete deck of the bridge, in accordance with the previous modeling techniques (Maleki 2002, Seo et al. 2017a). To simulate the girder-deck composite action, all the nodes from the frame elements for the stringers were linked to those of the adjacent shell elements by modeling their respective centroids at the same elevation as conducted in previous research by Maleki (2002) and considering the modeling procedure available in the software (Computer and Structures Inc. 2017b).

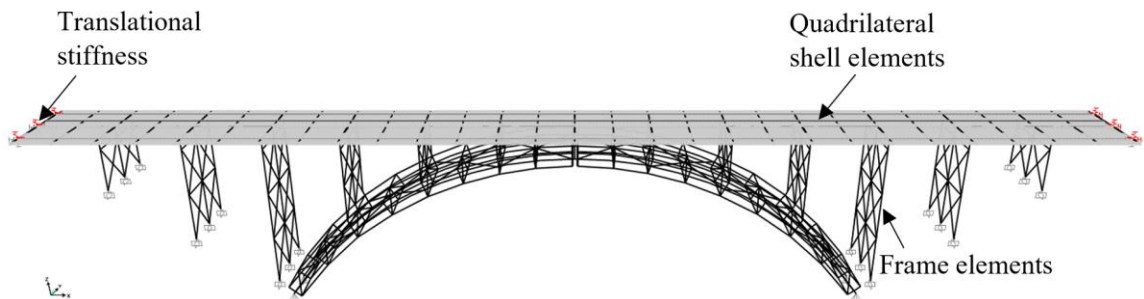


Fig. 4-2. SAP2000 3D bridge model schematic.

The dimensions of the FE model were assigned based upon the as-built bridge plan provided by the South Dakota Department of Transportation (SDDOT). In addition, the material properties for the concrete deck and Douglas-Fir Larch glued-laminated timber components used for the bridge were assigned following the AASHTO LRFD Bridge Design Specifications (AASHTO 2014) as seen in **Table 4-1**. To determine the stiffness of the translational springs, an equivalent spring model was developed according to the methodology provided by past work (Shi et al. 2015). The stiffness values were determined

by applying different small distributed loads from 11 N/cm to 57 N/cm on the stringer to determine the corresponding displacement of the translational and rotational springs. Once the displacements were obtained, the spring stiffness was determined based on the relationship between the applied force and the resultant displacement within the linear elastic range. The stiffness was determined as 87.6 kN/m and 20.3 kN-m/rad for the translational and rotational springs, respectively.

Table 4-1. Section and Material Properties for the FE model Components

Bridge Component	Element Type	Total Number of Elements	Width (cm)	Depth (cm)	Elastic Modulus (MPa)
Deck	Shell	7540	792 ¹	18.4 ²	24856
Stringer	Frame	870	31.1	74.7	11032
Column	Frame	48	30.5	Tapered from 45.7 (top) to 30.5 (bottom)	11032
Arch	Frame	60	36.2	156.2	11032
Cross braces	Frame	136	10.16	17.78	11032
Arch horizontal braces	Frame	32	22.9	15.24	11032

¹Denotes total width of deck

²Constant deck thickness along deck width

4.5 UAV SELECTION AND DAMAGE IDENTIFICATION

This section presents information regarding the UAV applied for the study and the identified bridge damage in the subsequent sections.

4.5.1 UAV SELECTION

The UAV selection process was based on a comparison among thirteen different drones, including: (1) DJI Inspire 1; (2) Voyager 3; (3) DJI Matrice 100; (4) DJI Phantom

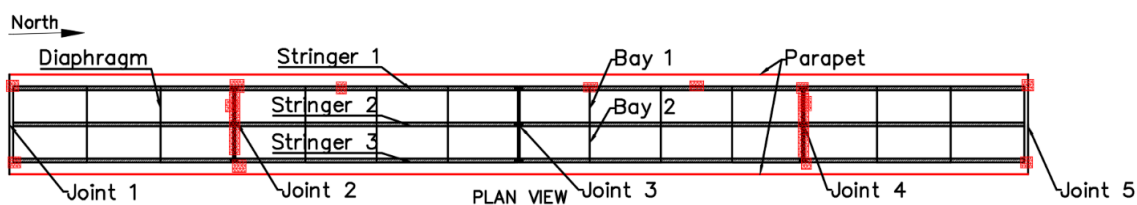
3 Pro; (5) DJI Phantom 4; (6) Yuneec Typhoon H; (7) DJI S900 airframe; (8) Yuneec Typhoon 4K; (9) Blade Chroma; (10) Autel Robotics X-Star Premium; (11) SenseFly eBee; (12) SenseFly Albris; and (13) Topcon Sirius Pro. For efficient selection of the suitable UAV for the bridge inspection, seven considerations involving fly time, camera location, camera low light capabilities, video resolution, payload capacity, drone lights, remote range were verified. The DJI Phantom 4 (see **Fig. 4-3**) was the best choice over the other considered UAVs due to higher values of the considerations. Additionally, the DJI Phantom 4 contains the ability to fly without GPS signal and incorporation of the Obstacle Avoidance (OA) technology. This ability allows the UAV to fly under the bridge and near structural components without the risk of accident. A comprehensive list of UAVs considered, and selection process can be found in Duque et al. (2017a).



Fig. 4-3. Selected DJI Phantom 4 UAV flying near the Keystone Wye Bridge (image captured by Junwon Seo).

4.5.2 DAMAGE IDENTIFICATION

Using the UAV, different types of damage such as crack, corrosion, and spalling were identified on the bridge as seen in **Fig. 4-4**. The bridge components were numbered to efficiently identify the damage location for the FE model updating. It is worth mentioning that the damage identification was completed only for the superstructure as the DFs and RFs determination was based upon the superstructure characteristics. The UAV-enabled bridge inspection was completed using a recommended inspection protocol found in Seo et al. (2017c) including bridge information review, site risk assessment, UAV-preflight check, UAV-enabled drone inspection, and damage identification. A detailed description of the UAV-enabled bridge inspection can be found elsewhere Seo et al. (2017c). Sample damage description and images per component are presented below.



Note: red marks and lines in plan view indicate damage and minor cracks along the parapet in a longitudinal direction, respectively.

Fig. 4-4. Plan view of superstructure with identified damage on the Keystone Wye Bridge.

4.5.2.1 Underside of Deck

The overall condition on the deck was good, despite various water damage locations, especially near joints. Sample concrete spalling and some rust stains due to moisture at Joint 4 captured using the UAV is presented in **Fig. 4-5**. Other critical damage such as concrete cracking and exposed corroded rebar was observed near Stringer 1 at Joint 4.



Fig. 4-5. Sample damage on Joint 4 captured with UAV (taken by Junwon Seo using UAV).

4.5.2.2 Stringers

The stringers were in good condition aside from some minor decay at the supports caused by water leakage from the deck, and corrosion of steel brackets at similar locations. For example, **Fig. 4-6** shows decay on Stringer 2 at Joint 4. Using the UAV, damage such as a shear crack on Stringer 1 and Joint 4 and salt deposits on Stringer 1 at Joint 2 were also observed.



Fig. 4-6. Damage identified on Stringer 2 at Joint 4 captured using UAV (taken by Luis Duque using UAV).

4.5.2.3 Abutments

The abutments were moderately damaged with cracks, water damage, and efflorescence. For instance, the North Abutment on Bay 1 has a transverse crack along almost the entire bay as seen in **Fig. 4-7**. Additional damage on the North and South abutments including concrete cracks, spalling, and water damage was also observed.



Fig. 4-7. Sample abutment damage detected using UAV on Bay 1 at North Abutment (taken by Luis Duque using UAV).

4.6 FE ANALYSIS

This section provides details regarding the FE model updating to reflect the identified damage captured using the UAV. The analytical DFs and RFs were determined and compared to codified values. The detailed information is given as indicated in the following subsections.

4.6.1 DAMAGE APPLICATION

After the damage identification using the UAV, the FE model was modified to reflect the damage per the bridge component. The damage quantification was conducted following a recommended four-stage quantification procedure found in Duque et al. (2017b) including UAV-enabled bridge inspection, image quality assessment, image-based damage quantification, and the AASHTO Manual damage level classification (AASHTO 2013). During the first stage, the inspection of the bridge using an UAV was completed following the protocol found in Seo et al. (2017c). The second stage presented the image quality assessment to identify high-quality images for a more efficient damage quantification. Then, during the third stage, the application of the image analysis-based measurement methods to quantify the damage on the bridge was completed. Finally, based upon the information obtained from the damage quantification, a damage level classification following the AASHTO Manual was assigned.

After completing the damage level classification, remaining structural capacity scales corresponding to bridge damage states, which were established by Shinozuka et al. (2001), were used for estimation of the damaged components on the selected bridge. The scale can

be seen in **Table 4-2**. The scale introduced by Shinozuka et al. (2001) classified the damage as minor, moderate, major, and collapse and assigned a corresponding bridge damage index (BDI). It can be noted that the BDI was established as the percent stiffness reduction for the bridge components. In order to provide a more systematic damage classification, the nomenclature for the damage level classification followed the AASHTO Manual description of good, fair, poor, and severe which is also presented in **Table 4-2** (AASHTO 2013). A comprehensive list of the identified damage with their corresponding the AASHTO damage level and BDI is presented in **Table 4-3**.

Table 4-2. Bridge Damage Index for Each Damage State Identified by Shinozuka et. al. (2001).

Bridge Damage State (AASHTO Damage Level)	BDI
Minor (Good)	0.1
Moderate (Fair)	0.3
Major (Poor)	0.75
Collapse (Severe)	1.0

Table 4-3. Identified Damage on Bridge and Damage level

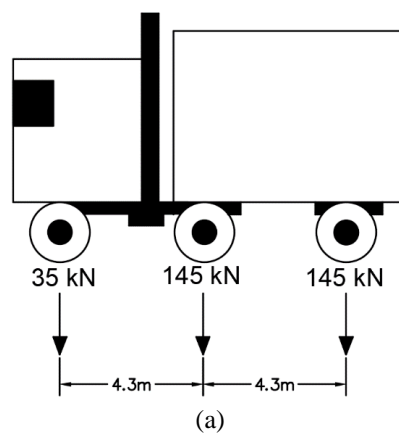
Structural Component	Damage Identified by UAV	Damage Level (AASHTO 2013)	BDI (Shinozuka et. al. 2001)
Underside of deck	Along the parapet near both Stringers 1 and 3: minor cracking	Fair	0.3
	Near Stringer 1 between Joints 2 and 3: stains and water leakage	Fair	0.3
	Near Stringer 1 at Joint 2, spalling: discoloration and corrosion	Poor	0.75
	Along Joints 2 and 4: spalling and stains	Poor	0.75
	Near Stringers 1 and 3 at Joint 5: concrete cracking, exposed corroded rebar, efflorescence and discoloration	Poor	0.75
	Near Stringer 1 at Joint 4: spalling and corroded exposed rebar	Poor	0.75
	Near Stringer 3 at Joint 2: spalling and stains	Poor	0.75
	Near Stringer 1 between Joints 3 and 4: minor moisture	Fair	0.3
	Near Stringers 1 and 3 at Joint 1: spalling, cracking, and exposed corroded rebar	Poor	0.75
	Near Stringer 1 between Joints 3 and 4: minor moisture	Fair	0.3
Abutment	North Abutment on Bay 1: large transverse crack, water accumulation and leakage, spalling, and efflorescence	Poor	0.75
	Near stringer 1 and 3 on North Abutment: concrete spalling, cracks, and moisture	Poor	0.75
	Near Stringer 3 on South Abutment: cracks under deck	Fair	0.3
	Near Stringer 1 on South Abutment: cracks near bottom of deck	Fair	0.3
Stringer	Near supporting areas of each stringer at Joints 2 and 4: stains and decay	Fair	0.3
	Stringer 1 between Joints 3 and 4: noticeable stains	Fair	0.3
	Stringer 1 between Joints 2 and 4: noticeable stains	Fair	0.3
	Stringer 1 at Joint 2: salt deposits	Fair	0.3
	Stringer 1 at Joint 4: shear crack and discoloration	Fair	0.3

After the BDI information per damage was gathered, the degradation of the elements stiffness to reflect the damage was completed on the FE model. The corresponding BDI reduction was applied by reducing the section properties of the elements following the

values recommended by Shinozuka et al. (2001). It is anticipated that the identified damage gathered from the UAV-enabled inspection in conjunction to the historical inspection reports provided by the SDDOT served as an acceptable benchmark for the damage quantification procedure to estimate the bridge damage state. Further, the values stipulated by Shinozuka (2001) provided a reference for the bridge damage condition, in order to estimate the load-carrying capacity of the as-built and damaged FE models.

4.6.2 LIVE-LOAD DFs

The DFs were calculated along the transverse and longitudinal direction of the bridge to identify the critical locations. The HL-93 truck (see **Fig. 4-8a**) locations varied transversely from the start position to the end position in 0.30 m intervals starting at 0.6 m from the inside of the curb per the AASHTO LRFD Bridge Design Specification requirements as seen in **Fig. 4-8b** (AASHTO 2014).



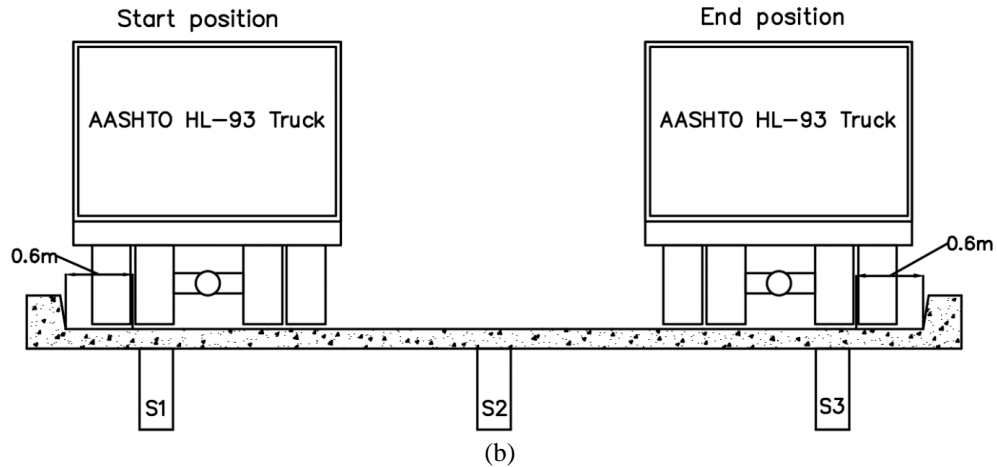


Fig. 4-8. Schematics for design truck and truck locations: (a) AASHTO HL-93 truck and (b) sample truck location along the transverse direction of the bridge deck.

To determine the flexural and shear DFs for a stringer accounting for damage on the bridge, a stress-based approach following a procedure found in Seo et al. (2013b) was implemented using Eqs. 4-1 and 4-2. To calculate the flexural and shear stresses, Eqs. 4-3 and 4-4 were applied.

$$DF = \frac{f_b}{\sum f_b} \quad (\text{Eq. 4-1})$$

$$DF = \frac{f_v}{\sum f_v} \quad (\text{Eq. 4-2})$$

$$f_b = \frac{M}{S} \quad (\text{Eq. 4-3})$$

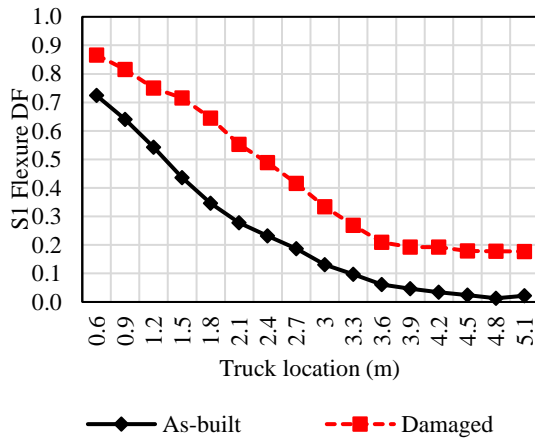
$$f_v = \frac{vQ}{It} \quad (\text{Eq. 4-4})$$

where DF = distribution factor; f_b = stringer flexural stress; $\sum f_b$ = sum of stringers flexural stresses at the same longitudinal location; f_v = stringer shear stress; $\sum f_v$ = sum of stringers shear stresses at the same longitudinal location; S = stringer section modulus; Q = first moment of the area; I = moment of inertia; and t = stringer thickness.

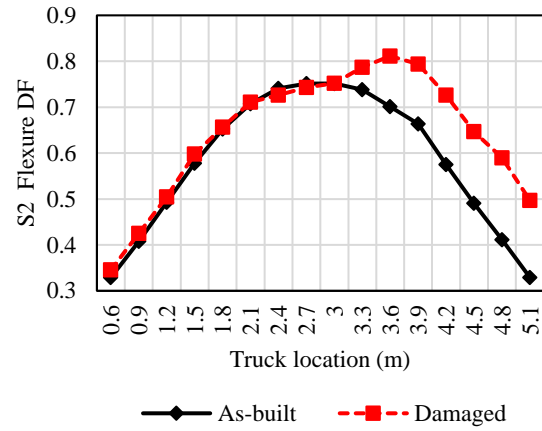
In comparison to the conventional force-based method, the use of the stress-based DFs allowed for a better observation of the DFs variation caused by the induced stress due to damage on the bridge. The estimated as-built flexure DFs for Stringers 1, 2 and 3 (S1, S2, and S3) with respect to the truck location along the transverse direction of the deck can be seen in **Figs. 4-9a** through **4-9c**, respectively. Similarly, the as-built shear DFs for S1, S2, and S3 are presented in **Figs. 4-9d** through **4-9f**, respectively.

A second analysis considering the stiffness degradation following the FE model updating method through the application of the BDI data to the bridge elements was conducted. The results for the damaged flexure and shear DFs can be seen superimposed in **Figs. 4-9a** through **4-9c** and **4-9d** through **4-9f**, respectively. It appears that the DFs for the as-built and damaged models exhibit obvious difference due to an increase in stress caused by the bridge damage. Depending on the location of the damage and the magnitude of the maximum moment and shear stress of the stringers, a significant variation of the DFs was observed. For example, S1 presented greater damage such as stains, salt deposits and a shear crack with a BDI of 0.3 at additional locations when compared to S2 and S3 as presented in **Table 4-3**. It should be noted that the magnitude of the damage for all stringers was equal, but S1 presented damage at more critical locations for moment such stains between Joints 3 and 4. The additional damage observed on S1 caused an unbalanced variation of the flexure DFs for S2 and S3 as shown in **Figs. 4-9b** and **4-9c**. Further, damage at critical locations for shear such as the stringers supports with a BDI value of 0.3 was identified. The increase of stress caused by the damage at the supports was reflected in the

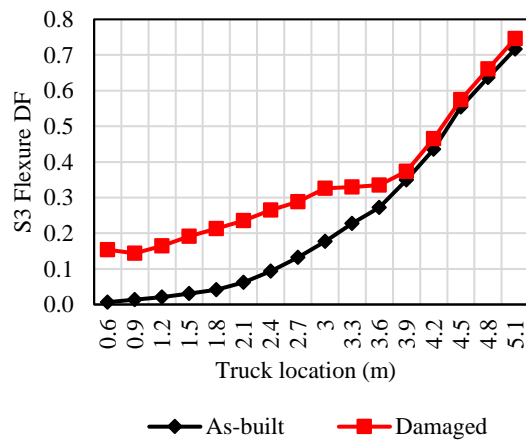
increase of shear DFs for the damaged FE model as seen in the plots of **Figs. 4-9d** through **4-9f**.



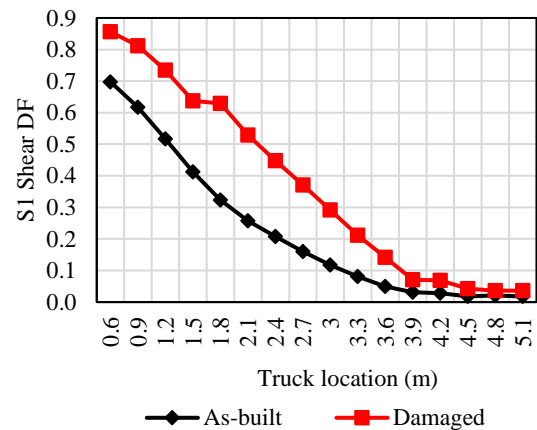
(a)



(b)



(c)



(d)

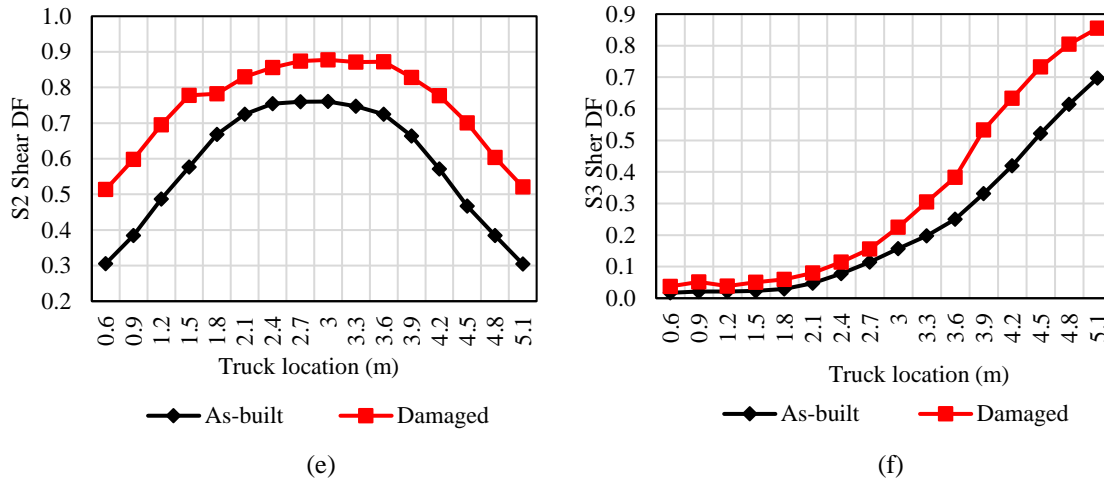


Fig. 4-9. Results for flexure and shear DFs with respect to HL-93 truck location: (a) stringer 1 flexure DFs; (b) stringer 2 flexure DFs; (c) stringer 3 flexure DFs; (d) stringer 1 shear DFs; (e) stringer 2 shear DFs; and (f) stringer 3 shear DFs.

To provide an envelope of the flexure and shear DFs, several critical sections based on the damage location on the stringers were studied. The selected sections were Joints 1, 2, 4, 5, and the three damage locations between Joints 2 and 4 as presented in **Fig. 4-4**. To identify the critical flexure and shear DFs along the longitudinal direction, the maximum DF value per stringer from the analysis was selected. The identified maximum, minimum and average values for the flexure and shear DFs are presented in **Figs 4-10a** and **4-10b**, respectively. Note that the values presented for the DFs do not sum to one as they represent the envelope of the DFs along the longitudinal direction of the bridge for the design truck at 0.6 m from the inside of the curb in the transverse direction. Finally, this procedure was replicated along the transverse direction of the bridge to determine the envelope of the DFs in both the transverse and longitudinal directions.

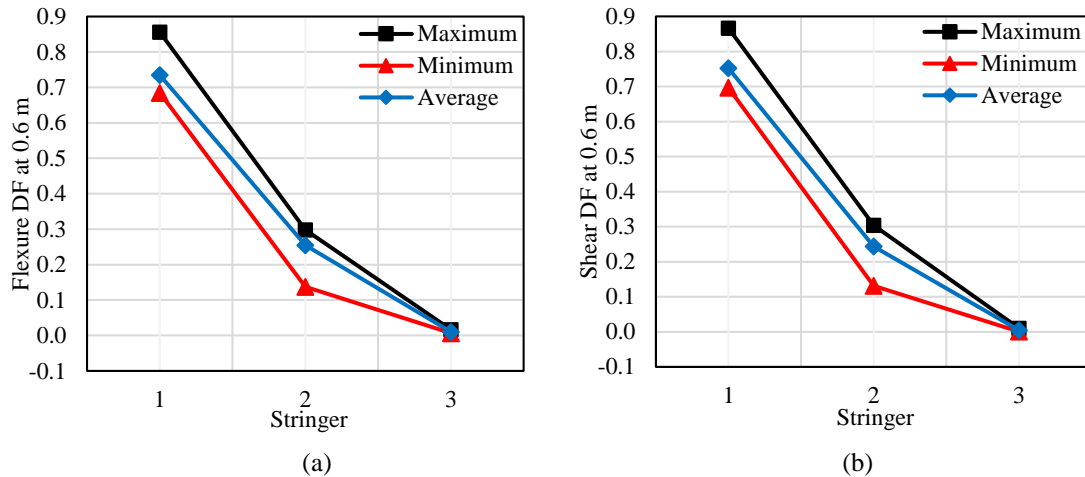


Fig. 4-10. Critical section analysis for truck location at 0.6 m from curb: (a) flexural DFs analysis for critical sections and (b) shear DFs analysis for critical sections.

After determining the analytical DFs obtained from the FE model analysis for both the as-built and damaged bridge, a comparison to the AASHTO codified values was completed. The AASHTO values were calculated using the lever rule as the bridge cross section was not within the range of applicability for the AASHTO LRFD Bridge Design Specifications standard equations (AASHTO 2014). The procedure to calculate the DFs based on the lever rule can be seen in section 4.6.2.2 in the AASHTO LRFD Bridge Design Specifications. The lever rule for both the exterior and interior stringers was applied following the recommended truck locations to generate the most critical loading condition as seen in Jenks et al. (2007). It is worth mentioning that Jenks et al. (2007) developed their lever rule equations following the standards seen in the AASHTO LRFD Bridge Design Specifications.

The envelope for the as-built and damaged flexure and shear DFs obtained from the FE modeling analysis in comparison to the codified values based on the AASHTO LRFD Bridge Design Specification can be seen in **Figs. 4-11a** and **4-11b**, respectively. It can be

observed that the induced damage on the bridge caused both the flexure and shear DFs to increase. Further, as previously described, the S1 presented additional damage locations with a BDI value of 0.3 at critical sections for flexure causing the flexure DF to increase significantly when compared to the S2 and S3. When compared to the codified values using the recommended lever rule by the AASHTO LRFD Bridge Design Specifications, the FE-based as-built and damage flexure DFs were less conservative. On the other hand, the as-built and damaged shear DFs were generally less conservative other than the interior damaged shear DF. Finally, the AASHTO codified flexural and shear DFs were, in most instances, more conservative demonstrating a need for more detailed equations to maximize the performance of bridges with special characteristics such as the Keystone Wye Bridge.

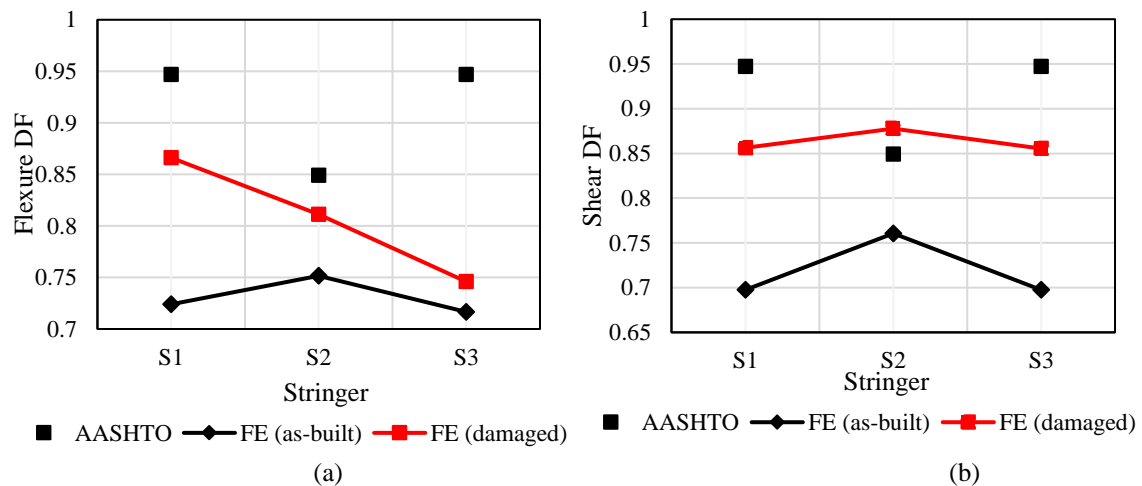


Fig. 4-11. Comparison analytical DFs for as-built and damaged models and the AASHTO values: (a) flexure DFs and (b) shear DFs.

After the critical flexure and shear DFs were calculated, the identification of the critical DFs location along the length of the bridge was checked. A summary of the envelope for the longitudinal (see **Fig. 4-10**) and the transverse (see **Fig. 4-11**) locations of the critical

flexure and shear DFs per stringer are summarized in **Table 4-4**. It was observed that the location of the critical DFs varied for the as-built and damaged FE models. The variation of the critical flexure and shear DFs was attributed to the fluctuation of the stringers stress along the longitudinal direction. For instance, the critical DF for the S1 varied from 65.5 m to 22 m in the longitudinal direction as there is an increase of stress near the Joint 2.

Table 4-4. Summary of Critical Flexure and Shear DF Location in the Transverse and Longitudinal Directions.

Bridge Condition	DF	Stringer	DF Value	Transverse Location (m)	Longitudinal Location (m)
As-built	Flexure	1	0.7240	0.6	65.5
		2	0.7515	3	37.6
		3	0.7166	5.1	65.5
	Shear	1	0.6975	0.6	56.7
		2	0.7606	3	50.6
		3	0.6976	5.1	56.7
Damaged	Flexure	1	0.8661	0.6	22.0
		2	0.8112	3.6	44.2
		3	0.7459	5.1	19.5
	Shear	1	0.8561	0.6	56.4
		2	0.8777	3	81.7
		3	0.8554	5.1	31.1

4.6.3 STRUCTURAL CAPACITY ESTIMATE

The structural capacity of the stringers is defined by the AASHTO LRFD Bridge Design Specifications as a product of the nominal resistance, resistance factor, condition factor, and system factor as seen in Eq. 4-5.

$$C = R_n \phi \varphi_c \varphi_s \quad (\text{Eq. 4-5})$$

where C = structural capacity; R_n = nominal flexure and shear resistance of the component; ϕ = resistance factor; ϕ_c = condition factor; and ϕ_s = system factor. The factors used in the structural capacity estimate for the strength limit state were adopted from the AASHTO Manual for Bridge Evaluation as $\phi = 0.85$ and 0.75 for flexure and shear, respectively; $\phi_c = 1.0$ referring to good or satisfactory condition; and $\phi_s = 1.0$ for flexure and shear for timber bridges. The condition factor referred to the member deterioration and was based on engineering judgement; thus, for the damaged FE model the condition factor was reduced to 0.95 .

To compute the nominal flexural and shear resistance of each stringer, the AASHTO LRFD Bridge Design Specification was referenced (AASHTO 2014). The nominal resistance was determined using the information from the design drawings of the Keystone Wye Bridge. The factors were applied in conjunction with the reference design values to determine nominal resistance of the stringer based on engineering judgement. For the structural glued-laminated timber, the wet service factor for moisture content less than 16% with in-service moisture content was taken as 1. The format conversion factor for LRFD is proportional to the resistance factor, which was determined as 0.85 and 0.75 for flexure and shear, respectively. The flat use factor, deck factor, and incising factor were taken as unity for the stringer flexure and shear capacity.

4.6.4 LOAD RATING FACTORS

The load rating was performed at the component level (e.g., stringers) to identify and evaluate the lowest rated stringer, and that value typically controls the bridge rating. The

rating is commonly performed at the inventory and operating level. The inventory level rating is determined for bridges with frequently carried vehicular loads and operating level rating for the heavier vehicular loads.

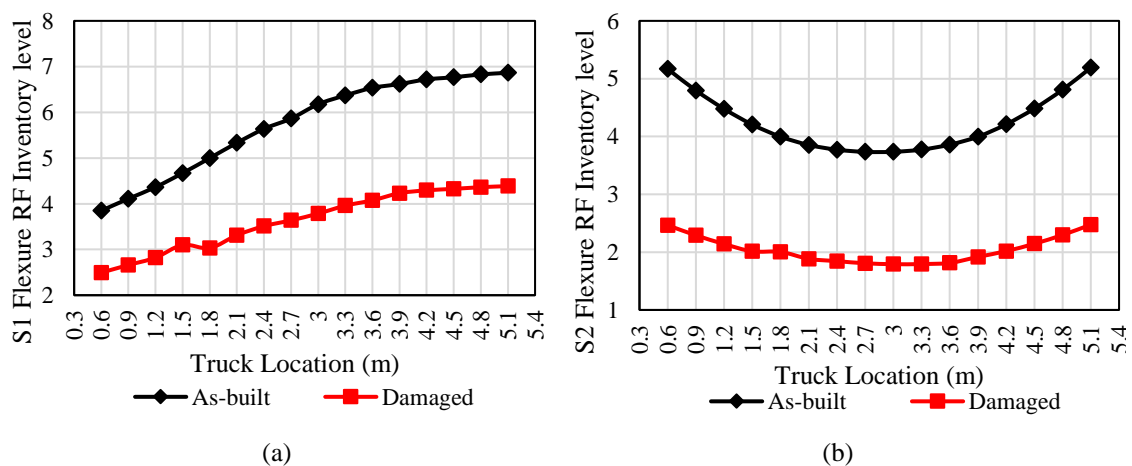
Generally, the bridge ratings can be performed either by the Load Factor Rating (LFR) or Load and Resistance Factor Rating (LRFR) methods as defined in the AASHTO LRFD Bridge Design Specification (AASHTO 2014). The LRFR procedure uses the equivalent strip width analysis (approximate analysis) method for evaluating straight bridges. The LRFR equation (Eq. 4-6) was used to calculate the RFs depending on the structural capacity of the bridge components and associated dead and live load factors including the DFs effect.

$$RF = \frac{(C - \gamma_{DC} * DC - \gamma_{DW} * DW)}{(\gamma_{LL} * LL * (1 + IM))} \quad (\text{Eq. 4-6})$$

where C = structural capacity; DC = dead-load effect due to structural components; DW = dead-load effect due to wearing surface; γ_{DC} = associated LRFD load factor for DC = 1.25; γ_{DW} = associated LRFD factor for DW = 1.5; LL = live-load associated to the vehicular loadings and lane loadings; γ_{LL} = live load factors corresponding to the inventory and operating level as 1.75 and 1.35, respectively; and IM = dynamic load allowance factor (impact factor) applied to the live-load effects caused by the vehicular loading. Note that the IM factor was neglected following the section 3.6.2.3 in the AASHTO LRFD Bridge Design Specifications. Further, the section C3.6.2.3 states that wood structures experience

a reduced dynamic load effect due to internal friction and the damping characteristics of wood.

For the Keystone Wye Bridge, the magnitudes of flexural and shear capacity of each stringer were computed as described in the structural capacity estimate section. The dead, live, and lane loads flexure and shear were computed directly from the FE model. Both the negative and positive moment regions for all the spans were evaluated. For each span, the critical section was utilized in the calculation of the RFs. The effect of the FE-based as-built and damaged DFs on the live load was applied when calculating the as-built and damaged flexure and shear RFs along the transverse and longitudinal directions for the inventory and operating level as presented in **Figs. 4-12** and **4-13**, respectively. It is anticipated that the bridges with RFs greater than 1 for the AASTHO HL-93 truck at inventory and operating level will have adequate capacity for all the AASHTO and state legal loads (AASHTO 2013).



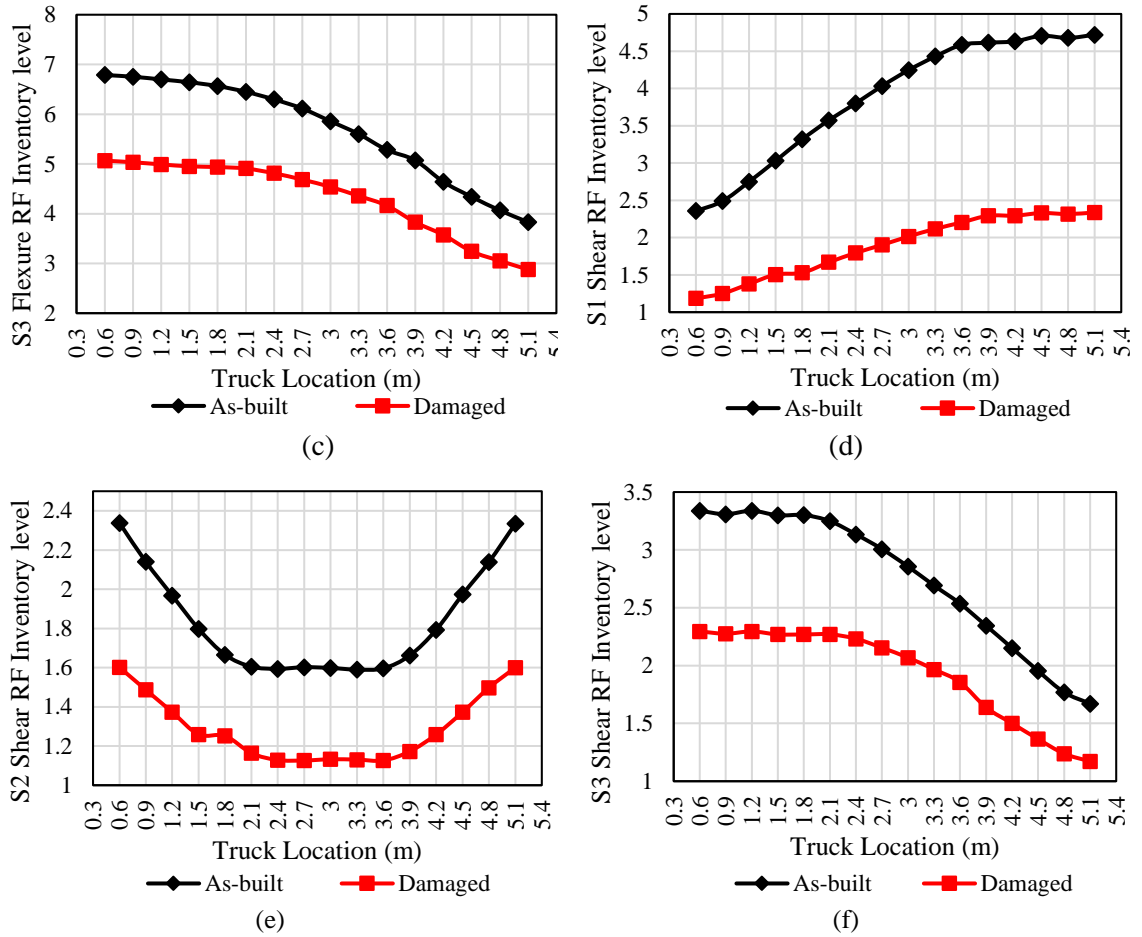
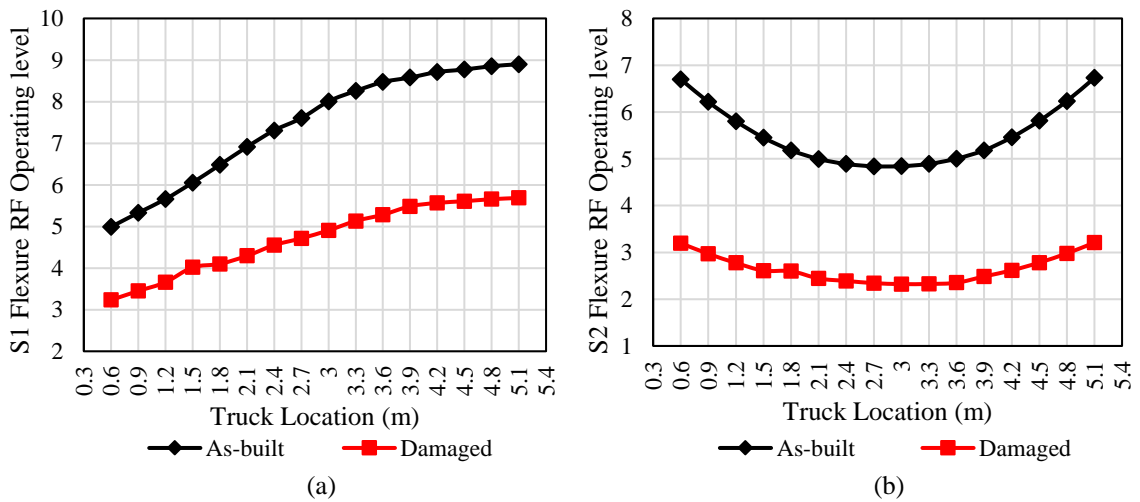


Fig. 4-12. Inventory RFs for flexure and shear: (a) stringer 1 flexural RFs for inventory level; (b) stringer 2 flexural RFs for inventory level; (c) stringer 3 flexural RFs for inventory level; (d) stringer 1 shear RFs for inventory level; (e) stringer 2 shear RFs for inventory level; (f) stringer 3 shear RFs for inventory level.



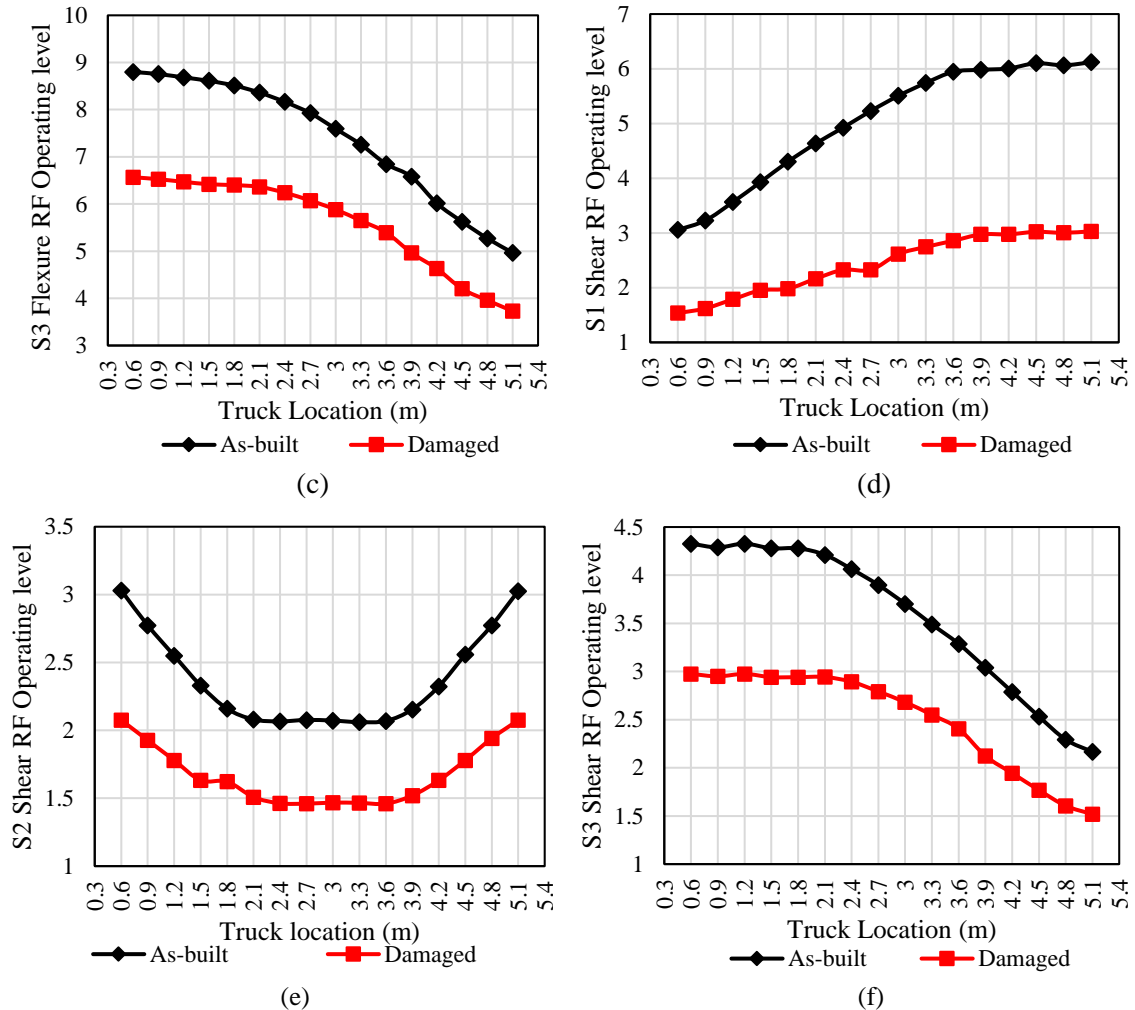


Fig. 4-13. Operating level RFs for flexure and shear: (a) stringer 1 flexural RFs for operating level; (b) stringer 2 flexural RFs for operating level; (c) stringer 3 flexural RFs for operating level; (d) stringer 1 shear RFs for operating level; (e) stringer 2 shear RFs for operating level; (f) stringer 3 shear RFs for operating level.

The RFs obtained using the conventional approach yielded higher values ($RF \geq 1$) representing an additional reserved load-carrying capacity of the bridge. The plots between the RFs and truck location for all the stringers as shown in **Figs. 4-12** and **4-13** show a decrease in the RFs after the updating of the FE-model. Furthermore, the values of the RFs were found to be higher for exterior stringers (S1 and S3) than for the interior stringer (S2) for both flexure and shear as seen in **Figs. 4-14a** through **4-14d**. **Figs. 4-14a** and **4-14b**

show the results for the inventory level and **Figs. 4-14c** and **4-14d** present the results for the operating level.

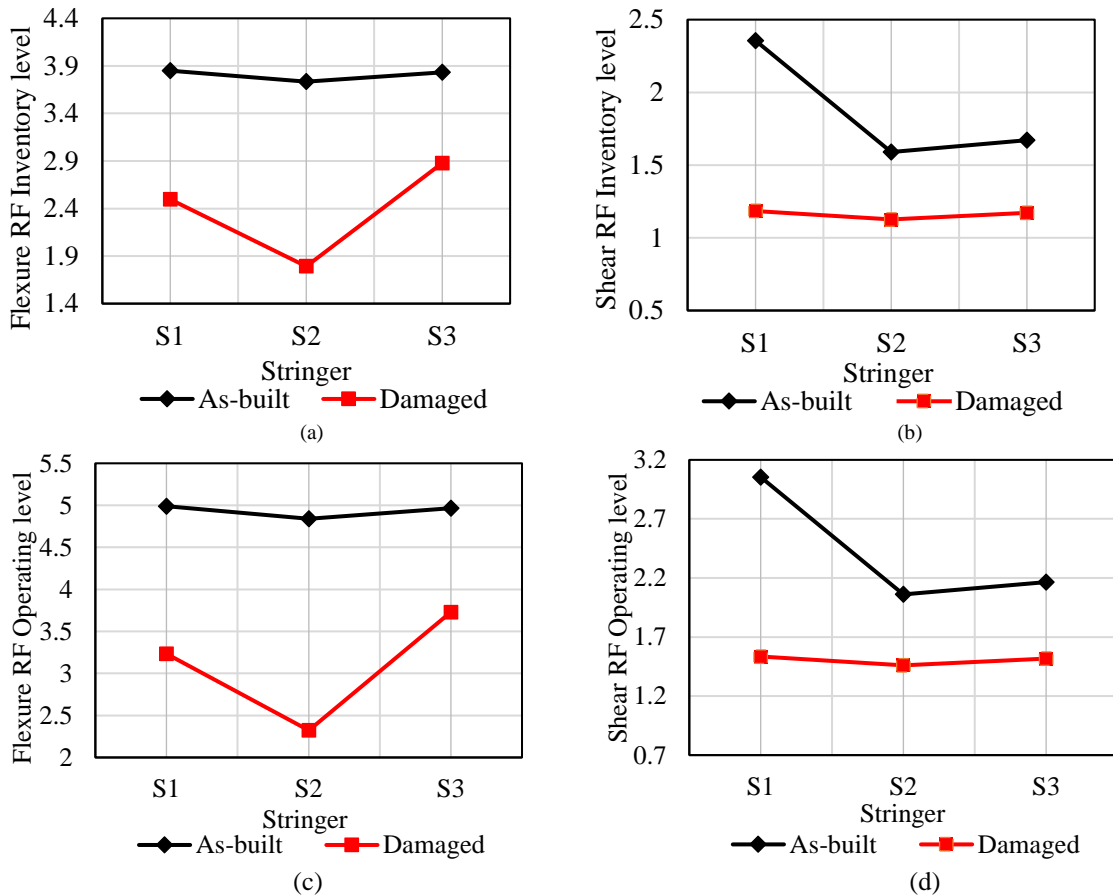


Fig. 4-14. Summary of RFs for the inventory and operating level: (a) flexure RFs for inventory level; (b) shear RFs for inventory level; (c) flexure RFs for operating level; and (d) shear RFs for operating level

4.7 CONCLUSIONS

This study aimed to evaluate the load-carrying capacity of a bridge using the proposed integrated UAV-FE method, following the AASHTO Manual for Bridge Evaluation. To complete the study, the damage identification of the Keystone Wye Bridge was conducted using the selected DJI Phantom 4. Then, a FE model was developed and modified to reflect the identified damage on the bridge to determine the variation of the as-built and damaged

DFs and RFs. Based on the results for the damage identification and FE modeling the following conclusions and recommendations for future work were drawn.

1. The UAV-enabled bridge inspection demonstrated the ability of the UAV to capture damage on different bridge components. The high-resolution camera allowed for an effective damage identification to efficiently modify the FE model to reflect the observed damage. Damage, such as cracking, spalling, and corrosion, was clearly observed by the UAV. Some concerns regarding the GPS signal while flying under the bridge arose during the literature review, but during the study of the Keystone Wye Bridge, it was determined that the UAV maintained GPS signal connection at all times.
2. The explored damage updating method served as an acceptable approach to update the FE model based on the observed damage using the UAV. It was determined that the identified damage gathered from the UAV-enabled inspection and the historical inspection reports provided by the SDDOT was considered an acceptable benchmark for the damage quantification procedure to estimate the bridge damage state. In addition to the damage quantification, the use of the BDI values served as a conservative approach to estimate the load-carrying capacity of the bridge.
3. The use of the stress-based approach to evaluate the effect of damage on the bridge through the FE model updating was determined to be an adequate method to estimate variation of the as-built and damaged DFs. The DFs for the damaged FE model were larger when compared to those of the as-built FE model as expected due to an increase of stress caused by the damage. When compared to the AASHTO

codified values, the analytical as-built and damaged DFs were, in most cases, less conservative.

4. The study of the variation of the RFs caused by the increase in the DFs provided a satisfactory estimation of the “*true*” bridge behavior in terms of its load-carrying capacity. It was observed that the damaged RFs were lower when compared to the as-built values due to the decrease in the bridge capacity and an increase in the live-load effects caused by the larger damaged DFs.

The proposed integrated UAV-FE method was deemed suitable to evaluate the variation of the DFs and RFs due to the damage on the timber bridge and their effect on the load-carrying capacity. Although the methods implemented in this study were acceptable, it is recommended that analysis of other bridge types, such as concrete and steel, be implemented. It is also suggested that a field testing using a network of strain gages to evaluate the true in-situ performance of the bridge due to an applied design truck load be completed and compared to analytical methods such as those presented in this study.

4.8 REFERENCES

- AASHTO. (2011). *Manual for Bridge Evaluation, 2th ED.*, Washington, D.C
- AASHTO (2013). *Manual for Bridge Element Inspection, 1st ED.*, Washington, DC.
- AASHTO. (2014). *AASHTO LRFD Bridge Design Specifications, 7th ED.*, Washington, DC.
- ASCE. (2016). *ASCE 2017 Report Card for America's Infrastructure*, ASCE, Reston, VA
- Baskar, K., Shanmugam, N. E., Thevendran, V. (2002). Finite-element analysis of steel–concrete composite plate girder. *Journal of Structural Engineering*, 128(9), 1158-1168.
- Cai, C. S. (2005). “Discussion of AASHTO LRFD Load Distribution Factors for Slab-on-Girder Bridges.” *Pract. Period. Struct. Des. Constr.*, 10(3), 171–176.
- Chen, S., Rice, C., Boyle, C., Hauser, E. (2011). “Small-Format Aerial Photography for Highway-Bridge Monitoring” *Journal of Performance of Constructed Facilities*, 25(4), 205-122.
- Chung, W., Sotelino, E. D. (2006). “Three-Dimensional Finite Element Modeling of Composite Girder Bridges”. *Engineering Structures*, 28(1), 63-71.
- Computer and Structures Inc. (2017a). “Shell - Technical Knowledge Base - Computers and Structures, Inc.” *CSI Knowledge Base*, <<https://wiki.csiamerica.com/display/kb/Shell>> (Nov. 17, 2017).
- Computer and Structures Inc. (2017b). “Composite section - Tutorials - Computers and Structures, Inc.” *CSI Knowledge Base*, <<https://wiki.csiamerica.com/display/tutorials/Composite+section>> (Nov. 17, 2017).

- Duque, L., Seo, J., Wacker, J. (2017a) “Synthesis of Unmanned Aerial Vehicle Applications for Infrastructures.” *Journal of Performance of Constructed Facilities*. In review
- Duque, L., Seo, J., Wacker, J. (2017b) “Bridge Damage Quantification Methodology using UAV.” *Journal of Bridge Engineering*, In review.
- Duque, L., Seo, J., Wacker, J. (2017c) “Timber bridge inspection using UAV” *ASCE Structures Congress*, ASCE, Fort Worth, Tx. In print
- Eamon, C. D., Chehab, A., Parra-Montesinos, G. (2016). “Field Tests of Two Prestressed-Concrete Girder Bridges for Live-Load Distribution and Moment Continuity.” *Journal of Bridge Engineering*, 21(5), 1–12. doi: 10.1061/(ASCE)BE.1943-5592.0000859.
- Eschmann, C., Kuo, C.-M., Boller, C. (2012). “Unmanned Aircraft Systems for Remote Building Inspection and Monitoring.” *Proceedings of the 6th European Workshop on Structural Health Monitoring, July 3-6, 2012, Dresden, Germany*, 2, 1–8.
- Fanous, F., May, J., Wipf, T., Ritter, M. (2011). *Live-Load Distribution on Glued-Laminated Timber Girder Bridges Final Report: Conclusions and Recommendations*. General Technical Report FPL-GTR-197. Madison, WI: U.S. Department of Agriculture, Forest Service, Forest Products Laboratory. 23 p.
- Fatemi, S. J., Mohamed Ali, M. S., Sheikh, A. H. (2016). “Load Distribution for Composite Steel-Concrete Horizontally Curved Box Girder Bridge.” *Journal of Constructional Steel Research*, 116, 19–28. doi: 10.1016/j.jcsr.2015.08.042

- Gheitasi, A., and Harris, D. K. (2015a). "Overload Flexural Distribution Behavior of Composite Steel Girder Bridges." *Journal of Bridge Engineering*, 20(5), 4014076. doi: 10.1061/(ASCE)BE.1943-5592.0000671
- Gheitasi, A., and Harris, D. K. (2015b). "Implications of Overload Distribution Behavior on Load Rating Practices in Steel Stringer Bridges." *Transportation Research Record: Journal of the Transportation Research Board*, Transportation Research Board, 2522(2522), 47–56.
- Henriques, M., and Roque, D. (2015). "Unmanned Aerial Vehicles (UAV) as a Support to Visual Inspections of Concrete Dams." *Second International Dam World Conference*, LNEC, Lisbon, Portugal, 1–12.
- Huo, X. S., and Wasserman, E. P. (2004). "Simplified Method of Lateral Distribution of Live Load Moment." *J. Bridge Eng.*, 9(4), 382–390
- Huseynov, F., Brownjohn, J. M. W., O'Brien, E. J., Hester, D. (2017). "Analysis of Load Test on Composite I-Girder Bridge." *Journal of Civil Structural Health Monitoring*, 7(2), 163–173. doi: 10.1007/s13349-017-0223-x
- Hodson, D. J., Barr, P. J., Halling, M. W. (2011). "Live-Load Analysis of Post-Tensioned Box-Girder Bridges." *Journal of Bridge Engineering*, 17(4), 644-651.
- Hou, J., Jankowski, Ł., Ou, J. (2015). "Frequency-Domain Substructure Isolation for Local Damage Identification." *Advances in Structural Engineering*, 18(1), 137-153.
- Irizarry, J., and Bastos, D. (2016). "Exploratory Study of Potential Applications of Unmanned Aerial Systems for Construction Management Tasks." *J. Manage. Eng.*, 32(3). doi: 10.1061/(ASCE)ME.1943-5479.0000422.

- Jáuregui, D. V., Licon-Lozano, A., Kulkarni, K. (2010). “Higher Level Evaluation of a Reinforced Concrete Slab Bridge.” *Journal of Bridge Engineering*, 15(2), 172-182.
- Jenks, C. W., Jencks, C. F., Beal, D. B., Delaney, E. P., Hatch, B. (2007). *NCHRP Report 592. Simplified Live Load Distribution Factor Equations. Distribution.*
- Ju, M., Moon, D., Kim, G., Sim, J. (2015). “Evaluating Rating Factor for Prestressed Concrete Girder Bridges by Nonlinear Finite Element Analysis.” *Structure and Infrastructure Engineering*, 11(9), 1250–1262. doi: 10.1080/15732479.2014.950302
- Khaloo, A., Lattanzi, D., Cunningham, K., Dell’Andrea, R., Riley, M. (2017). “Unmanned Aerial Vehicle Inspection of the Placer River Trail Bridge Through Image-Based 3D Modeling.” *Structure and Infrastructure Engineering*, 1–13. doi: 10.1080/15732479.2017.1330891
- Kim, H., Lee, J., Ahn, E., Cho, S., Shin, M., and Sim, S.-H. (2017). “Concrete Crack Identification Using a UAV Incorporating Hybrid Image Processing.” *Sensors*, 17(9), 1-14. doi: 10.3390/s17092052
- Kwasniewski, L., Li, H., Wekezer, J., Malachowski, J. (2006). “Finite Element Analysis of Vehicle–Bridge Interaction.” *Finite Elements in Analysis and Design*, 42(11), 950-959.
- Lovelace, B., and Zink, J. (2015). *Unmanned Aerial Vehicle Bridge Inspection Demonstration Project Report No. MN/RC 2015-40.* Minnesota Department of Transportation Research Services & Library, St. Paul, MN.
- Moller, P. (2008). *CALTRANS Bridge Inspection Aerial Robot Report No. CA08-0182.* Office of Transportation Management Final Report Federal Highway Administration,

Washington, DC.

- Schlune, H., Plos, M., Gylltoft, K. (2009). "Improved Bridge Evaluation Through Finite Element Model Updating Using Static and Dynamic Measurements." *Engineering Structures*, 31(7), 1477-1485.
- Semendary, A. A., Steinberg, E. P., Walsh, K. K., and Barnard, E. (2017). "Live-Load Moment-Distribution Factors for an Adjacent Precast Prestressed Concrete Box Beam Bridge with Reinforced UHPC Shear Key Connections." *Journal of Bridge Engineering*, 22(11), 4017088. doi: 10.1061/(ASCE)BE.1943-5592.0001127
- Seo, J., Chandra, T. K., Phares, B., Lu, P. (2017a). "Agricultural Vehicle Load Distribution for Timber Bridges." *J. Bridge Eng.* 22(11): 04017085. doi: 10.1061/(ASCE)BE.1943-5592.0001112
- Seo, J., Czaplewski, T. M., Kimn, J. H., and Hatfield, G. (2015a). "Integrated structural health monitoring system and multi-regression models for determining load ratings for complex steel bridges." *Measurement: Journal of the International Measurement Confederation*, 75, 308–319. doi: 10.1016/j.measurement.2015.07.043
- Seo, J., Duque, L., and Wacker, J. (2017b). "Field application of UAS-based bridge inspection." *Transportation Research Board 97th Annual Meeting*. In press.
- Seo, J., Duque, L., Wacker, J. (2017c). "Bridge Inspection Protocol Using Drone Technology." *Automation in Construction*. In review
- Seo, J., Hatfield, G., and Kimn, J.-H. (2016). "Weigh-in-motion-based live-load fragility analysis for a steel bridge using structural health monitoring system." *Transportation Research Board 95th Annual Meeting*, Transportation Research Board, Washington, D.C.

- Seo, J., and Hu, J. W. (2014). "Influence of Atypical Vehicle Types on Girder Distribution Factors of Secondary Road Steel-Concrete Composite Bridges." *J. Perform. Constr. Facil.* doi: 10.1061/(ASCE)CF.1943-5509 .0000566, 04014064.
- Seo, J., Kilaru, C., Phares, B. M., Lu, P. (2015b). "Live load distribution factors for a short span timber bridge under heavy agricultural vehicles." *Structures Congress 2015*, N. Ingraffea and M. Libby, eds., ASCE, Reston, VA, 2164–2173.
- Seo, J., Phares, B. M., Dahlberg, J., Wipf, T. J., Abu-Hawash, A. (2014a). "A Framework for Statistical Distribution Factor Threshold Determination of Steel-Concrete Composite Bridges Under Farm Traffic." *Eng. Struct.*, 69, 72–82.
- Seo, J., Phares, B. M., Lu, P., Wipf, T. J., Dahlberg, J. (2013a). "Bridge Rating Protocol Using Ambient Trucks Through Structural Health Monitoring System." *Eng. Struct.*, 46(Jan), 569–580.
- Seo, J., Phares, B., Wipf, T. (2013b). "Lateral Live-Load Distribution Characteristics of Simply Supported Steel Girder Bridges Loaded with Implements of Husbandry." *J. Bridge Eng.*, 04013021. doi: 10.1061/(ASCE)BE.1943-5592.0000558.
- Seo, J., Phares, B., Wipf, T. (2014b). "Lateral Live-Load Distribution Characteristics of Simply Supported Steel Girder Bridges Loaded with Implements of Husbandry." *J. Bridge Eng.* doi: 10.1061/(ASCE)BE.1943-5592.0000558, 04013021.
- Seo, J., Teja Kilaru, C., Phares, B., P Lu (2017d). "Agricultural Vehicle Load Distribution for Timber Bridges." *ASCE J. Bridge Eng.*, 22 (11), 04017085.
- Seo, J., Wacker, J., Duque, L. (2017e). Evaluation of Unmanned Aircraft Systems as a Bridge Inspection Tool. Madison, WI: U.S. Department of Agriculture, Forest Service, Forest Products Laboratory. In final editing

- Shi, D., Wang, Q., Shi, X., Pang, F. (2015). “An Accurate Solution Method for the Vibration Analysis of Timoshenko Beams with General Elastic Supports.” *Journal of Mechanical Engineering Science*, 229(13), 2324–2340. doi: 10.1177/0954406214558675
- Shinozuka, M., Feng, M. Q., Kim, H., Uzawa, T., Ueda, T. (2001). *Statistical analysis of fragility curves, technical report FHWA DTFH61-92-C00106*. University of California, Los Angeles, California.
- Vaghefi, K., de Melo e Silva, H. a., Harris, D. K., and Ahlborn, T. M. (2011). “Application of thermal IR imagery for concrete bridge inspection.” *Convention and National Bridge Conference*, 13.
- Wells, J., and Lovelace, B. (2017). *Unmanned Aircraft System Bridge Inspection Demonstration Project Phase II Report No. MN/RC 2017-18*. Minnesota Department of Transportation Research Services & Library, St. Paul, MN.
- Yan, J., Deng, L., He, W. (2017). “Evaluation of Existing Prestressed Concrete Bridges Considering the Randomness of Live Load Distribution Factor due to Random Vehicle Loading Position.” *Advances in Structural Engineering*, 1–10. doi: 10.1177/1369433216664350
- Yost, J. R., Schulz, J. L., Commander, B. C. (2005). “Using NDT data for finite element model calibration and load rating of bridges.” *Structures Congress 2005: Metropolis and Beyond* (pp. 1-9).
- Zhang, Q. W., Chang, T. Y. P., Chang, C. C. (2001). “Finite-Element Model Updating for The Kap Shui Mun Cable-Stayed Bridge.” *Journal of Bridge Engineering*, 6(4), 285-293.

Živanović, S., Pavić, A., Reynolds, P. (2007). "Finite Element Modelling and Updating of a Lively Foot-bridge: The Complete Process." *Journal of Sound and Vibration*, 301(1), 126-145.